Design optimization of jacket structures for mass production

Sandal, Kasper

Link to article, DOI:
10.11581/DTU:00000023

Publication date:
2017

Document Version
Publisher's PDF, also known as Version of record

Design Optimization of Jacket Structures for Mass Production

Department of Wind Energy PhD Report 2017

Kasper Sandal

DTU Wind Energy PhD-0077(EN)
DOI number: 10.11581/DTU:00000023

July 2017

DTU Wind Energy
Department of Wind Energy

Authors: Kasper Sandal

Title: Design Optimization of Jacket Structures for Mass Production

Department: Wind Energy

2017

Project Period:

August 1st 2014 – July 31st 2017

Education:

PhD

Supervisor:

Professor Jesper Mathias Stolpe

Co-supervisors:

Associate Professor Henrik Bredmose

Technical University of Denmark
Department of Wind Energy
Frederiksborgvej 399
Building 118
4000 Roskilde
Denmark

www.vindenergi.dtu.dk

DTU Wind Energy
Department of Wind Energy

PhD Thesis

Design optimization of jacket structures for mass production

Models and applications

Kasper Sandal

DTU Risø campus, Roskilde, 2017

DTU

Technical University of Denmark
Department of Wind Energy

DTU Risø Campus
Frederiksborgvej 399 Building 115
4000 Roskilde, Denmark
Phone +45 93511076
kasp@dtu.dk
kasper.sandal@outlook.com
www.vindenergi.dtu.dk

Title of thesis
Design optimization of jacket structures for mass production

PhD student:
Kasper Sandal
Department of Wind Energy
Technical University of Denmark
Address: Frederiksborgvej 399, 4000 Roskilde, Denmark
E-mail: kasp@dtu.dk

Supervisors:
Professor Jesper Mathias Stolpe
Department of Wind Energy
Technical University of Denmark
Address: Frederiksborgvej 399, 4000 Roskilde, Denmark
E-mail: matst@dtu.dk

Associate Professor Henrik Bredmose
Department of Wind Energy
Technical University of Denmark
Address: Energivej, 2800 Kgs. Lyngby, Denmark
E-mail: hbre@dtu.dk

PhD Committee
Associate Professor, dr.techn. Niels Leergaard Pedersen, Technical University of Denmark
Professor Pierre Duysinx, University of Liége
Professor Dr.-Ing. habil. Raimund Rolfes, Leibniz Universität Hannover

Preface

This thesis is submitted in partial fulfilment of the requirements for obtaining the degree of PhD at the Technical University of Denmark. This PhD project is a part of the strategic research project ABYSS: Advancing BeYond Shallow waterS - Optimal design of offshore wind turbine support structures (`www.abyss.dk`). The project is funded by the Danish Council for Strategic Research, Grant no. 1305-00020B. The funding is gratefully acknowledged.

My motivation for pursuing a PhD in structural optimization of jacket structures stems from a passion for mathematics, and a dream of moving the green shift forward. I am most grateful for the opportunity, and have had the privilege of working with many smart, kind, and creative people.

First I would like to thank Professor Mathias Stolpe, who has been the best supervisor I could ever have wished for. I also want to thank my office mate Alexander Verbart for our fun and interesting times, especially during the development of the software JADOP. Many thanks also to Susana Labanda Rojas, who has helped me continuously the past few years. Thanks to all of my collaborators, from my closest colleagues in the section, to Varvara Zania and Chiara Latini at DTU Civil Engineering, Jacob Oest from Aalborg University (Denmark), and Michael Muskulus, Sebastian Schafhirt, and Lars-Einar S. Stieng from the Norwegian University of Science and Technology (Norway). I also wish to thank my co-supervisors Thomas Buhl (previously DTU Wind Energy) and Henrik Bredmose (DTU Wind Energy) for their support whenever I asked for it. It has been a privilege to work with all of you, and this thesis is better because of you. A special thanks to Alexander and Jacob, who have really helped me develop as a reasearcher.

I would also like to express my deep gratitude to my family. Mom, dad, and Agathe, it means a lot to know that you are never more than a phone call or flight away. Finally, I would like to thank my wife and best friend Elin, for making my life so much richer, and for keeping me sane and effective these past few months. Soon we will be three.

DTU Risø campus, Roskilde, July 28, 2017

Kasper Sandal

Summary

This thesis presents models and applications for structural optimization of jacket structures for offshore wind turbines. The motivation is that automatic design procedures can be used to obtain more cost efficient designs, and thus reduce the levelized cost of energy from offshore wind.

A structural finite element model is developed specifically for the analysis and optimization of jacket structures. The model uses Timoshenko beam elements, and assumes thin walled tubular beams and a linear elastic structural response. The finite element model is implemented in a Matlab package called JADOP (Jacket Design Optimization), and the static and dynamic structural response is verified with the commercial finite element software Abaqus. A parametric mesh of the offshore wind turbine structure makes it relatively easy to represent various structures from the literature, as well as exploring conceptual designs. Stress concentrations in welds are modelled using design dependent stress concentration factors. Simplified models are also implemented for both piled foundations and suction caissons. Wind and wave loads are applied according to a realistic offshore environment.

An optimal design problem is formulated to optimize the design of the jacket structure using analytical gradients. The diameter and wall thickness of the jacket members are considered as design variables, making it a sizing optimization problem. Structural integrity constraints are implemented based on the relevant industrial design guidelines. These constraints include fatigue damage in the welded joints, shell buckling, and yield stress. The most challenging structural integrity constraint is fatigue, as it generally requires computationally expensive time-domain simulations. A simplified fatigue constraint based on damage equivalent loads is presented, and results indicate that the method gives realistic designs. The objective and constraint functions, including sensitivities, are implemented in JADOP, and this package is used throughout the thesis.

The devised framework is applied to the optimal design of jacket structures and foundations, with continuous and discrete design variables. Design criteria such as mass, fatigue, stress, and frequency are considered, and the validity of the modelling assumptions are investigated with aeroelastic simulations. The proposed framework can thus be applied to automate the design of jackets and foundations, and be a powerful tool in the whole design process of offshore wind turbine structures.

Resumé (in Danish)

Denne afhandling præsenterer modeller og anvendelser til strukturel optimering af jacket-konstruktioner for havvindmøller. Motivationen er at automatiske designprocedurer kan bruges til at lave mere omkostningseffektive designs, og dermed reducere den endelige pris på elektricitet fra havvindmøller.

En strukturel elementmetodemodel er udviklet specifikt til analyse og optimering af jacket-konstruktioner. Modellen bruger Timoshenko bjælkeelementer, og antager tyndvæggede cylindriske bjælker og en lineær-elastisk strukturel respons. Elementmetodemodellen er implementeret i en Matlab-pakke som hedder JADOP (Jacket Design Optimization), og den statiske og dynamiske strukturelle respons er verificeret med det kommercielle elementmetode-software Abaqus. Et parametrisk mesh af havvindmøllekonstruktionen gør det relativt nemt at repræsentere forskellige konstruktioner fra litteraturen, samt at udforske konceptuelle designs. Spændingskoncentrationer i svejsninger er modelleret med designafhængige spændingskoncentrationsfaktorer. Forenklede modeller er også implementeret for både pælefundamenter og sugebøttefundamenter. Vind- og bølgelaster er påført i henhold til et realistisk offshore miljø.

Et optimeringsproblem er formuleret for at optimere designet af en jacket-konstruktion ved brug af analytiske gradienter. Diameteren og vægtykkelsen af jacketdelene er valgt som designvariable, hvilket gør det til et sizing-optimeringsproblem. Strukturelle integritetsbetingelser er implementeret baseret på relevante industrielle retningslinjer. Disse betingelser inkluderer udmattelse i svejsesamlingerne, buling, og flydespænding. Den mest udfordrende af disse betingelser er udmattelse, da det generelt kræver beregningstunge tidsdomænesimuleringer. En forenklet udmattelsesbetingelse baseret på skade-ækvivalente laster er præsenteret, og resultater indikerer at metoden giver realistiske designs. Objekt- og betingelsesfunktionerne er implementeret i JADOP, og denne Matlab-pakke er brugt igennem hele afhandlingen.

Den udviklede fremgangsmåde er anvendt på det optimale design af jacket-konstruktioner og -fundamenter, med kontinuerlige og diskrete designvariable. Designkriterier så som masse, udmattelse, spændinger, og frekvenser behandles, og gyldigheden af modelleringsantagelserne er undersøgt gennem aeroelastiske simuleringer. Den fremsatte optimeringsmetodik kan derfor anvendes til optimering af jacket-konstruktioner og -fundamenter, og kan være et kraftfuldt værktøj i hele designprocessen af havvindmøllekonstruktioner.

Contents

Introduction

The objective of this thesis is to develop analysis models and design methods for optimal design of jacket structures for mass production.

Jacket structures have so far not been used in many offshore wind projects, mainly because monopiles have been cheaper, or been perceived as a safer option [59]. However, with very large turbines in deeper waters subjected to waves and varying soil conditions, jackets are expected to be the preferred substructure [20]. As in every other part of the industry, there is a strong motivation to bring down the cost. Since the design of jacket structures is a complex task, including advanced analysis and many design variables, computer-aided design methods should be developed to adress this design task. The currently avaiable design and analysis tools are not developed from an optimization point of view, which make them challenging to use for structural optimization. This motivates the development of new analysis and optimization tools for structural optimization of jackets.

This thesis presents an approach to optimal design of jacket structures which begins with the optimization problem, and then introduces different analysis models which are tailored to the specific problem. This is demonstrated for example in Paper I, with the optimal conceptual design problem. In Paper III, the design of foundations is included, again by introducing appropriate analysis models which work well in an optimization problem.

Summary of the thesis

The thesis is divided in two parts. **Part I** of the thesis provides context and background for the reseach conducted during the PhD studies. This part is organized as follows:

Chapter 1 presents the substructures for offshore wind turbines, and motivates the specific focus on jacket structures. The relevant design standards are listed, and the analysis of offshore wind turbines is discussed.

Chapter 2 contains a brief literature review of structural optimization of frames and support structures. Then the optimal design problem is discussed, followed by the identification of research gaps adressed in this thesis.

Chapter 3 presents the main conclusions of the work presented in this thesis, examines the main contributions, and suggests topics for future research.

Part II includes all the manuscripts associated with this thesis. This part consists of the following chapters, each referring to a different manuscript.

Paper I K. Sandal, A. Verbart, M. Stolpe, Conceptual optimal design of jacket structures. Submitted to *Wind Energy*, under review.

Paper II J. Oest, K. Sandal, S. Schafhirt, L. E. S. Stieng, M. Muskulus, On gradient-based optimization of jacket structures for offshore wind turbines. Submitted to *Wind Energy*, under review.

Paper III K. Sandal, C. Latini, V. Zania, M. Stolpe, Integrated optimal design of jackets and foundations. To be submitted to *Marine Structures*.

Paper IV M. Stolpe, K. Sandal, Structural optimization with several discrete design variables per part by outer approximation. To be submitted to *Structural and Multidiciplinary Optimization*.

Paper V K. Sandal, JADOP - JAcket Design OPtimization. To be submitted as a *Technical report at DTU Wind Energy*.

Part I

Background

CHAPTER 1
Support structures for offshore wind turbines

This chapter paints the bigger picture of substructure design in the offshore wind industry. First the terminology is explained in section 1.1, and some different foundation and substructure concepts are presented. Section 1.2 discusses the various design standards and recommended practises commonly applied to offshore wind turbine substructures. Then section 1.3 contains a brief introduction to the analysis of offshore wind turbines, with emphasis on what is required for different purposes. Section 1.4 discusses cost drivers and market trends, motivating the focus on jacket substructures. Finally, design for mass production is adressed in section 1.5, where the contributions from this thesis are briefly presented.

1.1 Definition of foundations and substructures

The terminology in this thesis defines the support structure as everything which supports the turbine, including tower, transition piece, substructure and foundation, see Figure 1.1. In the following, three foundation concepts and three substructure concepts are briefly presented. Floating support structures are not discussed.

The foundation is what anchors the bottom-fixed structure to the soil, and three main categories exists:

- Gravity Base Structures (GBS): The GBS is a heavy foundation, usually concrete, which is placed on top of the seabed, with or without a small steel or concrete skirt. The objective of the gravity based foundation is to avoid tensile loads between the support structure and the soil. The first offshore wind farm (Vindeby [59]) used GBS, and it has been used many times since.
- Piled foundation: The piled foundation are slender pipes which are driven deep into the seabed. The friction between the soil and the pile surface ensures that the structure stays in place. Most offshore wind turbines are installed with piled foundations, primarily monopiles [33].
- Suction bucket foundation: The suction bucket foundation is lowered into the seabed by decreasing the pressure on the inside of the upside-down bucket, so that a suction force pulls it down. The suction bucket is relatively unproven in the offshore wind industry, but is now reaching a good stage of maturity for both jackets and monopiles [25].

The substructure is the structure going from the seabed and up to above the surf zone,

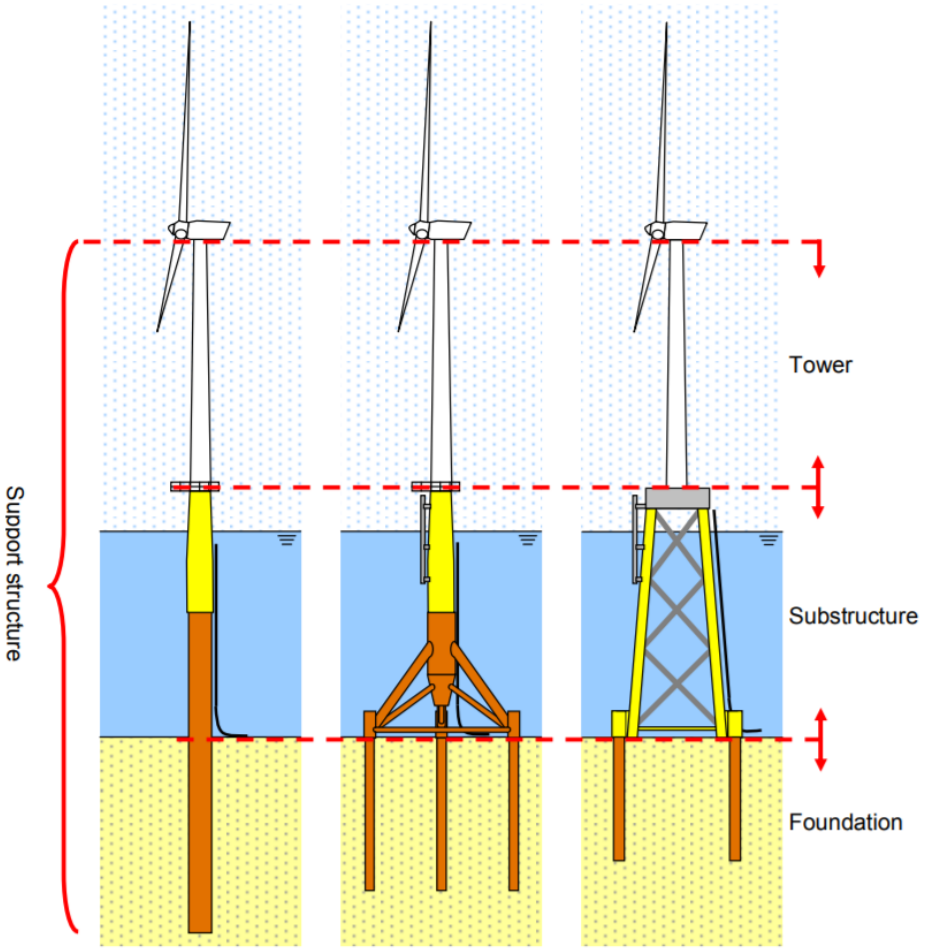

Figure 1.1: Definition of terminology and concepts. Monopile (left), tripod (middle), and jacket (right) are three different substructure concepts for offshore wind turbines. In the figure all foundations are placed on piled foundations, but suction bucket foundations or gravity based foundations can also be used. Figure credit: [20].

approximately 16 meters above the mean water level, depending on the site conditions. The substructure is usually a welded steel structure. The majority of the substructure is made up of the load carrying part, also known as primary steel, but it also includes boat landings and J-tube (steel tube protecting the power cables), which is referred to as secondary steel. The main substructures in Figure 1.1 are:

- Monopile: The monopile is a large diameter steel pipe. The monopile can be installed with both gravity based and suction bucket foundation, but it is most commonly seen as in Figure 1.1, where the substructure and foundation are combined into one very large pile.
- Jacket: The jacket is a space-frame steel structure welded together in Y-, K-, and X-joints. Since it has a larger footprint than the monopile, it is much stiffer, and is also more transparent to waves.
- Tripod: The tripod is similar to the monopile substructure, but distributes the forces out to three foundations.

Examples of concepts not presented here are the tripile and twisted jacket [26].

1.2 Design standards

Design of offshore wind turbine structures is subject to diffent requirements depending on country, and are often adopted from oil and gas. The main international standard for offshore wind turbine structures is the IEC 61400-3. This document is perhaps most famous for the thousands of aeroservoelastic time-domain analyses it requires to properly assess all limit states for an offshore wind turbine.

An offshore standard for design of offshore steel structures is presented for example in DNVGL-OS-C101 [23], and NORSOK and Eurocode provide similar codes. An offshore standard specifically for design of offshore wind turbine structures is the DNV-OS-J101 [21] (since April 2014 superseded by DNVGL-ST-0126 [24]). Because fatigue is often a design driver, the recommended practice for fatigue design of offshore steel structures DNVGL-RP-C203 [22] is also important to consult. In Germany, the design and installation of offshore wind turbine structures must be certified by the BHS [9], which pose much more stringent requirements than what is used in other countries [59]. The design of the substructure and foundation cannot be completly decoupled, as will be shown in Paper III. The most common standard used for the foundation design is one from the americal petroleum institute (API) [3].

Recommended practices and standards can be very good tools for engineers, and development of these are viewed as an important part of maturing new technnology. It is also important for banks and insurance companies that all procedures are "according to rules and guidelines". However, is should be mentioned that rules and guidelines can also have a backfiring effect. First of all, it can be cumbersome to introduce new innovations, because as long as they are not included in the right documents, they can be almost impossible to introduce to the market. So if the codes are not continuosly adopting new knowledge, innovation and cost reduction efforts are delayed. Secondly,

a recommended practice or standard can give a sense of false security. This was the case with the infamous "slippage" of the grouted connections in many monopiles [59]. Although designs were performed according to the at-the-time current design standard from DNV, the grouted connection failed to bear the intended load, and costly repairs had to be made.

1.3 Analysis of offshore wind turbines

Good design procedures for offshore wind turbine structures depend on accurate estimation of the structural behaviour throughout the lifetime. For monopiles, both wind and wave loads contribute significantly to the load. For jackets the load is dominated by the wind, which actually makes the analysis simpler, although the structure is more complex.

Certification of an offshore wind turbine structure according to the IEC-61400 Part 3 [32] requires thousands of time domain simulations in an aero-servo-hydro-elastic software. Not many softwares can do this, and a simplified analysis would be to decouple the rotor and the structure. This way, the load is first generated in one software, and then the load is applied to the structure in another software. This is sometimes done because turbine designers and support structure designers are unwilling to share all details of their models with the other. A decoupled model assumes that the load is independent of the structural design, something which is not necessarily true [46].

Another simplification one can make is to ignore dynamic effects, and use a quasi-static analysis. Since the wave-spectra often overlaps with the first natural frequency of the monopile, this is not recommended for monopiles. However, with brace-vibrations at much higher frequencies than the waves, it can be sufficient to use quasi-static analysis for wave loads on jackets [59]. Since the frequencies of the rotor loads are often comparable to the first natural frequency of the structure, it is not recommended to use quasi-static analysis for the wind loads.

Finite element or multi-body analysis with beam elements are the most common types of analysis for offshore wind turbine structures. This is because the beam element is computationally cheap, while providing a good representation of these types of structures [16]. A thorough description of beam finite elements is provided in Paper V of this thesis. Paper V also discusses how the reference structures from the literature have been interpreted by a generalized parametric jacket model, as shown in Figure 1.2.

1.4 Substructure costs and market trends

Monopiles are becoming much heavier with deeper waters, and installation is noisy. Jackets are lightweight, becoming cheaper, and soon considered proven technology.

The offshore wind industry has seen an impressive growth, both in volume, but also in size of turbines, support structures, and vessels. Many had predicted that the monopile would be replaced by the jacket long ago, but new fabrication facilities and vessels have allowed the dimensions of the monopile to grow way beyond expectations. One reason is that monopiles are seen as "proven technology", which is something banks and insurance

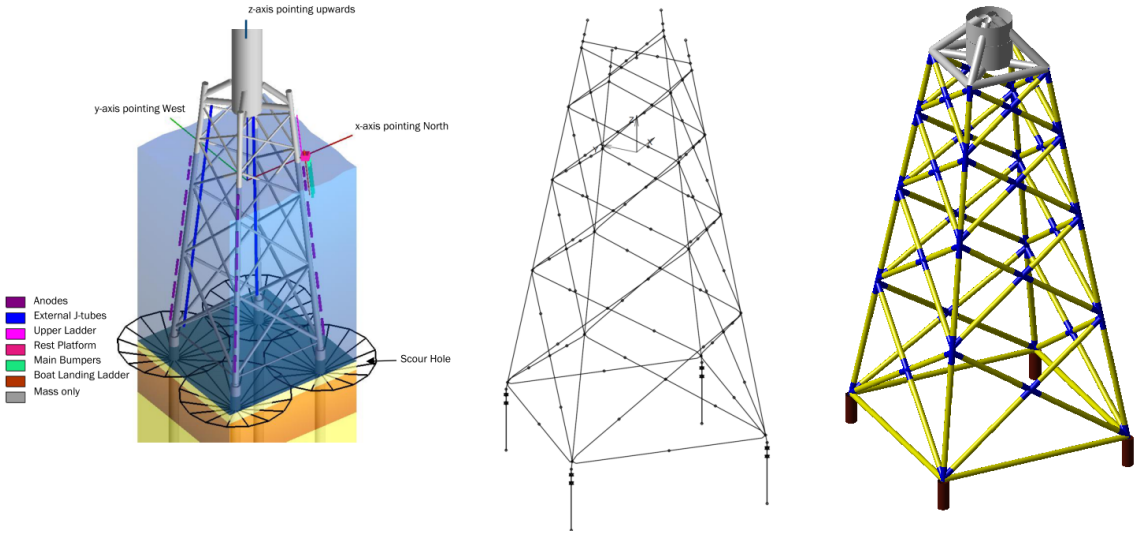

Figure 1.2: The figure shows the INNWIND.EU reference jacket [10] and the interpretation of it in this thesis. Note that only primary steel is modelled. The figure is adopted from Paper V.

companies prefer [59]. Another reason is that the jacket has failed to deliver on cost. Although it uses much less steel than the monopile, it is a complicated design with many welds.

During the past few years, the jacket has been the second most installed foundation, after the monopile [25]. In the Wikinger wind farm, 67 jacket foundations were installed in 2016, accounting for 12 percent of the all the foundations installed that year [67]. An important step towards cheaper jacket designs are mass producible tubular joints. The tubular joint is both the most complex part of the structure to manufacture, as well as the part most prone to failure, due to fatigue in the welds. Some general trends are that automatic welding [54] and weld treatment can be used to improve the fatigue properties of the weld. However, it is still uncertain whether welded nodes, cast nodes, or something else will turn out to be the most cost effective solution [58].

All jackets installed to date are using piled foundations. However, suction buckets are expected to enter the market soon [25]. Suction buckets can be used both for jackets and monopiles, and are more silent to install than piles [25]. This is because they are pulled into the soil by a suction on the inside of the bucket, while piles are driven into the soil by a hammer.

1.5 Mass production of jacket structures

Mass production is a core element of bringing down the cost of any product. In this thesis, mass production of jacket structures is adressed in four different ways.

- **Cost versus complexity:** In Paper I, the four-legged jacket is optimized with varying levels of design complexity. Both the number of sections, and the number of independent design variables in each section was varied. As expected, a higher number of independent variables leads to a lower mass, see Figure 1.3. Lower mass means a reduced raw material costs, and possibly also reduced installation and transportation costs. However, with more complex designs, other costs such as assembly and logistics increase.
- **Validation of models:** In Paper II, the state-of-the-art methods for fatigue constraint design optization of jackets are compared with aeroelastic analysis. It was found that static models are computationally cheap, and therefore useful in conceptual design, while dynamic models can be used to generate final designs.
- **Repeatable designs:** In Paper III, the sensitivity of the jacket design to variations in soil conditions are investigated. The conclusion is that this sensitivity is low for most soil types. This means that one jacket design can be used for all sites with similar water depth, even though soil conditions vary.
- **Discrete variables:** In paper IV, the jacket is optimized with discrete design variables. Instead of letting the variables vary continuously between a lower and upper bound, the diameters and thicknesses are chosen from predefined catalogues. The implication is that the structure can be designed from low-price, off-the-shelf pipes, instead of from tailor-made pipes.

The contribution of these three articles are thus important steps towards design for mass production of jacket structures. The investigations in Paper I can potentially be of assistance to someone who wants to find the ideal design complexity for a mass producible jacket. The validation in Paper II means that the models used in structural optimization are indeed advanced enough to be used for real world design problems. The conclusions from Paper III means that the number of different jacket designs can be kept to a minimum. Finally, the methodology in Paper IV can be used to design jackets from existing parts, instead of having the parts tailor-made.

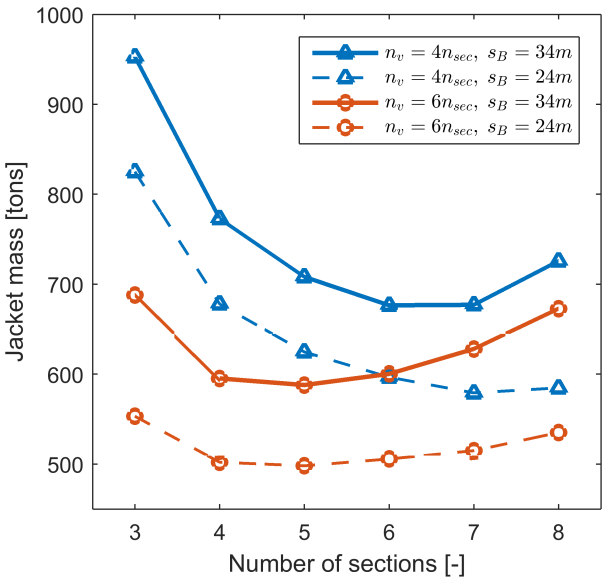

Figure 1.3: The plot shows how the optimized mass for a jacket in 50 meter water depth varies with the number of sections, n_{sec} in the jacket and with the number of independent design varables per section. The top leg distance of the jacket is 14 meters, while the bottom leg distance, s_B, is set to both 24 and 34 meters, where the latter is the same as the INNWIND.EU reference jacket [10]. The plot is adopted from Paper I.

CHAPTER 2
Structural optimization

This chapter contains two brief literature reviews, and then motivates the research contributions in the second part of this thesis. The first review is on structural optimization of frames, as this is the foundation on which gradient-based optimization of support structures is built. The second review considers optimal design of support structures, including gradient-free approaches. Then the optimal design problem is briefly discussed, and related to the papers in the thesis. Finally, research gaps are identified and linked to the publications.

2.1 Review of structural optimization of frames

Numerical structural optimization of frames is an extension of truss optimization, and many of the same methods are challenges are encountered. Therefore this review begins with truss optimization, and then continues with frame optimization.

2.1.1 Truss optimization

Truss optimization is a popular topic, and both topology, sizing and joint position (shape) problems are well studied. A review of truss topology optimization is given in [7], and topology optimization in general is described in [8].

Truss optimization with discrete design variables is a related field, which is of "major practical relevance if the truss must be built from pre-produced bars with given areas" [1]. Using the solution to the continuous problem to find an optimal design in discrete variables, however, is certainly not easy [61]. The mathematical properties of truss optimization with discrete design variables is discussed in [68], and the complexity of finding an optimal solution is emphasized. The segmental method presented in [62] for truss optimization with discrete variables avoids the combinatorial problem, but also gives no guarantee for a global optimal solution. Guaranteed global optimality of truss optimization (topology and sizing) is discussed in [1]. The authors also presents benchmark problems which can be used to evaluate other methods and heuristics. Application of discrete truss optimization to realistic problems is presented for example in [43]. Buckling constraints in truss topology optimization is discussed in [44]. Optimization of trusses including both sizing and joint position variables is applied to practical problems in [51].

2.1.2 Frame optimization

Less discussed than truss optimization, is the extension to structures with beam elements (also known as frames). The difference between truss elements and beam elements is

that the beam element also has bending capacity. Minimum mass of a frame is presented in [52] for continuous design variables, with stress constraints. Euler-Bernoulli and Timoshenko elements are shown to yield different solutions for non-slender beams, which is expected since Timoshenko beams also account for shear stiffness. Frame optimization with emphasis on joint modelling is given in [11, 27]. Optimal design of frame structures for crashworthiness in transient analysis with continuous variables is given in [50].

Gradient based optimization of frames with discrete variables are presented for example in [66]. In this work, the Eurocode building standards has been used to define constraints, thereby making the optimization as close as possible to realistic engineering design. Also, the presented methods can guarantee global optimality.

Optimal design of frames with heuristic methods has been extensively documented in [53]. The heuristic methods can in general be applied to both discrete and continuous problems. Since these methods do not guarantee global optimality, they are often applied to larger problems.

All of the research in this thesis considers gradient based frame optimization, mostly with static loads and continuous design variables. Constraints are inspired by industrial design guidelines, but are generally related to frequency, stress, and displacement constraints. Joints are modelled as rigid, and joint location variables have not been included. However, in Paper I, a brute-force approach is applied, where one hundred jackets with varying leg distances are optimized to investigate the influence of leg distance on optimized mass and natural frequency.

2.2 Review of structural optimization of support structures for offshore wind turbines

Structural optimization of support structures for wind turbines can from a numerical optimization perspective be divided in gradient-free and gradient-based approaches. Due to the very complex analysis tools generally recommended for simulation of offshore wind turbine structures, most researchers have traditionally opted for the gradient-free methods. The gradient-free methods are based on design update schemes such as genetic algorithms [30] or other heuristics [41].

2.2.1 Early work

Early work on design optimization of offshore wind turbine structures [36] emphasized the importance of tailoring wind turbine dynamics to reduce fatigue damage. Whereas support structures today are almost always designed for the soft-stiff frequency range, [37] also considers the possibility of soft-soft monopiles. This is realized by increasing the rotor speed and reducing the pile diameter. An interesting quote from [37], is "Series installation of the soft-stiff monopile with the diameter of 4.7 m and enormous weight of over 350 t is challenging and beyond the capabilities of most contractors". The largest monopile produced in 2016, 15 years later, weighs 1,300 tonnes, have a diameter of 7.8 m, and is over 80m in length [25].

2.2.2 Onshore towers

Optimal design of an onshore wind turbine tower has been presented in [69] using a genetic algorithm. Optimizations of onshore towers have also been presented in [31] with the objective of minimizing energy payback time, and in [64] with the objective of minimizing cost. The latter builds on a long tradition of estimating cost functions for steel structures, but it is unclear whether these earlier cost models can be used for wind turbines [47]. In [2] an onshore truss tower with L-profiles was optimized using a genetic algorithm.

2.2.3 Monopiles

Optimization of an offshore monopile is presented in [63], using a genetic algorithm and uncoupled simulation of wind and wave loads. Integrated optimization of the monopile and tower is performed in [29] with elastic soil springs, including aeroelastic and hydrodynamic modelling. The article [28] describes a method of optimizing a monopile using genetic algorithm together with a finite element analysis where also the soil model is included. Fatigue and structural frequency were found to be design drivers. A multidiciplinary optimization of blades and tower was done in [4, 6], and of tower and layout in [5].

2.2.4 Topology optimization

Topology optimization of a transition piece for a jacket was performed in [38]. The optimization was performed with continuous 3D elements in a commercial software, and then interpreted into a shell structure. Topology optimization of a jacket using genetic algorithm was attempted in [42], where the ground structure approach was used with frame elements. Combined joint-location and sizing optimization of a jacket is demonstrated in [49] with a genetic algorithm. It is argued that this method can also be used for discrete dimensions, but this is not demonstrated. Improvements to this approach is presented in [56], but without the joint location variables.

2.2.5 Jacket optimization with simplified physics

A comprehensive software for structural optimization of jackets is developed at NREL [19, 17]. The software is a module in the Wind-Plant Integrated System Design & Engineering Model toolbox from NREL. The main disadvantage of this software is that it is currently lacking fatigue constraints. The advantage is that the structure is highly parametrized, allowing the user to create many types of parameter studies. In [18] the tool is used for scenario analysis of support structures in the US.

Structural optimization of offshore wind turbine lattice-towers in the fatigue and ultimate limit state were done in [40, 39], and properties such as optimal leg distance was investigated. In these studies, the wind turbine model was approximated, and the frequency domain fatigue calculation proposed in [65] was applied.

2.2.6 Simulation-based jacket optimization

One approach to jacket optimization is the simulation-based, where aero-elastic simulations are used to obtain a structural response which is as realistic as possible. A simulation based iterative design update scheme for a full-height lattice tower was presented in [70]. Here the authors use very short time-domain aero-elastic simulations to estimate the structural response in fatigue and ultimate limit states, and use an iterative scheme to update the designs. The iterative scheme works very well, and the designs converge nicely. However, it is concluded that the very short time-domain simulation is not sufficient to estimate lifetime loads. An extension of this approach is presented in [55], where convexity of the iterative scheme, and the accuracy of the load basis are discussed. Another extension of this work is presented in [57]. In [45] a stochastic search algorithm was used to optimize the dimensions of a full-heigh lattice tower, and some non-intuitive but well-performing designs were obtained.

2.2.7 Gradient-based jacket optimization

From the literature presented, it is observed that gradient-free methods have dominated the field of wind turbine support structure optimization. This is mainly because obtaining function sensitivities of time dependent multidisciplinary analyses is quite involved, and thus not many researchers have attempted the challenging path of gradient-based optimization. Recent developments, however, show a promising future for gradient-based optimization of jackets. Gradient-based structural optimization of a jacket structure using quasi-static analysis and fatigue constraint was presented in [48]. Combining time-domain analysis with gradient-based optimization gives a unique possibility to constrain the fatigue damage. However, quasi-static analysis is not widely accepted for offshore wind turbine structures, due to the many dynamic effects that might influence the structural response.

Gradient-based structural optimization of a jacket structure using dynamic transient analysis was developed in [12, 13, 14, 15]. This combination of dynamic transient analysis and gradient-based optimization is in the authors opinion a leap forward, at least from an optimization perspective.

The main disadvantage with the gradient-based approach compared with the simulation-based optimizations, is that the rotor loads are assumed decoupled from the structural dynamics. Traditionally this has been criticized, arguing that the loads are indeed design dependent [47]. However, recent numerical experiments involving deconvolution of loads using the Duhamel integral has shown very promising results, as shown in Paper II. If the structure can be optimized with predefined loads, that would mean that gradient-based optimization will likely become the state-of-the-art optimization approach for offshore wind turbine structures.

2.2.8 Reliability-based optimization

A relatively unexplored field for offshore wind turbine structures are reliability-based optimization [47]. Although more difficult and time-consuming, it could potentially be a

good approach due to the highly probabilistic nature of offshore wind turbine systems [47]. Reliability-based optimization of offshore towers and jackets are presented in [35, 34].

2.3 Optimal design problem

The general problem adressed in this thesis is

$$\begin{aligned} \underset{\boldsymbol{x}\in\mathbb{R}^m}{\text{minimize}} \quad & f(\boldsymbol{x}) \\ \text{subject to} \quad & \mathbf{A}\boldsymbol{x} \leq \mathbf{b} \\ & g_i(\boldsymbol{x}) \leq 0 \;\; \forall \;\; i = 1, ..., n \\ & \underline{\boldsymbol{x}} \leq \boldsymbol{x} \leq \overline{\boldsymbol{x}}, \end{aligned} \tag{P}$$

which is a nonlinear, constrained optimization problem. The design variable $\boldsymbol{x}$ describes the design of the jacket. More specifically it contains the cross sectional diameters and wall thicknesses of the tubular members in the jacket. The objective function $f(\boldsymbol{x})$ models the mass of the structure, and this mass we would like to minimize. The linear constraints $\mathbf{A}\boldsymbol{x} \leq \mathbf{b}$ and the variable bounds $\underline{\boldsymbol{x}}$ and $\overline{\boldsymbol{x}}$ are imposed to include design and manufacturing limitations. The nonlinear inequality constraints $g_i(\boldsymbol{x}) \leq 0$ contain the structural integrity constraints, and is mostly inspired by rules and guidelines for these types of structures. The design parametrization used in this thesis is illustrated in Figure 2.1.

Analytical sensitivities can be derived for the structural analysis and the structural integrity constraints, such as frequency and stresses. A more elaborate description of the

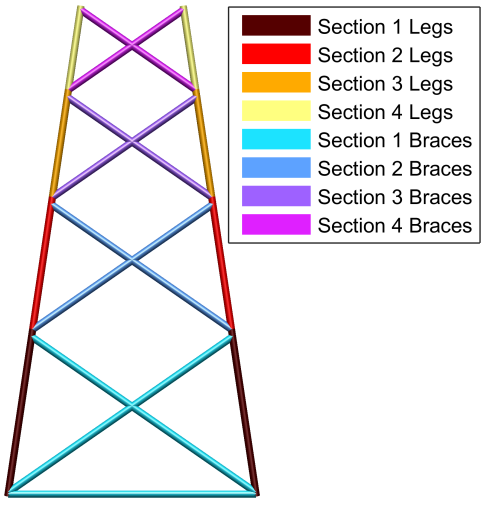

Figure 2.1: The design parametrization used in this thesis is to consider the outer diameter and wall thickness for each of the eight groups shown in the figure, giving a total of 16 design variables. The figure is adopted from Paper IV. Other parametrizations are discussed in Paper I..

optimal design problem as well as design sensitivities are presented in the Paper V of this thesis.

This optimal design problem is the foundation for this thesis. Paper I aims to simplify the structural integrity constraints so that the problem can be solved fast enough to be used in conceptual design. Paper II compares and evaluates three different methods for constraining fatigue, which is perhaps the most challenging structural integrity constraint. Paper III extends (P) to also consider design of piles and suction buckets. Paper IV presents an approach for solving (P) with discrete design variables. Paper V is a theory manual for an analysis and design optimization software which models (P) and interfaces to optimization solvers.

2.4 Static fatigue constraint

A key concept in this thesis is the static fatigue constraint introduced in Paper I. Based on an observation in [60], a weighted combination of tower top damage equivalent loads can be used with relatively good accuracy to design the jacket. The method is therefore applicable in the conceptual design phase. In the following is an explanation of how the fatigue constraint is applied in combination with the damage equivalent load, and how it relates to normal fatigue calculations.

A structure is subjected to one of two loading scenarios over a liftime of n_T seconds.

- Scenario A is a combination of n_s seconds long loads $P^\ell(t)\ \forall\ \ell = 1, \dots, n_\ell$ which are extrapolated to lifetime by c^ℓ such that $\sum_{\ell=1}^{n_\ell} c^\ell n_s = n_T$.
- Scenario B is a harmonic load with a frequency of 1 Hz, and amplitude of ΔP^{1Hz}.

Lifetime fatigue damage at point i is computed by Palmgren-Miners rule

$$D_i^A = \sum_{\ell=1}^{n_\ell} c^\ell \sum_{j=1}^{m} \frac{n_{ij}^\ell}{N_{ij}^\ell}, \qquad \frac{1}{N_{ij}^\ell} = \frac{\left(2\Delta\sigma_{ij}^\ell\right)^m}{\bar{a}} \tag{2.1}$$

$$D_i^B = \frac{n_T}{N_i^{1Hz}}, \qquad \frac{1}{N_i^{1Hz}} = \frac{(2\Delta\sigma_i)^m}{\bar{a}}. \tag{2.2}$$

where n_{ij}^ℓ is the number of cycles at axial stress amplitude $\Delta\sigma_{ij}^\ell$. The material parameters $\bar{a}$ and m relates the stress range $2\Delta\sigma_{ij}^\ell$ to the number of cycles to failure, N_{ij}^ℓ, through the empirically determined SN-curves [22]. Assuming one-degree-of-freedom loading and quasi-static structural response, the stresses scale linearly with the load, $\sigma_i(t) = \alpha_i P(t)$. We set $D_i^B = D_i^A$, and solve for the load amplitude:

$$\frac{n_T \left(\alpha_i \Delta P^{1Hz}\right)^m}{\bar{a}} = \sum_{\ell=1}^{n_\ell} c^\ell \sum_{j=1}^{n_j} \frac{n_j^\ell \left(\alpha_i \Delta P_j^\ell\right)^m}{\bar{a}} \tag{2.3}$$

$$\Rightarrow \Delta P^{1Hz} = \left(\frac{1}{n_T} \sum_{\ell=1}^{n_\ell} c^\ell \sum_{j=1}^{n_j} n_j^\ell \left(\Delta P_j^\ell\right)^m \right)^{\frac{1}{m}}. \tag{2.4}$$

The stress amplitude $\Delta\sigma_i$ from the harmonic load is found as the absolute value of the stress computed when ΔP^{1Hz} is applied as a static load. The fatigue constraint

$$D_i^A = D_i^B = \frac{n_T \left(2|\sigma_i|\right)^m}{\bar{a}} \leq \eta, \tag{2.5}$$

where η is the utilization factor, can thus be reformulated to a stress constraint under the static load $P = \Delta P^{1Hz}$

$$-\left(\frac{\eta\bar{a}}{n_T}\right)^{\frac{1}{m}} \leq \sigma_i \leq \left(\frac{\eta\bar{a}}{n_T}\right)^{\frac{1}{m}}. \tag{2.6}$$

Note that the static fatigue constraint assumes one-degree-of-freedom-loading and quasi-static structural response, but that based on the observations and specific methodology in [60], good results are also achieved for the jacket support structure. This is further studied in Paper II in this thesis, where the static fatigue constraint is compared with time-domain fatigue calculations using qusi-static as well as dynamic analysis.

2.5 Research gaps and motivation of publications

The objective of this section is to identify gaps in the research field, and motivate the research contributions of this thesis. Focus of the motivation is more on application to real world problems than to solving fundamental theoretical problems.

2.5.1 Conceptual design

Structural optimization is an excellent tool for conceptual design because it can deal with many design variables and constraints and automatically identify favourable feasible solutions. However, in structural optimization of jackets, the state-of-the-art methods are very computationally expensive, and can require days of computations for sizing the members of a singe jacket. In the conceptual design phase it would be advantageous to use a less accurate but much faster approach.

This research gap is adressed in Paper I, where an optimal design problem for conceptual design is presented.

2.5.2 Validation of models

All gradient-based methods for optimal design of jackets use some sort of simplification in the analysis models. However, none of the methods have validated or evaluated their analysis models against state-of-the-art analysis models. A common simplification is for example to use precalculated rotor loads. Whether this can provide acceptable accuracy in the analysis has been a topic for discussion, even though it is not uncommen in industrial projects.

This research gap is adressed in Paper II, where optimized designs from three state-of-the-art optimization methods for jackets are evaluated with aero-elastic simulations.

2.5.3 Interfacing components

The jacket is only a subcomponent of the offshore wind turbine support structure, and the design of different subcomponents are likely to influence each other. Identifying interaction effects between the design of the jacket, and the design of for example the transition piece or the foundation could therefore lead to a better understanding of the global design.

This research gap is adressed in Paper III, where integrated design of jacket and foundation is adressed. Figure 2.2 from Paper II shows how the structural frequency is a function of both jacket leg distance and soil stiffness.

2.5.4 Discrete variables

The practical problem of designing a jacket for mass production is perhaps not subjected to continuous design variables, but discrete. This is because it might be cheaper to pick steel pipes from a predefined catalogue than to have each pipe profile tailor made.

This reesearch gap is adressed in Paper IV, where the problem from Paper I is solved with discrete design variables.

2.5.5 Software

One of the bottlenecks stopping structural optimization of jackets to spread into industry is the lack of appropriate software. Most research codes are developed to adress one specific research challenge. An important part of making research beneficial to society, is the right form of dissemination. For structural optimization to be applied and have a positive impact, it needs to be implemented in user-friendly software which practicing engineers can make use of without too much education or prior knowledge.

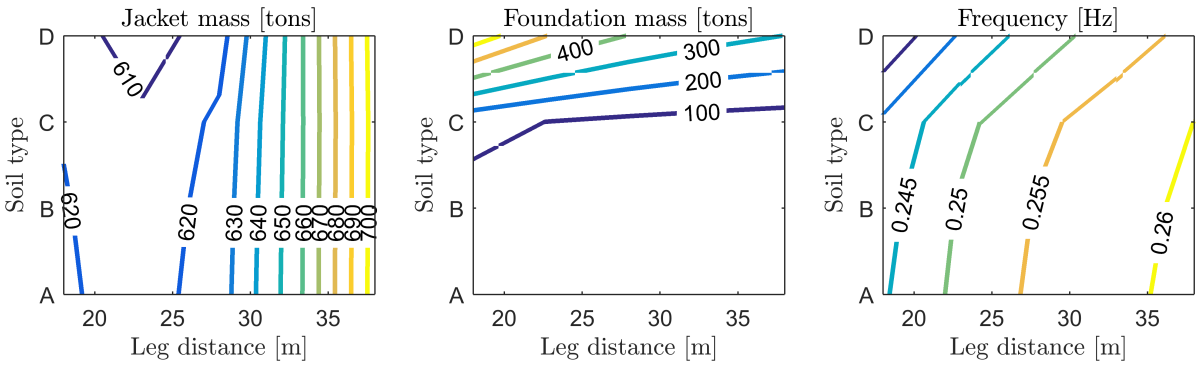

Figure 2.2: Influence of bottom leg distance and soil stiffness on the first natural frequency of the offshore wind turbine on a jacket substructure with suction caisson foundation. "A" is the stiffest soil. Figure adopted from Paper III.

This industrial adoptation gap is adressed in Publication V, which is a theory manual for the JAcket Design OPtimization (JADOP) software developed during this PhD project.

CHAPTER 3

Conclusions

The most important conclusions and contributions of this thesis are presented in this chapter along with suggestions for future research directions. This thesis describes work done in the field of structural optimization of frame structures, with emphasis on application to the offshore wind turbine jacket support structure. The resulting design tool includes several state-of-the-art design approaches, and has been extended towards foundation design and discrete optimization.

This chapter is organized as follows. A summary of the results obtained in each individual publication is presented next in Section 3.1. The main contributions and impact of the research presented in this thesis is subsequently outlined in Section 3.2. Finally, in Section 3.3, several directions for future research are suggested.

3.1 Summary of the results

The most important results and conclusions from each of the publications are summarized here. The PhD candidate is the first author of Paper I, Paper III, and Paper V, and the second author of Paper II and Paper IV. At the date of submission of this thesis, Paper I and Paper II are submitted to peer-reviewed international journals. Paper III and Paper IV are scheduled to be submitted to peer-reviewed international journals in August/September 2017, and Paper V is scheduled to be submitted as a technical report at DTU Wind Energy in September/October 2017.

Paper I: Conceptual optimal design of jacket structures

This paper focuses on sizing optimization of jacket structures. The jacket is modelled with Timoshenko beam finite elements, and the outer diameter and wall thickness of the thin-walled circular cross sections are chosen as design variables. Damage equivalent loads are used to approximate the fatigue damage in the structure, following recommendations for conceptual design. The optimal design problem is formulated with seven static load cases, and includes constraints on both fatigue and ultimate limit states. The resulting optimal designs look realistic, and the impact of higher or lower design freedom (number of independent cross sections in the structure) is investigated. Although the optimal design problem only considers sizing of cross sections, a study of optimal leg distance is performed by optimizing one hundred jackets with varying leg distance. The main results are that by increasing the number of independent cross sections, for example by reinforcing the joints, a mass reduction of 23 percent can be achieved. Furthermore it was found that by decreasing the leg distance from 34 meters in the reference design to 24 meters, and by increasing the number of sections from four in the reference design to

five, an additional 17 percent mass reduction could be achieved.

Remarks This paper presents the core work of this thesis. The presented design tool, JADOP, includes a parameterized mesh, structural analysis, and many constraints. The following papers make use of everything presented herein. Details which did not fit into this article are thouroughly explained in Paper V.

Paper II: On analytical gradient-based optimization of jacket structures for offshore wind turbines

This paper focuses on comparing three state-of-the-art approaches to fatigue constraints in sizing optimization of jacket structures. All three methods use gradient-based optimization, but the analysis required to compute the fatigue constraints are based on static, quasi-static, and dynamic load simulations, respectively. The three methods are implemented in the same optimization framework, and applied to the same optimization problem. The optimized designs are then exported to an aeroelastic software for a realistic evaluation of the fatigue damage. The results show that while all three approaches converge to relatively similar designs, the dynamic method is the most accurate. This is mainly because the static and quasi-static analyses do not capture all the vibrations, espacially at the first natural frequency of the structure. It is concluded that the dynamic optimization approach can produce designs that are ready to be used, while the static and quasi-static methods are more suitable at a conceptual design stage.

Remarks This paper compares the method from Paper I with the state-of-the art alternative formulations. Since the two other methods are implemented in JADOP, this improves the possibilities of this software.

Paper III: Integrated optimal design of jackets and foundations

This paper proposes an approach for integrated design of jackets and foundations. Such an approach takes into account both global design requirements, as well as local design requirements in the jacket and the foundation respectively. The aim of this paper is to investigate the interraction effects between the jacket design and the foundation design, and to establish how much there is to gain from an integrated design approach. Six differente design procedures are implemented as nonlinear constraints, covering both piles and suction buckets in both clay and sand soils. The results indicate that the foundation design depend highly on the jacket design, while the jacket design is relatively independent on the foundation design. This is because the design driver in most cases were found to be the pull-out forcec on the pile, which depends directly on the jacket mass. The design driver for the jacket is mostly fatigue, which did not depend on the foundation.

Remarks This paper extends the model presented in Paper I to also account for foundation models and foundation design. It is concluded that the jacket design is not

dependent on the foundation design (at least not for the conditions examined), which means that the clamped-at-seabed-assumption used in Paper I, II and IV is valid.

Paper IV: Structural optimization with several discrete variables per part

This paper proposes a method for optimal design of structures with discrete design variables. The structure is assumed to be assembled by parts, where each part has several design variables associated with it. These design variables are then to be chosen from a discrete catalogue. The motivation for this design parametrization is that it is suitable for many industrial problems. It also allows for new types of objective and constraint functions which cannot be modelled if the variables are continuous or only one variable is associated with each part. The method proposed to solve the problem is based on the concept of outer approximation, and the problem to be solved is modelled as a mixed 0–1 nonlinear problem with nonconvex continuous relaxations. The method is used to minimize the mass of a jacket structure with constraints on frequency, strength, and fatigue lifetime.

Remarks This paper solves the jacket sizing problem from Paper I with discrete variables. It also outlines which possibilities this includes, such as modular design, and more realistic cost and constraint functions.

Paper V: JADOP - JAcket Design OPtimization

This paper is a documentation of the software package JADOP, which has been developed during this PhD project. The two-noded Timoshenko beam element is described, and the static and dynamic finite element analysis is derived from the principle of virtual work. Stresses in tubular welds are computed by stress concentration factors which are incorporated into the strain displacement matrix. The design parametrization and optimal design problem are presented, along with sensitivity analysis of relevant functions. Nested and simultaneous analysis and design (SAND) are both implemented and explained. A parametric offshore wind turbine structural mesh is used to interprete structures from the literature, and the static and dynamic analyses are validated with commercial finite element software.

Remarks The documentation describes the software package used in Paper I, II, III, and IV. JADOP has been developed not only by the PhD student, and a summary of contributions is included at the end of the documentation. This documentation is still in development.

3.2 Contributions and impact

The main contributions of this thesis are the proposed methods for optimal design of jacket structures. Although the methods can be applied to other types of frame structures as

well, this thesis contributes with specific constraints, design parametrizations, validation, and extensions, demonstrating that structural optimization can be a valuable tool for real world offshore wind turbine jacket design problems.

The contributions according to each individual paper are as follows. Paper I concerns conceptual design of jacket structures. The presented method automates the conceptual design using numerical optimization with both fatigue and ultimalte limit state constraints. It is demonstrated how this method together with a parametrized mesh can be used to very quickly explore a large design space, and find not only optimal cross sectional dimensions, but also favourable leg distance and number of sections. The impact of this method is that conceptual jacket design can become more analysis-based instead of experience-based, and potentially lead to significant cost reductions. Paper II concerns the accuracy of state-of-the-art gradient-based optimization methods for jackets. The new knowlegde presented here allows designers to better understand the available tools, and their limitations. The impact of this should be that all optimization approaches dealing with final designs should use a dynamic analysis, while the methods for conceptual design should consider computationally cheaper methods such as a static analysis. Paper III demonstrates that not only jacket design, but also foundation design can be automated using structural optimization. The impact of this is that the foundation and the jacket can be designed simultaneously, reducing the number of design iterations between the jacket designer and the foundation designer. Paper IV concerns discrete variables, and it is shown that this is in fact very possible to solve, even for very large catalogues of available dimensions. The impact of this is that the number of different dimensions can be constrained, which is an important step towards mass producible designs.

3.3 Future work

This section presents several future research topics which can either be a direct continuation of the work in this thesis, or which can use this thesis as a starting/reference point.

Interfaces: Clear interfaces and data formats for exhanging informations between optimization and analysis software would improve the useability of optimization in the design flow. This could lead to more integrated design processes, and enable research on optimal design flow. One could for example envision a flow where new information is added to the optimization problem as the design process moves from conceptual to basic to detailed design.

Weld modelling: Current models of the tubular joints in the jacket structure assumes conservative stress concentration factors developed several decades ago. As industry adopts more advanced materials and welding techniques, as well as weld-treatments, significantly better fatigue properties can be achieved. This should of course also be modelled in the optimization problem.

Bolt modelling: Some of the welded connections in the jacket could possibly be replaced

by bolted connections. This could reduce the stress concentrations, and thus reduce the mass of the structure. It could also simplify the assembly, as fastening bolts is faster and easier than welding.

Other joint types: The joint type assumed in this thesis is the welded tubular joint. However, it is also possible to create cast nodes or forged nodes, or use a different material. One research idea could be topology or shape optimization of cast/forged joints for minimum stress concentrations. Another one could be composite design of joints for high strength and high flexibility. The advantage of high flexibility is that it would reduce the stresses in the tubular members.

All-in-one: A realistic design optimization of jacket structures must take many aspects into account. First of all the loads need to be realistic. Second, all structural integrity constraints must be properly modelled, which implies that the analysis must be sufficiently accurate and that the ultimate limit state must be controlled at every time step in every part of the structure.

Support structure: The work in this thesis is focused on the jacket substructure, and partly also the foundation. Future work should aim at including also the transition piece and the tower in the design approach. This is especially advantageous when it comes to tailoring the natural frequency, which becomes more and more difficult with increasing turbine size.

Frequency domain: Frequency domain analysis can be a very effective tool for obtaining the structural response. While it is not as accurate as dynamic analysis, it can probably be comparable to damage equivalent static loads. That makes it an interesting tool for structural optimization in the conceptual design phase.

Floating support structures: A very interesting extension of the work in this thesis would be optimal design of support structures for floating offshore wind turbines. This is an intrinsically more difficult modelling task, as the hydrodynamic interaction is much more complex, and because the boundary condition can not be assumed rigid. In addition, the large displacements of the floating structure probably calls for multibody dynamics. However, the cost comes with a gain. Designs of floating structures are much less matured than the jacket design, and thus inspire more conceptual design. The choice of design parametrization is in no way given, and one can envision both topology, sizing, and shape optimization problems, as well as multiple interesting objective and constraint functions. One of the main objectives in design of floating structures is the minimization of the maximum acceleration at the nacelle. This is an obvious task for structural optimization, if only the modelling can be appropriately handled in an optimization framework.

Bibliography

[1] W. Achtziger and M. Stolpe. Truss topology optimization with discrete design variables — Guaranteed global optimality and benchmark examples. *Structural and Multidisciplinary Optimization*, 34:1–20, 2007.

[2] P. Américo, A. Magalhães, I. G. Rios, T. Simão, F. Pedro, H. Deogene, D. D. E. Mecânica, P. Universidade, C. D. Minas, and A. D. Jose. Design of Lattice Wind Turbine Towers With Structural Optimization. *Int. Journal of Engineering Research and Applications*, 4(8):38–51, 2014.

[3] API. Geotechnical and foundation design considerations. ANSI/API RP 2GEO 1st edition Petroleum and natural gas industries: Specific requirements for offshore structures, Part 4. Technical report, American Petroleum Institute, 2011.

[4] T. Ashuri. *Beyond Classical Upscaling : Integrated Aeroservoelastic Design and Optimization of Large Offshore Wind Turbines*. PhD thesis, Technische Universiteit Delft, 2012.

[5] T. Ashuri. Integrated Layout and Support Structure Optimization for Offshore Wind Farm Design. *Journal of Physics: Conference Series*, 753:092011, 2016.

[6] T. Ashuri, M. B. Zaaijer, J. R. R. A. Martins, G. J. W. van Bussel, and G. A. M. van Kuik. Multidisciplinary design optimization of offshore wind turbines for minimum levelized cost of energy. *Renewable Energy*, 68:893–905, 2014.

[7] M. P. Bendsøe, A. Ben-Tal, and J. Zowe. Optimization methods for truss geometry and topology design. *Structural Optimization*, 7:141–159, 1994.

[8] M. P. Bendsøe and O. Sigmund. *Topology Optimization - Theory, Methods and Applications*. Springer, second edition, 2004.

[9] BHS. The Bundesamt für Seeschifffahrt und Hydrographie (Federal Maritime and Hydrographic Agency), 2017.

[10] T. Borstel. Design report - reference jacket. Technical Report D4.3.1, INNWIND.EU, 2013.

[11] T. M. Cameron, A. C. Thirunavukarasu, and M. E. M. El-Sayed. Optimization of frame structures with flexible joints. *Structural and Multidisciplinary Optimization*, 19(3):204–213, 2000.

[12] K. H. Chew. Optimization of offshore wind turbine support structures using analytical gradient-based method. Technical report, Norwegian University of Science and Technology, Trondheim, 2015.

[13] K. H. Chew, M. Muskulus, K. Tai, and E. Y. K. Ng. Fatigue Sensitivity Analysis of Offshore Wind Turbine Structures. In *11th World Congress on Structural and Multidisciplinary Optimization*, 2015.

[14] K.-H. Chew, K. Tai, and E. Ng. Optimization of Offshore Wind Turbine Support Structures Using an Analytical Gradient-based Method. *Energy Procedia*, 80:100–107, 2015.

[15] K.-H. Chew, K. Tai, E. Ng, and M. Muskulus. Analytical gradient-based optimization of offshore wind turbine substructures under fatigue and extreme loads. *Marine Structures*, 47:23–41, may 2016.

[16] R. D. Cook, D. S. Malkus, M. E. Plesha, and R. J. Witt. *Concepts and Applications of Finite Element Analysis*. John Wiley & Sons, fourth edition, 2007.

[17] R. Damiani. JacketSE : An Offshore Wind Turbine Jacket Sizing Tool Theory Manual and Sample Usage with Preliminary Validation. Technical Report NREL/TP-5000-65417, National Renewable Energy Laboratory (NREL), 2016.

[18] R. Damiani, A. Ning, B. Maples, A. Smith, and K. Dykes. Scenario analysis for techno-economic model development of U.S. offshore wind support structures. *Wind Energy*, 20(4):731–747, 2017.

[19] R. Damiani and H. Song. A Jacket Sizing Tool for Offshore Wind Turbines within the Systems Engineering Initiative. In *Offshore Technology Conference*, page OTC 24140, Houston, 2013. Offshore Technology Conference.

[20] W. de Vries. Final report WP 4 . 2 Support Structure Concepts for Deep Water Sites. Technical report, Delft University of Technology, 2011.

[21] DNV. DNV-OS-J101 Design of Offshore Wind Turbine Structures. Technical report, DNV, 2011.

[22] DNVGL. RP-C203 Fatigue design of offshore steel structures. Technical report, DNVGL, 2014.

[23] DNVGL. OS-C101 Design of Offshore Steel Structures, general - LRFD method. Technical Report July, DNVGL, 2015.

[24] DNVGL. DNVGL-ST-0126 : Support structures for wind turbines. Technical report, DNVGL, 2016.

[25] ETIP. Strategic research and innovation agenda 2016. Technical report, European Technology and Innovation Platform on Wind Energy, 2016.

[26] B. Foley. Inward Battered Guide Structure the “Twisted Jacket”. Technical report, Keystone engineering inc., 2016.

[27] H. Fredricson, T. Johansen, A. Klarbring, and J. Petersson. Topology optimization of frame structures with flexible joints. *Structural and Multidisciplinary Optimization*, 25(3):199–214, 2003.

[28] T. Gentils, L. Wang, and A. Kolios. Integrated structural optimisation of offshore wind turbine support structures based on finite element analysis and genetic algorithm. *Applied Energy*, 199:187–204, 2017.

[29] R. Haghi, T. Ashuri, P. L. C. van der Valk, and D. P. Molenaar. Integrated Multidisciplinary Constrained Optimization of Offshore Support Structures. *Journal of Physics: Conference Series 555*, page 012046, 2014.

[30] J. H. Holland. Genetic Algorithms. *Scientific American*, 267(1):66–72, 1992.

[31] C. Horgan. Using energy payback time to optimise onshore and offshore wind turbine foundations. *Renewable Energy*, 53:287–298, 2013.

[32] IEC. IEC 61400-3: Wind turbines - Part 3: Design requirements for offshore wind turbines. Technical Report 300 V, IEC, 2009.

[33] IRENA. Series, Renewable Energy Technologies: Cost Analysis Wind Power. Technical Report 5, International Renewable Energy Agency, 2012.

[34] H. Karadeniz, V. Togan, A. Daloglu, and T. Vrouwenvelder. Reliability-based optimisation of offshore jacket-type structures with an integrated-algorithms system. *Ships and Offshore Structures*, 5(1):67–74, mar 2010.

[35] H. Karadeniz, V. Togan, and T. Vrouwenvelder. An integrated reliability-based design optimization of offshore towers. *Reliability Engineering and System Safety*, 94(10):1510–1516, 2009.

[36] M. Kühn. Design optimization of an offshore wind energy converter by means of tailored dynamics. In *European Wind Energy Conference and Exhibition*, number Ewec 99, pages 1–4, Nice, 1999. European Wind Energy Conference and Exhibition.

[37] M. J. Kuhn. *Dynamics and design optimisation of offshore wind energy conversion systems*. PhD thesis, Delft University, 2001.

[38] Y.-S. Lee, J. A. Gonzalez, J. Hyun, Y. Il, K. C. Park, and Y.-s. Lee. Structural topology optimization of the transition piece for an offshore wind turbine with jacket foundation. *Renewable Energy*, 85:1214–1225, 2016.

[39] H. Long and G. Moe. Preliminary Design of Bottom-Fixed Lattice Offshore Wind Turbine Towers in the Fatigue Limit State by the Frequency Domain Method. *Journal of Offshore Mechanics and Arctic Engineering*, 134(3):031902, 2012.

[40] H. Long, G. Moe, and T. Fischer. Lattice Towers for Bottom-Fixed Offshore Wind Turbines in the Ultimate Limit State: Variation of Some Geometric Parameters. *Journal of Offshore Mechanics and Arctic Engineering*, 134(2):021202, 2012.

[41] D. G. Maringer. Heuristic Optimization. In *Portfolio Management with Heuristic Optimization*, chapter 2, pages 38–76. Springer, 2005.

[42] J. H. Martens, D. Zwick, and M. Muskulus. Topology Optimization of a Jacket Structure for an Offshore Wind Turbine with a Genetic Algorithm. In *11th World Congress on Structural and Multidisciplinary Optimization*, Sydney, 2015.

[43] K. Mela. *Mixed Variable Formulations for Truss Topology Optimization*. PhD thesis, Tampere University of Technology, 2013.

[44] K. Mela. Resolving issues with member buckling in truss topology optimization using a mixed variable approach. *Structural and Multidisciplinary Optimization*, 50(6):1037–1049, 2014.

[45] H. Molde. Simulation-based optimization of lattice support structures for offshore wind energy converters with the simultaneous perturbation algorithm. *Journal of Physics: Conference Series 555*, 2014.

[46] M. Muskulus. Why design load calculations for offshore wind turbine support structures cannot use load time series from moving rotors. In *Proceedings of the 25th International Ocean and Polar Engineering Conference*, pages 525–29, 2015.

[47] M. Muskulus and S. Schafhirt. Design Optimization of Wind Turbine Support Structures – A Review. *Journal of Ocean and Wind Energy*, 1(1):12–22, 2014.

[48] J. Oest, R. Sørensen, L. C. T. Overgaard, and E. Lund. Structural optimization with fatigue and ultimate limit constraints of jacket structures for large offshore wind turbines. *Structural and Multidisciplinary Optimization*, 55(3):779793, 2017.

[49] L. Pasamontes, F. G. Torres, D. Zwick, S. Schafhirt, and M. Muskulus. Support structure optimization for offshore wind. In *Proceedings of the ASME 2014 33rd International Conference on Ocean, Offshore and Arctic Engineering*, pages 1–7, San Francisco, 2014. The American Society of Mechanical Engineers (ASME).

[50] C. B. W. Pedersen. Crashworthiness design of transient frame structures using topology optimization. *Computer Methods in Applied Mechanics and Engineering*, 193(6-8):653–678, 2004.

[51] N. Pedersen and a.K. Nielsen. Optimization of practical trusses with constraints on eigenfrequencies, displacements, stresses, and buckling. *Structural and Multidisciplinary Optimization*, 25(5-6):436–445, dec 2003.

[52] P. Pedersen and L. Jørgensen. Minimum mass design of elastic frames subjected to multiple load cases. *Computers and Structures*, 18(1):147–157, 1984.

[53] M. P. Saka. Optimum Design of Steel Frames using Stochastic Search Techniques Based on Natural Phenomena : A Review Optimum Design of Steel Frames Using Stochastic Search. In B. H. V. Topping, editor, *Civil Engineering Computations: Tools and Techniques*, chapter 6, pages 105–147. Saxe-Coburg Publications, Glasgow, first edition, 2007.

[54] Salzgitter Mannesmann Forschung GmbH. Automated welding technology, 2017.

[55] K. Sandal. Convex optimization of space frame support structures for offshore wind turbines. *10th PhD Seminar on Wind Energy in Europe*, 2014.

[56] S. Schafhirt, D. Zwick, and M. Muskulus. Reanalysis of jacket support structure for computer-aided optimization of offshore wind turbines with a genetic algorithm. *Journal of Ocean and Wind Energy*, 1(4):209–216, 2014.

[57] S. Schafhirt, D. Zwick, and M. Muskulus. Two-stage local optimization of lattice type support structures for offshore wind turbines. *Ocean Engineering*, 117:163–173, 2016.

[58] M. Seidel. Jacket substructures for the REpower 5M wind turbine. In *Conference Proceedings European Offshore Wind 2007*, 2007.

[59] M. Seidel. Substructures for offshore wind turbines Current trends and developments. *Festschrift Peter Schaumann*, 2014.

[60] M. Seidel, S. Voormeeren, and J. van der Steen. State-of-the-art design processes for offshore wind turbine support structures. *Stahlbau*, 85(9):583–590, 2016.

[61] A. B. Templeman. Discrete optimum structural design. *Computers and Structures*, 30(3):511–518, 1988.

[62] A. B. Templeman and D. F. Yates. a Segmental Method for the Discrete Optimum Design of Structures. *Engineering Optimization*, 6(3):145–155, 1983.

[63] A. Thiry, F. Bair, L. Buldgen, B. G. Raboni, and P. Rigo. Optimization of monopile offshore wind structures. *Advanced Marine Structures*, pages 633–642, 2011.

[64] P. Uys, J. Farkas, K. Jármai, and F. van Tonder. Optimisation of a steel tower for a wind turbine structure. *Engineering Structures*, 29(7):1337–1342, jul 2007.

[65] J. van der Tempel. *Design of Support Structures for Offshore Wind Turbines*. PhD thesis, Technische Universiteit Delft, 2006.

[66] R. Van Mellaert. *Optimal design of steel structures according to the Eurocodes using mixed-integer linear programming methods*. PhD thesis, KU Leuven, 2017.

[67] WindEurope. The European offshore wind industry - Key trends and statistics 2016. Technical Report January, WindEurope, 2017.

[68] D. F. Yates, A. B. Templeman, and T. B. Boffey. The complexity of procedures for determining minimum weight trusses with discrete member sizes. *International Journal of Solids and Structures*, 18(6):487–495, 1982.

[69] S. Yoshida. Wind turbine tower optimization method using a genetic algorithm. *Wind Engineering*, 30(6):453–469, 2006.

[70] D. Zwick, M. Muskulus, and G. Moe. Iterative optimization approach for the design of full-height lattice towers for offshore wind turbines. *Energy Procedia*, 24(January):297–304, 2012.

Part II

Manuscripts

Paper I

K. Sandal, A. Verbart, M. Stolpe, Conceptual optimal design of jacket structures. Submitted to *Wind Energy*, under review.

WIND ENERGY
Wind Energ. 2010; **00**:1–14
DOI: 10.1002/we

RESEARCH ARTICLE

Conceptual optimal design of jacket structures

Kasper Sandal, Alexander Verbart, Mathias Stolpe

DTU Wind Energy, Frederiksborgvej 399, 4000 Roskilde, Denmark

ABSTRACT

We present an approach for sizing optimization of jacket structures, and apply it to investigate the conceptual design of jackets for offshore wind turbines. Conceptual design is an input to early structural and financial models, and is not based on integrated load analysis. A four-legged jacket for the DTU 10 MW wind turbine in 50 meter water depth is modelled by Timoshenko beam finite elements, and the structural dimensions of the beam cross sections are considered as continuous design variables. A structural optimization problem is formulated to minimize the jacket mass, with constraints on fatigue and ultimate limit states. The optimal design problem is then used to investigate how the optimized mass depends on the jacket leg distance, the number of sections, and the number of independent design variables. Results show that reinforcing joints with stubs and cans can reduce the jacket mass with 22 percent. The conceptual design investigation also shows that the legs should be almost vertical, and with at least four levels of X-braces. We conclude that structural optimization can provide useful insights in the conceptual design phase and lead to a better starting point for the further design and planning processes.

KEYWORDS

Structural optimization; Offshore wind turbines; Jacket support structures; Fatigue; Numerical optimization; Static structural analysis.

Correspondence

Kasper Sandal, DTU Wind Energy, Frederiksborgvej 399, 4000 Roskilde, Denmark.

Received . . .

1. INTRODUCTION

There is high pressure on the offshore wind industry to reduce the levelized cost of energy, and cheaper support structures have been identified as one of the major cost reduction potentials [31]. One type of support structure is the jacket, which is very stiff, transparent to waves, and can be installed with limited harm to the oceanic environment [24]. In this paper we present a numerical structural optimization approach which designs the primary steel of a jacket structure, and demonstrate that the method can be used in a conceptual design phase. The conceptual design phase is where an integrated load analysis is not necessarily available, but important design decisions have to be given as an input to early structural and financial models [29].

Structural optimization is a set of techniques which have aided auto and aerospace industries in decades, and is increasingly being applied to wind energy and offshore structures [13]. The benefit of structural optimization is that it explores a large design space in a short time, and thereby can often find better designs than a human engineer on his own [22]. To the authors knowledge, all published efforts on design optimization of jackets for wind turbines are based on frame structure modelling and analysis with beam finite elements, see e.g. [10, 23]. The advantage of the beam element is that it can model the structural response of a jacket with a relatively low number of elements and degrees of freedom compared to shell or solid elements. The disadvantage is that e.g. welding stresses are not accurately captured.

Numerical structural optimization of frame structures dates back to as early as the 1960s. More recent articles proposing sizing optimization of frames under Timoshenko beam assumptions are e.g. [26, 9]. An important application related to the automotive industry is optimal design of frames for crash-worthiness. An approach for this application based on topology optimization is presented in [25]. Common for the above mentioned articles is that they rely on nested analysis and design formulations, i.e. computations of the response requires one or several calls to a finite element solver at every optimization iteration.

Simultaneous Analysis and Design (SAND), see e.g. [16] and the review article [4] and the references therein, is an increasingly popular approach for modelling and solving structural optimization problems. With this approach both the design variables and the state variables are included in the optimization problem and the governing equations are explicitly stated as constraints. The problems increase in size compared to the classical nested formulations, but the sensitivity analysis becomes simplified, even to the point that second order sensitivity analysis can be provided, and for problems with expensive analysis SAND can be advantageous. SAND formulations are also the main reason that many structural optimization problems with discrete design variables can be reformulated as convex mixed 0-1 problems, see e.g. [15] and [30]. A recent and comprehensive comparison of models, including SAND and nested formulations, and numerical optimization methods for structural topology optimization is presented in [27].

Design optimization of jackets is an application of frame optimization with some specific challenges. These challenges, and recommendations for future developments, are summarized in the review article [22]. The challenges are e.g. fatigue as design driver, the need for specialized analysis software, and that a jacket structure has many design variables and constraints. Of the recommendations mentioned in [22], this paper specifically deals with gradient-based optimization and demonstration of cost reduction potential.

A central challenge in design optimization of wind turbine support structures is to model the fatigue response in a manner such that simulations are fast while also sufficiently accurate. The most accurate is to run coupled aero-servo-hydro-elastic simulations in the time domain for multiple hours, and extrapolate the response to lifetime. This approach was used for gradient-free optimization in [28]. A common, but less accurate approach is to use a decoupled model, where the rotor loads are extracted from an aero-servo-elastic tool, and subsequently applied to the structure. This approach was used for gradient-based optimization in [23] for a quasi-static analysis, and in [10] for a dynamic analysis. The two last approaches are frequency domain analysis, which was used in [18] with a gradient-free optimization, and static load approaches.

This paper differs from the recent works [10, 23, 28] in two important ways. First, the applied load in the optimal design problem is a small set of static loads, and not a transient load. As a transient load basis typically requires analysis and sensitivity analysis at hundreds of thousands of time steps, a static load basis of less than ten load cases will make the optimization run four to five orders of magnitude faster, depending on the implementation. Second, the result is design trends, and not a final design. The idea is that the method presented in this paper is used to guide the designer in early design decisions such as leg distance and number of sections. When these parameters are specified, a more accurate design optimization can be performed to find the final design. The scope of this paper is therefore more similar to the work in [19, 18, 12], but with a clearly defined optimal design problem, and fatigue constraints. The motivation for using gradient-based optimization, rather than gradient-free methods such as genetic algorithm [17] or other meta heuristic methods [20] to update the variables, is that the gradient-based optimization generally requires fewer function calls and can easily deal with a large number of design variables and constraints.

The design problem for sizing optimization of a jacket can be summarized as finding the cross section dimensions of all the steel members in the jacket which minimizes the primary steel mass, subject to fatigue and ultimate limit state constraints. In this paper we formulate the optimal design problem for jackets in the SAND formulation with multiple static load cases and a new fatigue constraint based on damage equivalent load. Furthermore, the optimal design problem is used to investigate the influence of leg distance on the mass and natural frequencies of the full structure.

In the next section, the analysis model and the optimal design problem are explained, as well as some of the constraints and sensitivities. In the results section follows some numerical examples which demonstrate how the presented optimal design problem can be used to generate conceptual designs and investigate design trends. The article ends with a conclusion and suggestions for future work.

2. ANALYSIS AND DESIGN MODELS

This section describes the structural design and analysis models and presents the optimal design problem which uses the simultaneous analysis and design formulation. Then the sensitivity of stress and frequency constraints are given, and the fatigue and ultimate limit constraints are explained. At last the implementation details are presented briefly.

2.1. Model and design parametrization

We consider a frame structure with thin-walled tubular members and apply sizing optimization on outer diameter and wall thickness of the members. There is a limited design freedom, and the design vector $\mathbf{x} = (\mathbf{d}, \mathbf{t}) \in \mathbb{R}^{2n}$ has many linked variables. The variable linking is controlled by the Boolean matrix $\mathbf{B} \in \mathbb{Z}^{2n \times n_v}$, such that $\mathbf{x} = \mathbf{B}\mathbf{v}$. Here n is the number of design elements, and n_v is the number of independent design variables. The independent design variables $\mathbf{v} \in \mathbb{R}^{n_v}$ is used in the optimal design problem, and can vary in size from 2, where all members have the same diameter and thickness, to $2n$, where all design elements have independent diameters and thickness. Displacement vectors $\mathbf{u}^\ell \in \mathbb{R}^d$ are considered

Wind Energ. 2010; **00**:1–14 © 2010 John Wiley & Sons, Ltd.
DOI: 10.1002/we
Prepared using weauth.cls

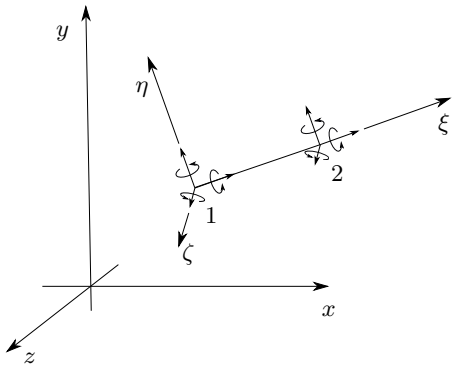

Figure 1. A 3D beam element with global coordinate system (x, y, z), and local coordinate system (ξ, η, ζ).

as state variables in the optimization problem, where d is the number of free degrees of freedom in the whole structure and ℓ refers to the static load case.

2.2. Structural analysis

The frame model is based on two-noded Timoshenko beam elements [11] with six degrees of freedom in each node, see Figure 1. Let the element displacement vector in local coordinates $\mathbf{u}_e^l \in \mathbb{R}^{12}$ be defined as

$$\mathbf{u}_e^l = \begin{pmatrix} u^1 & v^1 & w^1 & \theta_\xi^1 & \theta_\eta^1 & \theta_\zeta^1 & u^2 & v^2 & w^2 & \theta_\xi^2 & \theta_\eta^2 & \theta_\zeta^2 \end{pmatrix}^T,$$

where u^i, v^i, w^i and $\theta_\xi^i, \theta_\eta^i, \theta_\zeta^i$ are displacements and rotations, respectively, in the local coordinate system ξ, η, ζ. The element rotation matrix, $\mathbf{T}_e \in \mathbb{R}^{12\times12}$, maps the global element displacement vector $\mathbf{u}_e \in \mathbb{R}^{12}$ which is part of $\mathbf{u}^\ell$ to local coordinates, $\mathbf{u}_e^l = \mathbf{T}_e\mathbf{u}_e$. The stiffness matrix $\mathbf{K}_e(\mathbf{v}) : \mathbb{R}^{n_v} \mapsto \mathbb{R}^{12\times12}$ and mass matrix $\mathbf{M}_e(\mathbf{v}) : \mathbb{R}^{n_v} \mapsto \mathbb{R}^{12\times12}$ for element e are derived as

$$\mathbf{K}_e(\mathbf{v}) = \mathbf{T}_e^T \left(\int_{V_e} \mathbf{B}(\mathbf{v};\boldsymbol{\gamma})^T \mathbf{C}\, \mathbf{B}(\mathbf{v};\boldsymbol{\gamma})\, \mathrm{d}V_e \right) \mathbf{T}_e$$
$$\mathbf{M}_e(\mathbf{v}) = \mathbf{T}_e^T \left(\int_{V_e} \rho\mathbf{N}(\mathbf{v};\boldsymbol{\gamma})^T\, \mathbf{N}(\mathbf{v};\boldsymbol{\gamma})\, \mathrm{d}V_e \right) \mathbf{T}_e,$$

where $\mathbf{B}(\mathbf{v};\boldsymbol{\gamma}) : \mathbb{R}^{n_v+3} \mapsto \mathbb{R}^{6\times12}$ and $\mathbf{N}(\mathbf{v};\boldsymbol{\gamma}) : \mathbb{R}^{n_v+3} \mapsto \mathbb{R}^{3\times12}$ are the strain-displacement matrix and the shape function matrix in element coordinates $\boldsymbol{\gamma} = (\xi, \eta, \zeta)$ [7]. $\mathbf{C} \in \mathbb{R}^{6\times6}$ is the material constitutive matrix, and $\rho \in \mathbb{R}$ is the material density. When the cross section is constant over the element length, the expressions for $\mathbf{K}_e(\mathbf{v})$ and $\mathbf{M}_e(\mathbf{v})$ reduces to simple functions of the element cross section area $A_e(d_e, t_e)$ and second moment of area about a transverse axis $I_e(d_e, t_e)$.

The assembly of the global stiffness matrix $\mathbf{K}(\mathbf{v}) \in \mathbf{R}^{d\times d}$ and mass matrix $\mathbf{M}(\mathbf{v}) \in \mathbf{R}^{d\times d}$ are sums of a non-design dependent and a design dependent part

$$\mathbf{K}(\mathbf{v}) = \mathbf{K}_0 + \sum_{e=1}^{n} \mathbf{K}_e(d_e, t_e) \tag{1}$$

$$\mathbf{M}(\mathbf{v}) = \mathbf{M}_0 + \sum_{e=1}^{n} \mathbf{M}_e(d_e, t_e), \tag{2}$$

where $\mathbf{K}_0 \in \mathbb{R}^{d\times d}$ and $\mathbf{M}_0 \in \mathbb{R}^{d\times d}$ are the global stiffness and mass matrices for the design independent elements such as transition piece, tower and rotor-nacelle-assembly (RNA). The RNA is modelled with lumped equivalent masses and inertias at the tower top. The summation operation in (1) and (2) also distributes the element matrices to the appropriate degrees of freedom.

We define the state variable $\mathbf{u}^\ell$ to be the solution to the static finite element problem

$$\mathbf{K}(\mathbf{v})\mathbf{u}^\ell = \mathbf{f}^\ell(\mathbf{v})$$

where $\mathbf{f}^\ell(\mathbf{v}) \in \mathbb{R}^d$ is the ℓth static, design dependent load vector. The eigenfrequencies ω_i are obtained from the eigenvalue problem

$$\mathbf{K}(\mathbf{v})\boldsymbol{\phi}_i = \lambda_i \mathbf{M}(\mathbf{v})\boldsymbol{\phi}_i, \quad \omega_i = \sqrt{\frac{\lambda_i}{2\pi}} \tag{3}$$

where we assume $\lambda_1 \leq \lambda_2 \cdots \leq \lambda_d$, and that $\boldsymbol{\phi}_i^T \mathbf{M}(\mathbf{v})\boldsymbol{\phi}_i = 1$, and $\boldsymbol{\phi}_j^T \mathbf{M}(\mathbf{v})\boldsymbol{\phi}_k = 0$ for $j \neq k$.

Let there be n_f fatigue load cases and n_u ultimate load cases. The normal stress in element e, position $\boldsymbol{\gamma}_h$, for the ultimate limit state load cases is then computed as

$$\sigma(\mathbf{v}, \mathbf{u}_e^\ell; \boldsymbol{\gamma}_h) = E\mathbf{b}_e(\mathbf{v}; \boldsymbol{\gamma}_h)\mathbf{T}_e\mathbf{u}_e^\ell, \quad \ell = n_f + 1, ...n_\ell$$

where $\mathbf{b}_e(\mathbf{v}; \boldsymbol{\gamma}_h) \in \mathbb{R}^{1\times 12}$ is the strain displacement vector for normal stress at postition $\boldsymbol{\gamma}_h$, and E is the material Young modulus. In the fatigue limit state load cases we must also account for uneven stress distribution in welded joints. The recommended practice [2] provides a method using stress concentration factors (SCFs, referred to as s). This method assumes superposition of the normal stress components coming from axial forces (ax), moments in plane (mi) and moments out of plane (mo). We decompose the normal stress by decomposing the strain displacement vector, $\mathbf{b}_e(\mathbf{v}; \boldsymbol{\gamma}_h) = \mathbf{b}_e^{ax}(\mathbf{v}; \boldsymbol{\gamma}_h) + \mathbf{b}_e^{mi}(\mathbf{v}; \boldsymbol{\gamma}_h) + \mathbf{b}_e^{mo}(\mathbf{v}; \boldsymbol{\gamma}_h)$, and multiply the respective SCF coefficients onto each stress component.

$$\mathbf{b}_e^s(\mathbf{v}; \boldsymbol{\gamma}_h) = s_e^{ax}(\mathbf{v}; \boldsymbol{\gamma}_h)\mathbf{b}_{eh}^{ax}(\mathbf{v}; \boldsymbol{\gamma}_h) + s_e^{mi}(\mathbf{v}; \boldsymbol{\gamma}_h)\mathbf{b}_{eh}^{mi}(\mathbf{v}; \boldsymbol{\gamma}_h) + s_e^{mo}(\mathbf{v}; \boldsymbol{\gamma}_h)\mathbf{b}_{eh}^{mo}(\mathbf{v}; \boldsymbol{\gamma}_h)$$

When there is a thickness transition along a member, such as when stubs and cans are used to reinforce the joints, we assume that there is a butt weld. Butt weld SCFs are simpler than the tubular joint SCFs, but the implementation is similar. For elements that are not part of a weld, the SCFs are all set to unity, i.e. $s_{eh}^{ax} = s_{eh}^{mi} = s_{eh}^{mo} = 1$. The fatigue stress in element e, position $\boldsymbol{\gamma}_h$, for the fatigue limit state load cases $\ell = 1, ..., n_f$ is now computed as $\sigma^f(\mathbf{v}, \mathbf{u}_e^\ell; \boldsymbol{\gamma}_h) = E\mathbf{b}_e^s(\mathbf{v}; \boldsymbol{\gamma}_h)\mathbf{T}_e\mathbf{u}_e^\ell$. In all load cases the stress is evaluated at $n_h = 8$ points along the circumference of the element.

2.3. Optimal design problem

The optimal design problem minimizes the mass of the n elements in the design domain while enforcing requirements on linear constraints, the state equation, fatigue equivalent stresses, ultimate stresses, frequencies, buckling limits and design variable bounds. We consider the non-linearly constrained optimization problem

$$\begin{aligned}
\underset{\mathbf{v}\in\mathbb{R}^{n_v}, \mathbf{u}\in\mathbb{R}^{dn_\ell}}{\text{minimize}} \quad & f(\mathbf{v}) = \rho \sum_{e=1}^{n} A_e(d_e, t_e) l_e \\
\text{subject to} \quad & \mathbf{A}\mathbf{v} \leq \mathbf{b} \\
& \mathbf{K}(\mathbf{v})\mathbf{u}^\ell - \mathbf{f}^\ell(\mathbf{v}) = \mathbf{0}, && l = 1, ..., n_\ell \\
& \underline{\Delta\sigma} \leq \sigma^f(\mathbf{v}, \mathbf{u}_e^\ell; \boldsymbol{\gamma}_h) \leq \overline{\Delta\sigma}, && e = 1, ..., n, h = 1, ..., n_h, \ell = 1, ..., n_f \\
& \sigma_e^b(\mathbf{v}) \leq \sigma(\mathbf{v}, \mathbf{u}_e^\ell; \boldsymbol{\gamma}_h), && e = 1, ..., n, h = 1, ..., n_h, \ell = n_f + 1, ..., n_\ell \\
& \underline{\omega_i} \leq \omega_i(\mathbf{v}) \leq \overline{\omega_i}, && i = 1, ..., n_\omega \\
& g_e(\mathbf{v}) \leq 0, && e = 1, ..., n \\
& \underline{\mathbf{v}} \leq \mathbf{v} \leq \overline{\mathbf{v}},
\end{aligned} \tag{P}$$

where l_e is the length of element e. The objective function $f(\mathbf{v})$ sums the masses of all elements in the design domain. The linear constraints $\mathbf{A}\mathbf{v} \leq \mathbf{b}$ enforce the SCF validity range [2], which states that for a joint where a brace element, B, is welded onto a leg element, L, the dimensions should satisfy the following relations:

$$\frac{d_L}{5} \leq d_B \leq d_L$$
$$\frac{t_L}{5} \leq t_B \leq t_L,$$

and that for all elements, the following should hold

$$16t_e \leq d_e \leq 64t_e, \quad e = 1, ..., n.$$

The equality constraint $\mathbf{K}(\mathbf{v})\mathbf{u}^\ell - \mathbf{f}^\ell(\mathbf{v}) = \mathbf{0}$, which is necessary in the SAND formulation, ensures that the state variables satisfy the static equilibrium at any feasible point of (P), and in particular for all optima. The stress constraints ensure that

Wind Energ. 2010; **00**:1–14 © 2010 John Wiley & Sons, Ltd.
DOI: 10.1002/we
Prepared using weauth.cls

the fatigue and ultimate limit states are satisfied in every stress evaluation point of the jacket. The frequency constraints $\underline{\omega_i} \leq \omega_i(\mathbf{v}) \leq \overline{\omega_i}$ set bounds on the n_f first natural frequencies of the structure, the non-linear constraints $g_e(\mathbf{v}) \leq 0$ prevents column buckling, and at last there is also an upper $\overline{\mathbf{v}}$ and lower $\underline{\mathbf{v}}$ bound on the design variables $\mathbf{v}$, which ensures realistic and manufacturable designs.

Problem (P) is in general non-convex and the feasible set may be empty if the requirements on the structure are too demanding. This can for example happen when the frequency constraint requires a softer structure, and the stress constraints require larger cross sections. Since $\omega_i(\mathbf{v})$ is obtained by solving the eigenvalue problem (3), problem (P) is not completely a traditional SAND formulation.

2.4. Design variable sensitivities

All the design variable sensitivities required by (P) can be computed analytically. In the SAND formulation, sensitivities of the normal stress with respect to the design and state variables are

$$\frac{\mathrm{d}\sigma(\mathbf{v},\mathbf{u}_e;\boldsymbol{\gamma}_h)}{\mathrm{d}\mathbf{v}_k} = \frac{\mathrm{d}\mathbf{b}_e(\mathbf{v};\boldsymbol{\gamma}_h)}{\mathrm{d}\mathbf{v}_k}\mathbf{T}_e\mathbf{u}_e$$

and

$$\frac{\mathrm{d}\sigma(\mathbf{v},\mathbf{u}_e;\boldsymbol{\gamma}_h)}{\mathrm{d}\mathbf{u}_e} = E\mathbf{b}_e(\mathbf{v};\boldsymbol{\gamma}_h)\mathbf{T}_e.$$

The latter follow since stresses are linear in the state variables. The sensitivity of the fatigue stress is similar, except that the sensitivity of the strain-displacement matrix $\mathbf{b}_e^s(\mathbf{v};\boldsymbol{\gamma}_h)$ with respect to the design variables is a bit more complicated since it also involves the design dependent SCFs. In the numerical examples we explain the assumptions made to ensure smoothness of the SCFs. The sensitivity of the eigenvalues are, under the assumption that the eigenvalues are distinct, given by [14]

$$\frac{\mathrm{d}\lambda_i}{\mathrm{d}\mathbf{v}_k} = \boldsymbol{\phi}_i^T\left(\frac{\mathrm{d}\mathbf{K}(\mathbf{v})}{\mathrm{d}\mathbf{v}_k} - \lambda_i\frac{\mathrm{d}\mathbf{M}(\mathbf{v})}{\mathrm{d}\mathbf{v}_k}\right)\boldsymbol{\phi}_i.$$

The model of the rotor-nacelle-assembly ensures that the lowest eigenfrequencies are indeed distinct.

2.5. Fatigue constraint

For conceptual optimal design the aim is to model the fatigue response to a collection of time dependent loads using only one or a few static loads. Let $p_w(t)$ be a time dependent load applied to the structure, with probability of occurrence β_w, for $w = 1, ..., n_w$,. The load is T^{sim} seconds long and $\sum_{w=1}^{n_w}\beta_w = 1$. The fatigue response D_{eh} in a specific point eh due to the loads $p_1(t), ..., p_{n_w}(t)$ can be obtained in three steps. First do the analysis to obtain the time dependent normal stresses $\sigma^s_{ehw}(t)$ in point eh for loads $w = 1, ..., n_w$. Second, do rainflow counting [5] on $\sigma^f_{ehw}(t)$ to bin it into pairs of stress amplitudes $\Delta\sigma^f_{ehw,i}$ and number of cycles $n_{w,i}$ for $i = 1, ..., q$, where q is the number of stress amplitude bins. Third, sum the damages at each stress level for all load cases using Miners rule [21]

$$D_{eh} = \sum_{w=1}^{n_w}\left(\beta_w\sum_{i=1}^{q}\frac{n_{w,i}(\Delta\sigma^f_{ehw,i})^m}{\bar{a}}\right). \tag{4}$$

Here we have used that $\log N_i = \log\bar{a} - m\log\Delta\sigma_i$ which describes the SN-curve with material properties $\bar{a}$ and m.

An alternative method to obtain the fatigue response is presented here. This method uses damage equivalent loads, and is in general limited to one-degree-of-freedom loads, and a linear SN-curve. If the load is applied at only one degree of freedom and the structural response is quasi-static, there is a linear relationship between the stress in any point eh, and the load, $\sigma^f_{ehw}(t) = \alpha_{eh}p_w(t)$. This means that we can do the rainflow counting on the load, and get that $\Delta\sigma^f_{ehw,i} = \alpha_{eh}\Delta p_{w,i}$. Assuming that a 1 Hz harmonic load, $p^{1Hz}(t)$ produces the same damage as the original loads $p_1(t), ..., p_{n_w}(t)$, we can solve for the harmonic 1 Hz load amplitude as

$$\Delta p^{1Hz} = \left(\frac{1}{T^{sim}}\sum_{w=1}^{n_w}\left(\beta_w\sum_{i=1}^{q}n_{w,i}(\Delta p_{w,i})^m\right)\right)^{\frac{1}{m}}$$

The fatigue damage from all load cases can now be computed as

$$D_{eh} = \frac{T^{sim}(\Delta\sigma^{1Hz}_{eh})^m}{\bar{a}}$$

We find $\Delta\sigma_{eh}^{1Hz}$ by doing the analysis with Δp^{1Hz} as the applied load. The fatigue constraint $D_{eh} \leq D^{max}$ can now be reformulated as a static stress constraint $\underline{\Delta\sigma} \leq \Delta\sigma_{eh}^{1Hz} \leq \overline{\Delta\sigma}$ where

$$\overline{\Delta\sigma} = \left(\frac{D^{max}\bar{a}}{T^{life}}\right)^{\frac{1}{m}} \quad \text{and} \quad \underline{\Delta\sigma} = -\overline{\Delta\sigma},$$

where T^{life} is the desired fatigue lifetime in seconds. We have now showed that under special assumptions, a transient load with fatigue constraint can be rewritten as a static load with stress constraints.

The above derivation assumes that the transient load is in only one degree of freedom, that the SN-curve is linear, and that the structural response is quasi-static. Neither of these assumptions are generally satisfied for offshore wind turbine structures. However, it is mainly the thrust F_x, overturning moment M_y, and torsion M_z which contribute to fatigue in the jacket. An approach used in the industry [29] is therefore to use a weighted superposition of the damage equivalent load Δp_{1Hz} from these three degrees of freedom. Regarding the linear SN-curve assumption, using the high-cycle part of the SN-curve will only give slightly conservative results. If one assures that the first natural frequencies of the structure avoids the rotor frequencies, it is the authors experience that it is conservative to assume quasi-static structural response. Future work focuses on the validity of these assumptions.

2.6. Ultimate constraints

Local shell buckling and column buckling are considered according to the offshore standard [3] and the recommended practice [1]. Shell buckling is formulated as a stress constraint in compression,

$$\sigma_e^b(\mathbf{v}) \leq \sigma(\mathbf{v}, \mathbf{u}_e^\ell; \boldsymbol{\gamma}_h),$$

where the shell buckling capacity $\sigma_e^b(\mathbf{v})$ is defined as

$$\sigma_e^b(\mathbf{v}) = \frac{-\sigma^y}{\gamma_M\sqrt{1+\left(\frac{\sigma^y}{f_{Em}}\right)^2}}, \qquad f_{Em} = C\frac{\pi^2 E}{12(1-\nu^2)}\left(\frac{t_e}{L_e}\right)^2, \qquad C = \sqrt{1+(\tilde{\rho}\tilde{\xi})^2}$$

$$\tilde{\rho} = \frac{1}{2\sqrt{1+\frac{d_e}{600t_e}}}, \qquad \tilde{\xi} = 1.404\frac{L_e^2}{d_e t_e}\sqrt{1-\nu^2}.$$

Here, L_e is the length of the member, from one joint to the next, to which element e belongs. σ^y is the material yield strength and ν is the Poissons ratio. Column buckling need only be assessed for element e if

$$\frac{(kL_e)^2 A_e}{I_e} \geq \frac{2.5E}{\sigma^y} \tag{5}$$

where $k = 0.7$ is the effective column length. To avoid assessing column buckling, the inverse of equation (5) is formulated as a non-linear constraint $g_e(\mathbf{v}) \leq 0$, where

$$g_e(\mathbf{v}) = \sqrt{\frac{3.2\sigma^y}{E}}kL_e - d_e^2 + 2d_e t_e - 2t_e^2.$$

2.7. Implementation

The structural analysis model and the design sensitivities are implemented in a Matlab package called JADOP (JAcket Design OPtimization), and is based on five modules:

- Mesh: Builds the finite element model based on parametric input describing the overall properties of the jacket, such as number of sections, bottom and top leg distances, and turbine properties. In this paper we use the DTU 10 MW reference turbine [6].
- Designcase: Sets boundary conditions, defines design and constraint domains, implements variable linking, and builds the load vectors.
- Analysis: Assigns cross sectional properties based on design variables, assembles structural matrices, and solve for displacements, frequencies and stresses. Note that in the SAND formulation the displacements do not need to be solved for since they are implicitly defined by the constraints.
- Sensitivity analysis: Computes analytical sensitivities of mass, stress, SCFs, structural matrices, displacements, shell buckling limit, column buckling limit and frequencies.

Wind Energ. 2010; **00**:1–14 © 2010 John Wiley & Sons, Ltd.
DOI: 10.1002/we
Prepared using weauth.cls

Table I. Non-default IPOPT parameters

Parameter	Value	Description
`mu_strategy`	`'adaptive'`	Update strategy for barrier parameter
`nlp_scaling_method`	`'none'`	Technique used for scaling the NLP
`hessian_approximation`	`'limited-memory'`	Indicates what Hessian information is to be used
`tol`	10^{-5}	Desired convergence tolerance (relative)
`max_iter`	10^3	Maximum number of iterations
`ma57_pre_alloc`	10	Safety factor for work space memory allocation for the linear solver MA57
`limited_memory_max_history`	4	Maximum size of the history for the limited quasi-Newton Hessian approximation

Table II. Details of the finite element models

Number of sections	Number of free degrees of freedom	Number of finite elements	Number of design elements
3	2430	452	396
4	3126	580	524
5	3822	708	652
6	4518	836	780
7	5214	964	908
8	5910	1092	1036

- Optimization: Includes SAND and Nested problem formulations and interfaces the interior point method implemented in IPOPT [32].

Time series at the tower top are extracted from Flex5 simulations of a rotor on top of a rigid tower, and are extracted for 11 wind speeds with an initial cut-off of 200 s, a time step of 0.02 s, and a length of 10 minutes.

IPOPT is an open source software package for large-scale nonlinear optimization. It uses a primal-dual interior point method with filters to promote global convergence. Non-default parameters for IPOPT used in the numerical experiments are listed in Table I. The adaptive strategy for the barrier parameter is used because it, for these problems, converges faster than the more robust monotone strategy. The scaling method is set to none, as it gave better performance to use a user-defined scaling method. The load, the structural matrices, and the objective function were all scaled with 10^{-5}. The Hessian was not computed analytically, and therefore the limited memory BFGS approximation was chosen. It was observed that the default tolerance of 10^{-8} was too strict, and it was set to 10^{-5}. The maximum number of iterations was set to 1000, though most problems converged in less than 100 iterations. Finally, two memory settings were altered to improve the solution time on the laptop. The problems were solved on a laptop with 8 GB RAM and i7-4600U CPU 2.7 GHz processor.

3. NUMERICAL EXPERIMENTS

The optimal design problem (P) is solved to propose jacket support structures for 50 m water depth. The influence of leg distance, variable linking and number of sections on the optimal design is investigated. Finally, the performance of the SAND formulation is compared with the nested formulation.

3.1. Definition of the reference jacket support structure

A structural finite element model with piles, jacket, transition piece, and tower is built in JADOP, see Figure 2. All cross sections are assumed to be thin-walled pipes with constant cross section along the element length, and with a shear correction factor of 0.5 [11]. The details of the model are given in Table II for different number of sections, n_{sec}. The position of the nodes and the element connectivities are not changed in the optimization. The jacket cross sections can be modelled with different alternatives of variable linking, leading the number of variables to range from 4 to $6n_{sec}$ as described in Table III.

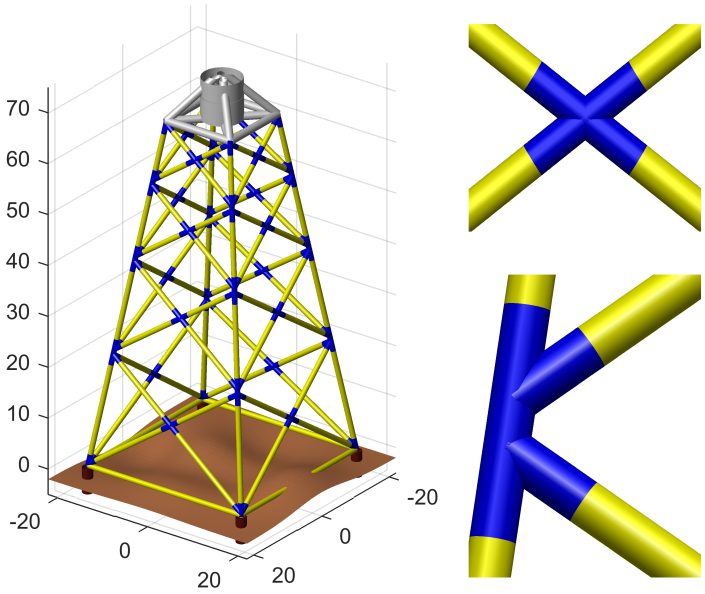

Figure 2. A 3D rendering of the reference structure in JADOP, showing the top of the piles, the jacket, and the transition piece. The members going straight from seabed and up to the transition piece are called legs, and they are connected to each other by braces. The blue part of the legs and braces are called stubs and cans, respectively. To the right is a zoom on an X-joint and a K-joint.

The jacket design under consideration in the first numerical example is a close replica of the INNWIND.EU reference jacket [8]. The jacket has four straight legs, four sections with X-joints, and the angle between braces is equal in all sections. The bottom leg distance, top leg distance, and height of the jacket are 34, 14, and 67 meters, respectively. A difference from the INNWIND.EU jacket is that an eccentricity of half a meter in the K-joints is included to avoid overlapping welds.

The transition piece is modelled as the frame of a pyramid with diagonal stiffening in the bottom. All transition piece members have a diameter of 1.5 meters and thickness of 65 millimetres. These values are chosen so that the transition piece mass matches the transition piece mass of the INNWIND.EU reference jacket, which is 330 tons. The piles are modelled as rigid, which might lead to an over-prediction of the first eigenfrequencies.

The tower is similar to the onshore tower described in [6], with the bottom 26 meters cut off, such that the hub-height remains at 113 meters. The bottom of the tower has diameter and thickness of 7.83 m and 36 mm, and the at the top the diameter and thickness are 5.58 m and 20 mm. The tower mass is 489 tons. Instead of conical tower sections, as are decribed in [6], the JADOP model uses cylindrical tower sections with stepwise decreasing diameters from one section to the next. Since the tower is modelled with more than 10 finite elements, this is not expected to have any noticeable effect on the global structural response.

The material used is offshore steel S355 with a Youngs modulus of 210 GPa, Poissons ratio of 0.3, and a density of 7850 kg per cubic meter. The tower is specified to have an increased density of eight percent, which accounts for non-structural mass [6]. While the rotor-nacelle-assembly (RNA) is not modelled, an equivalent lumped mass matrix is added at the tower top. The high cycle SN-curve used in the fatigue constraint is for tubular joints [2]. The mass of the RNA is 677 tons, and the equivalent inertia about x, y, and z are 166, 127, and 127 MNm, respectively [8]. The coordinate axes are oriented such that x points in the load direction and z points towards the skies.

The SCF factors were implemented with some assumptions to assure smoothness. First, the diameter of the upper and lower brace in a K-joint were assumed to be equal. Second, the parameter $\alpha = \frac{L}{2d_c}$ is assumed to be constant and equal to 12 meters. The recommended practice [2] refers to the brace as the member which is welded onto a chord. This means that in a K-joint the leg is the chord. In the X-joint we assume both braces to be the chord. Modifications to these assumptions could change the optimized designs.

3.2. First optimal design of the jacket structure

The optimal design problem (P) is solved for the jacket structure in Figure 2, with $6n_{sec}$ design variables. The problem is solved with seven static load cases, listed in Table IV. The four fatigue load cases are all based on the damage equivalent load, Δp^{1Hz}, described in Section 2.5. Based on recommendations for conceptual design of jackets [29], we neglect wave loads, and use the following two weighted superposition of damage equivalent loads at the tower top:

- Thrust dominated: F_x, M_y, and $\frac{1}{2}M_z$. This load combination is expected to be design driving for the jacket legs.

DOI: 10.1002/we
Prepared using weauth.cls

Table III. Description of the variable linking options considered.

Number of variables	Description
4	Separate diameter and thickness for legs and braces
$4n_{sec}$	Separate diameter and thickness for legs and braces per section
$6n_{sec}$	Separate diameter and thickness for legs and braces per section, plus separate thickness for stubs and cans per section

Table IV. Description of static load cases

	Load type	Limit state	Rotation [deg]	Tower top load
1	Thrust	Fatigue	0	F_x, M_y, and $\frac{1}{2}M_z$ from Δp^{1Hz}
2	Thrust	Fatigue	45	F_x, M_y, and $\frac{1}{2}M_z$ from Δp^{1Hz}
3	Torsion	Fatigue	0	$\frac{1}{2}F_x$, $\frac{1}{2}M_y$, and M_z from Δp^{1Hz}
4	Torsion	Fatigue	45	$\frac{1}{2}F_x$, $\frac{1}{2}M_y$, and M_z from Δp^{1Hz}
5	Thrust	Ultimate	0	F_x^{max} and M_y^{max} from [6]
6	Thrust	Ultimate	45	F_x^{max} and M_y^{max} from [6]
7	Torsion	Ultimate	0	M_z^{max} from [6]

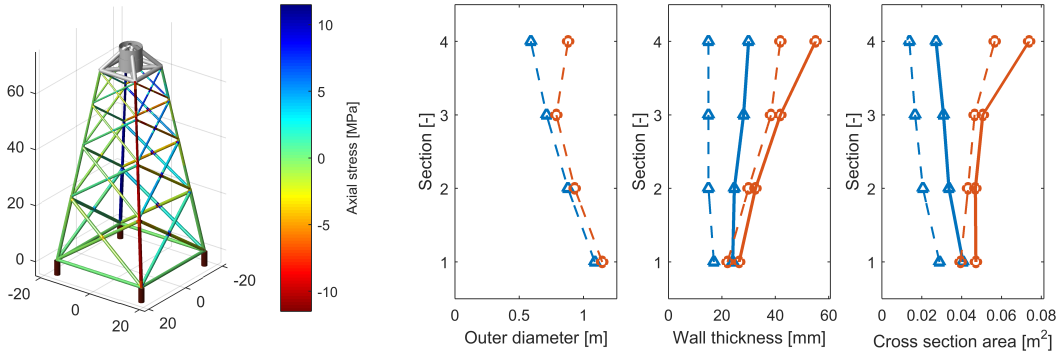

Figure 3. To the left is the optimized jacket with stress contours from load number four, one of the critical load cases. The mass of this jacket is 602 tons and the frequency is 0.258 Hz. The three other plots show how the mass is distributed in the jacket. Red lines with circles are for leg dimensions, and blue lines with triangles are for brace dimensions. Whole lines are for stub and can dimensions.

- Torsion dominated $\frac{1}{2}F_x$, $\frac{1}{2}M_y$, and M_z. This load combination is expected to be design driving for the jacket braces.

Both load combinations are applied from two directions to ensure that the worst case scenario is captured. It is emphasized that these design load assumptions are valid only for conceptual design of jackets, and are not accurate enough to use in preliminary or detailed design phases. For the ultimate limit state loads, we have used extreme loads for the DTU 10 MW reference wind turbine [6], recorded from onshore conditions. Also here, the loads are split into thrust, and torsion dominated, and applied from two directions.

Frequency constraints are placed on the three lowest eigenfrequencies of the full structure. The two lowest should be within the soft-stiff range with ten percent margin, and the third should be above the 3P range. The 1P range of the DTU 10 MW wind turbine is 0.10 to 0.16 Hz, which makes the soft-stiff range with 10 percent margin from 0.18 to 0.27 Hz.

The optimized jacket is shown in Figure 3. Note that $\overline{\Delta\sigma} = 11.5$ MPa. The jacket has a mass of 602 tons, and an eigenfrequency of 0.258 Hz. The leg cross section area increases towards the top of the jacket, while the brace cross section area decreases. The high diameter of both legs and braces towards the seabed is driven by the column buckling constraint. An investigation of the active constraints in the optimized jacket showed that

- 13 out of 48 linear constraints were active.
- Fatigue stress constraints were active in all four fatigue load cases, and spread around in the structure.
- The frequency constraints were not active, but they clearly influenced the solution time, at least in the SAND formulation.
- The shell buckling constraints were not active, although the utilization was as high as 90 percent for two evaluation points in load case six.

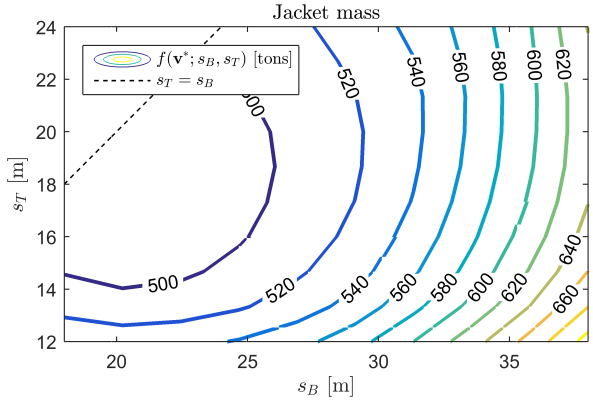

Figure 4. Optimized jacket mass as function of bottom leg distance s_B, and top leg distance s_T. Only designs where $s_T < s_B$ were investigated.

- The simplified column buckling constraints were active for all braces in the three bottom sections, and for the legs in the second section.
- The lower bound on wall thickness, 15 mm, was active for the braces in the three top sections.

It was observed that removing the frequency constraint could significantly speed up the solution time, see Table VII. This is likely due to the fact that a strict upper frequency bound significantly decreases the feasible design space. While active stress constraints generally push the design variables to increase, an active upper frequency constraint will push the design variables to decrease. It is therefore very difficult for to find a feasible design when both stress constraints and frequency constraints are active. In the rest of the numerical experiments, the frequency constraints are therefore removed unless otherwise specified.

3.3. Conceptual design investigations using structural optimization

In this numerical example we modify the reference structure by changing the leg distance, the variable linking, or the number of sections. For each change, we re-optimize the structure. Looking at the results from all these optimal designs allows us to investigate design trends, and provide a better justification for our design decisions.

The leg distance on the bottom and top of a jacket can have an influence on manufacturing, logistics, installation, as well as the frequency of the structure. With the following limits on the bottom leg distance s_B, and top leg distance s_T:

$$18m \leq s_B \leq 38m$$
$$12m \leq s_T \leq 24m,$$

we model 100 jacket designs with leg distances in these ranges. The jackets are optimized using $n_v = 6n_{sec}$ design variables, and without frequency constraints. As a reminder, the reference design has a bottom and top leg distance of 34 and 14 meters, respectively. The 100 optimization calls were solved with an average cpu-time of 110 seconds, using an average of 57 iterations to convergence.

Figure 4 shows how the optimized jacket mass is lower for jackets with a lower bottom leg distance, with a potential mass reduction of more than a hundred tons for the reference jacket. It also looks favourable to increase the top leg distance slightly. However, a larger top leg distance also increases the size of the transition piece. Figure 5 shows how the added mass of the larger transition piece motivates a low top leg distance. Figure 6 shows how increased leg distance, both at bottom and top of the jacket, gives a higher frequency.

Based on this investigation, a good design change would be to reduce the bottom leg distance from 34 to 24 meters, and make no change to the top leg distance. That would reduce reduce the jacket mass with almost 100 tons (16 percent), make no change to the transition piece, and reduce the frequency with almost 0.01 Hz (3 percent).

The number of independent variables in the design has an influence on how the jacket can be manufactured. The results presented so far has used the variable linking $6n_{sec}$, described in Table III, and we now present the motivation for using this variable linking. The reference structure was optimized with all three options for variable linking, both with and without frequency constraint, and the mass and frequency of the optimized structures are shown in Table V. The results show that the optimal design mass is highly dependent on the number of independent design variables. Changing from one cross section for legs and one for braces, to separate cross sections for each section reduces the mass with more than 400 tons, or 35 percent. Adding subs and cans decreases the mass even more, from 773 to 602 tons, corresponding to a 22 percent reduction.

Wind Energ. 2010; **00**:1–14 © 2010 John Wiley & Sons, Ltd.
DOI: 10.1002/we
Prepared using weauth.cls

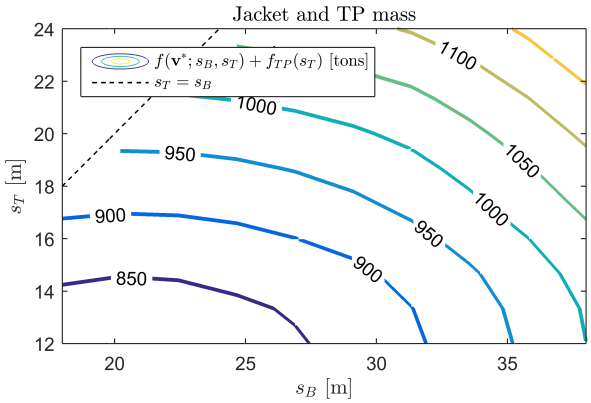

Figure 5. Optimized jacket mass plus transition piece mass as function of bottom leg distance s_B, and top leg distance s_T. Note that the transition piece mass increases with increasing top leg distance.

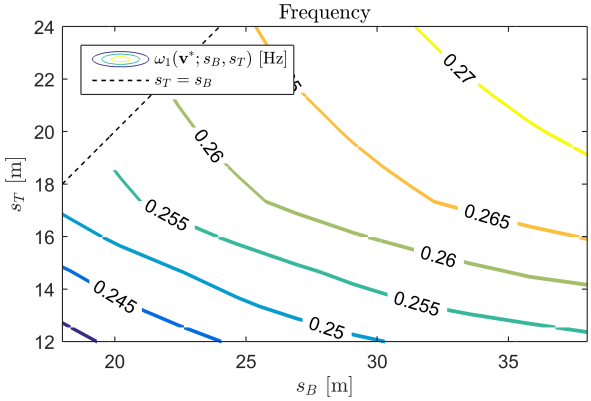

Figure 6. First fundamental frequency as function of bottom leg distance s_B, and top leg distance s_T. Note that the upper bound on the allowable frequency range is 0.27 Hz, but this constraint was not included in the optimization problem for this investigation.

Table V. Comparison of variable linking options.

	4	4 with $\boldsymbol{\omega}$-constraints	$4n_{sec}$	$4n_{sec}$ with $\boldsymbol{\omega}$-constraints	$6n_{sec}$	$6n_{sec}$ with $\boldsymbol{\omega}$-constraints
Jacket mass	1187 tons	-	773 tons	773 tons	602 tons	602 tons
Structural frequency	0.275 Hz	-	0.262 Hz	0.262 Hz	0.258 Hz	0.258 Hz

The number of sections in the jacket has consequences for buckling limits and manufacturing. Since the previous investigations indicated that both variable linking and bottom leg distance have significant influence on the optimized jacket mass, this investigation is done for two different bottom leg distances and two different variable linking options. Figure 7 shows how the number of sections influence the optimized jacket mass. The jacket with lowest mass according to Figure 7 has a bottom leg of 24 meters, six independent design variables per section, and five sections. The details of this design are given in Figure 8. Note that the dimensions of both legs and braces are relatively constant for the whole jacket. The jacket with 24 meter bottom leg distance, six independent design variables per section, and four sections is only two tons heavier than the one with five sections, and potentially cheaper to manufacture due to fewer welds.

3.4. Comparison of the nested and SAND problem formulations

The optimal design problem (P) was formulated and solved in the nested analysis and design as well. In the nested formulation the state variables are not included as variables in the optimization problem, and the displacements are instead found by solving the state equation, $\mathbf{u}(\mathbf{v}) = \mathbf{K}(\mathbf{v})^{-1}\mathbf{f}(\mathbf{v})$. Sensitivities of displacements are obtained by solving the system

$$\mathbf{K}(\mathbf{v})\frac{\mathrm{d}\mathbf{u}(\mathbf{v})}{\mathrm{d}\mathbf{v}_k} = \frac{\mathrm{d}\mathbf{f}(\mathbf{v})}{\mathrm{d}\mathbf{v}_k} - \frac{\mathrm{d}\mathbf{K}(\mathbf{v})}{\mathrm{d}\mathbf{v}_k}\mathbf{u}(\mathbf{v}).$$

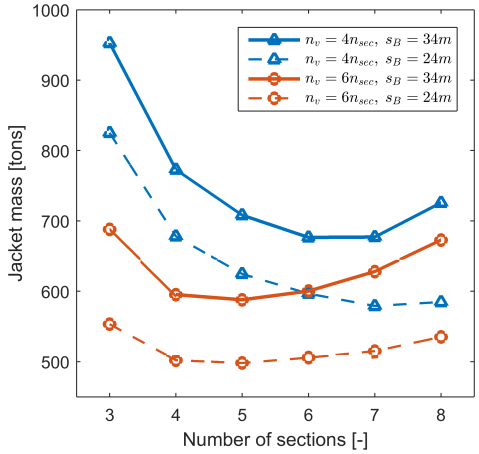

Figure 7. Optimized jacket mass as a function of number of sections. The plot is given for two bottom leg distances and two variable linking options.

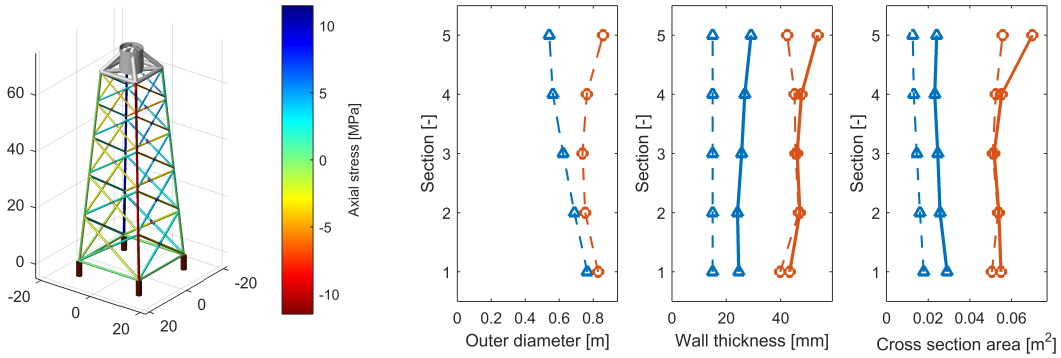

Figure 8. The solution to the optimal design problem with a bottom leg distance of 24 meters and five sections. The mass of this jacket is 506 tons and the frequency is 0.250 Hz. This is 96 tons, or 16 percent, less than the jacket in Figure 3. Red lines with circles are for leg dimensions, and blue lines with triangles are for brace dimensions. Whole lines are for stub and can dimensions.

Table VI. Comparison of optimization problem details for SAND and nested formulations for a four legged jacket with four sections and 6_{nsec} design variables.

	SAND	Nested
Number of variables	21570	24
Number of equality constraints	21546	0
Number of inequality constraints	42495	42495

for $k = 1, ..., n_v$. The sensitivity of the stress with respect to the design variables in the Nested formulation can now be computed as

$$\frac{\mathrm{d}\sigma(\mathbf{v}, \mathbf{u}_e(\mathbf{v}); \boldsymbol{\gamma}_h)}{\mathrm{d}\mathbf{v}_k} = \frac{\partial\sigma(\mathbf{v}, \mathbf{u}_e(\mathbf{v}))}{\partial\mathbf{v}_k} + \frac{\partial\sigma(\mathbf{v}, \mathbf{u}_e(\mathbf{v}); \boldsymbol{\gamma}_h)}{\partial\mathbf{u}_e(\mathbf{v})} \frac{\mathrm{d}\mathbf{u}_e(\mathbf{v})}{\mathrm{d}\mathbf{v}_k} \tag{6}$$

The details of the optimal design problem in the SAND and nested formulations are given in Table VI. The SAND formulation has more variables and equality constraints than the Nested formulation, and it can be expected that it requires more time in the solver (IPOPT). However, the design sensitivities are computationally cheaper, and it is therefore expected that the SAND formulation requires less time in the function evalutations (Matlab).

The result of the comparison is given in Table VII, for problems both with and without frequency constraints. It was observed that both SAND and nested problem formulations, both with and without frequency constraint, led to the exact same optimized design. Regarding solution time, the time per iteration is as expected lower for the SAND formulation, but when the frequency constraint is included, significantly more time is spent in the optimization solver. It is also interesting to note that while the number of iterations increases in the SAND formulation when frequency constraints are included, it

DOI: 10.1002/we
Prepared using weauth.cls

Table VII. Comparison of computation time for SAND and nested formulations with and without ω-constraint.

	SAND $6n_{sec}$ with ω-constraint	SAND $6n_{sec}$	Nested $6n_{sec}$ with ω-constraint	Nested $6n_{sec}$
Number of iterations	77	66	59	79
CPU-time IPOPT	252.8 s	58.9 s	13.2 s	11.9 s
CPU-time Matlab	150.5 s	90.0 s	165.1 s	134.4 s
CPU-time Total	403.3 s	148.9 s	178.3 s	146.3 s
Time in Matlab per iteration	1.95 s	1.36 s	2.80 s	1.70 s

decreases for the nested formulation. For the specific problem studied here, SAND and Nested formulations are therefore equivalently effective in terms of solving the problem, but that the solution time is more stable for the Nested formulation.

4. CONCLUSION

In this paper we presented an approach for conceptual optimal design of jacket structures. The method uses static load cases to model fatigue constraints and the problems are solved using gradient based optimization. Sizing optimization of a jacket is performed in a few minutes on a laptop. We also demonstrated how this optimization approach can be used in a conceptual design investigation by providing design trends for changes to leg distance, variable linking options, and number of sections.

We found that the linear constraints, static fatigue and column buckling constraints were mostly driving the design. When the member lengths were decreased by either decreasing the leg distance or increasing the number of sections, the column buckling constraints had less influence on the design. The first frequency was only slightly affected by changes to the jacket design, but the frequency constraint had a significant effect on the performance of the optimal design problem. Because the frequency constraints significantly reduces the feasible design space, the problems solved faster when those constraints were removed.

Based on the conceptual design investigations, it seems that a good jacket design has almost vertical legs. This reduces the stress concentrations in the welds, and avoids the case where some members are very much longer than others. Since the welded joints are design driving, a mass reduction of about 22 percent can be gained from using stubs and cans. Further mass reduction of 16 percent can be gained by reducing the bottom leg distance and adding an extra section compared to the reference structure.

In future works, the static fatigue model should be compared with more advanced analysis techniques, and the optimal design from the presented approach should also be compared with optimal designs from other optimization methods. It would also be of interest to investigate other conceptual design decisions, such as number of legs, foundation type, transition piece type, pile stick up length, and jacket height.

ACKNOWLEDGEMENT

The research presented in this manuscript is part of the strategic research project ABYSS (www.abyss.dk) sponsored by the Danish Council for Strategic Research, Grant no. 1305-00020B. The funding is gratefully acknowledged.

REFERENCES

1. DNV-RP-C202 Buckling Strength of Shells. Technical report, DNV, 2013.
2. DNVGL-RP-C203 Fatigue design of offshore steel structures. Technical report, DNVGL, 2014.
3. DNVGL-OS-C101 Design of Offshore Steel Structures, general - LRFD method. Technical report, DNVGL, 2015.
4. J S Arora and Q Wang. Review of formulations for structural and mechanical system optimization. *Structural and Multidisciplinary Optimization*, 30(4):251–272, 2005.
5. ASTM. Standard Practices for Cycle Counting in Fatigue Analysis. Technical Report Reapproved 2011, ASTM, 1985.
6. C Bak, F Zahle, R Bitsche, T Kim, A Yde, L C Henriksen, A Natarajan, and M Hansen. The DTU 10 MW reference wind turbine. Technical report, DTU Wind Energy, 2013.
7. A Bazoune, Y A Khulief, and N G Stephen. Shape functions of three-dimensional Timoshenko beam element. *Journal of Sound and Vibration*, 259(2):473–480, 2003.

8. T Borstel. Design report - reference jacket. Technical Report D4.3.1, Ramboll, 2013. url: http://www.innwind.eu/publications/deliverable-reports, accessed 2017-02-13.
9. T M Cameron, A C Thirunavukarasu, and M E M El-Sayed. Optimization of frame structures with flexible joints. *Structural and Multidisciplinary Optimization*, 19(3):204–213, 2000.
10. K H Chew, K Tai, E Y K Ng, and M Muskulus. Analytical gradient-based optimization of offshore wind turbine substructures under fatigue and extreme loads. *Marine Structures*, 47:23–41, 2016.
11. R D Cook, D S Malkus, M E Plesha, and R J Witt. *Concepts and Applications of Finite Element Analysis*. John Wiley & Sons, fourth edition, 2007.
12. R Damiani, Ning A, B Maples, A Smith, and K Dykes. Scenario analysis for techno-economic model development of U.S. offshore wind support structures. *Wind Energy*, 20(4):731–747, 2017.
13. European Technology and Innovation Platform on Wind Energy. Strategic research and innovation agenda 2016. Technical report, European Technology & Innovation Platform on Wind Energy (ETIP Wind), 2016.
14. R L Fox and M P Kapoor. Rate of change of eigenvalues and eigenvectors. *AIAA Journal*, 6(12):2426–2429, 1968.
15. I Grossman, V T Voudouris, and O Ghattas. Mixed-integer linear programming formulations of some nonlinear discrete design optimization problems. In C A Floudas and P M Pardalos, editors, *Recent Advances in Global Optimization*. Princeton University Press, 1992.
16. R T Haftka. Simultaneous analysis and design. *AIAA Journal*, 23(7):1099–1103, 1985.
17. J H Holland. Genetic Algorithms. *Scientific American*, 267(1):66–72, 1992.
18. H Long and G Moe. Preliminary Design of Bottom-Fixed Lattice Offshore Wind Turbine Towers in the Fatigue Limit State by the Frequency Domain Method. *Journal of Offshore Mechanics and Arctic Engineering*, 134(3):031902, 2012.
19. H Long, G Moe, and T Fischer. Lattice Towers for Bottom-Fixed Offshore Wind Turbines in the Ultimate Limit State: Variation of Some Geometric Parameters. *Journal of Offshore Mechanics and Arctic Engineering*, 134(2):021202, 2012.
20. D G Maringer. Heuristic Optimization. In *Portfolio Management with Heuristic Optimization*, chapter 2, pages 38–76. Springer, 2005.
21. M A Miner. Cumulative damage in fatigue. *Journal of Applied Mechanics*, 12(3):A159–A164, 1945.
22. M Muskulus and S Schafhirt. Design Optimization of Wind Turbine Support Structures A Review. *Journal of Ocean and Wind Energy*, 1(1):12–22, 2014.
23. J Oest, R Sørensen, L C T Overgaard, and E Lund. Structural optimization with fatigue and ultimate limit constraints of jacket structures for large offshore wind turbines. *Structural and Multidisciplinary Optimization*, 55(3):779–793, 2017.
24. 4C Offshore. Jacket or Lattice Structures, 2013. url: www.4coffshore.com/windfarms/jacket-or-lattice-structures-aid5.html, accessed 2017-06-01.
25. C B W Pedersen. Crashworthiness design of transient frame structures using topology optimization. *Computer Methods in Applied Mechanics and Engineering*, 193(6-8):653–678, 2004.
26. P Pedersen and L Jørgensen. Minimum mass design of elastic frames subjected to multiple load cases. *Computers and Structures*, 18(1):147–157, 1984.
27. S Rojas Labanda and M Stolpe. Benchmarking optimization solvers for structural topology optimization. *Structural and Multidisciplinary Optimization*, 52(3):527–547, 2015.
28. S Schafhirt, D Zwick, and M Muskulus. Two-stage local optimization of lattice type support structures for offshore wind turbines. *Ocean Engineering*, 117:163–173, 2016.
29. M Seidel, S Voormeeren, and J B van der Steen. State-of-the-art design processes for offshore wind turbine support structures. *Stahlbau*, 85(9):583–590, 2016.
30. M Stolpe and K Svanberg. Modeling topology optimization problems as linear mixed 0–1 programs. *International Journal for Numerical Methods in Engineering*, 57(5):723–739, 2003.
31. The Crown Estate. Offshore wind cost reduction-Pathways study. 2012.
32. A Wächter and L T Biegler. On the Implementation of a Primal-Dual Interior Point Filter Line Search Algorithm for Large-Scale Nonlinear Programming. *Mathematical Programming*, 106(1):25–57, 2006.

DOI: 10.1002/we
Prepared using weauth.cls

Paper II

J. Oest, K. Sandal, S. Schafhirt, L. E. S. Stieng, M. Muskulus, On gradient-based optimization of jacket structures for offshore wind turbines. Submitted to *Wind Energy*, under review.

WIND ENERGY
Wind Energ. 0000; **00**:1–15
DOI: 10.1002/we

Research Article

On gradient-based optimization of jacket structures for offshore wind turbines

Jacob Oest[1], Kasper Sandal[2], Sebastian Schafhirt[3], Lars Einar S. Stieng[3], Michael Muskulus[3]

[1]Department of Materials and Production, Aalborg University, Aalborg East, Denmark
[2]Department of Wind Energy, Technical University of Denmark, Risø Campus, Roskilde, Denmark
[3]Department of Civil and Environmental Engineering, Norwegian University of Science and Technology NTNU, Trondheim, Norway

ABSTRACT

During the bidding or very early design phases of jacket structures for offshore wind turbines, there may be very limited information available on weather conditions, soil conditions, turbine specifications etc. However, it is still extremely important to quickly produce near-optimal designs with production costs similar to that of the final support structure. Numerical optimization methods can be used to this purpose. This paper investigates three gradient-based optimization methods where preliminary designs are produced by minimization of mass optimization of cross-sectional areas with fatigue and frequency constraints. The three methods are based on (i) damage equivalent loads, (ii) quasi-static analysis, and (iii) dynamic analysis. The optimizations are carried out using in-house software JADOP (JAcket Design OPtimization), and the optimized designs are evaluated using state-of-the-art integrated time-domain simulation software FEDEM Windpower. The findings show that each analysis can be applied with success. However, if excitations of structural frequencies contribute significantly to the overall damage, special care must be taken with quasi-static and static modeling. It is observed that wave-loading does not contribute considerably to the fatigue damage. Additionally, the aerodynamic loading does not change significantly with large sizing changes of cross-sectional areas. The optimized designs are partly driven by reducing stress concentration factors, which can be achieved by reducing the chord diameter to thickness ratio. Thus, the optimized designs resemble each other to a certain extent. Copyright © 0000 John Wiley & Sons, Ltd.

KEYWORDS

offshore wind; jacket support structures; optimization; analytical sensitivities; fatigue

Correspondence
J. Oest, Department of Materials and Production, Aalborg University, Fibigerstraede 16, 9220 Aalborg East, Denmark.
E-mail: oest@make.aau.dk

Received . . .

1. INTRODUCTION

Wind energy is a reliable and important supplier of sustainable energy. In favourable site conditions, the levelized cost of energy can be comparable to conventional energy sources. However, such site-conditions are limited. Off-coastal areas often contain great wind conditions and space for large wind-farms, but offshore wind energy is in general more expensive than onshore wind energy [1, 2]. In deep waters, jacket structures are generally considered the most cost-effective bottom-fixed support structure. Deep water conditions increase the levelized cost of energy due to larger support structures, more expensive infrastructure and higher installation and maintenance costs. Support structures account for about 19% of the total cost of an offshore wind farm [3]. Design, manufacturing, and installation of support structures have been identified as areas of large cost saving potential [4, 5].

Human designers are often restricted to a very limited number of design iterations due to time- and cost-related considerations. Computer-aided structural optimization techniques are not restricted in the same manner. For this reason, structural optimization techniques are increasingly being applied in wind energy. In general, there are two types of numerical optimization techniques that can be applied. There are heuristic methods and gradient-based methods. Both methods have their strengths and weaknesses, and both have been applied to optimization of support structures.

Prepared using weauth.cls [Version: 2010/06/17 v1.00]

Heuristic methods are update schemes often based on analogies from behaviours observed in nature. Heuristic methods rely on function values alone and are therefore also referred to as gradient-free methods. However, as the methods do not utilize design sensitivities, they often require many design iterations before convergence.

Some of the first work in the field of structural optimization of wind turbine support structures was using gradient-free methods to optimize monopile structures [6]. Since then, much work has been done on optimizing both onshore and offshore monopile structures using gradient-free methods [7, 8, 9]. As jackets gained in popularity, different gradient-free methods have also been applied in the design thereof [10, 11, 12, 13, 14]. A different approach to efficient optimization is shown in [15]. By using a two-stage approach where the optimization of cross-sectional area and Stress Concentration Factors (SCFs) are assumed independent of the structural analysis, the computational effort is greatly reduced in the jacket optimization.

Gradient-based optimization methods often converge in fewer iterations than gradient-free optimization. However, at least first order derivatives of cost and constraint functions are necessary. In [16] a method of gradient-based optimization of tower and turbine to reduce the levelized cost of energy is presented. In the optimization, stress, fatigue, and frequency constraints on both tower and turbine, as well as blade tip deflection are considered. The design sensitivities are estimated using finite difference approximations. The optimization framework was further developed in [17], where both the wind farm layout and the offshore monopile are optimized, again using finite difference approximations of the design sensitivities. Using finite difference schemes can be efficient, but care must be taken as the sensitivities are very sensitive to perturbation size [18, 19].

Analytical gradient-based optimization of a jacket structure is solved in [20, 21], where a dynamic analysis is employed. The optimization reduces the overall mass subject to ultimate limit state (ULS) constraints, to fatigue limit state (FLS) constraints, and to frequency constraints. In [19] analytical gradient-based optimization of a jacket is solved using a quasi-static analysis to lower the computational costs. For a more detailed overview of optimization of support structures, see [22].

The designer of the support structure may be different from the designer of the tower and turbine. Thus, it may prove time-consuming to obtain updated loading conditions when the substructure is altered. The challenge is to design a jacket based on initial information, that has an accumulated damage near the fatigue limit when re-evaluated with updated loading conditions. This paper investigates this problem using three state-of-the-art analytical gradient-based sizing optimization methods with fatigue and frequency constraints. All three methods utilize linear finite element theory and beam elements. Additionally, all three methods use the Hot Spot Stress (HSS) method where SCFs are applied according to the recommended practice [23]. The three different approaches can be classified by their respective structural analysis method. In other words, the approaches are using (i) a static analysis, (ii) a quasi-static analysis, and (iii) a dynamic analysis. The approach in (i) uses damage equivalent loads (DEL) [24]. It follows that a static analysis is much faster than a quasi-static analysis. In turn, the quasi-static analysis is faster than the dynamic analysis. However, it also follows that the dynamic analysis is more accurate than the quasi-static analysis and the static analysis.

Neither of the three optimization approaches attempt to produce fully validated and readily producible designs, but rather very good preliminary designs. In this framework, a good design is defined as having a low mass and fatigue damage levels near the desired value when reevaluated using state-of-the-art integrated time-domain simulations, here performed with the commercial software FEDEM Windpower (Fedem Technology AS, Trondheim, Norway, Version R7.2.1). It must be noted that the optimized designs should not be directly compared to the original reference design, as the design basis is completely different.

2. METHODS

The applied design process can be described using a flow chart, see Figure 1. An initial design is used to generate a finite element representation of the structure in JADOP. This structure is exported to FEDEM Windpower using the application programming interface. In FEDEM Windpower the jacket is attached to a predefined wind turbine. Next, a transient analysis of the entire structure is performed, and the results are extracted. The results are used to deconvolute the loading conditions, such that forces and moments corresponding to the wind-induced loads can be applied in JADOP. Then, the optimal design problems are formulated in JADOP, where cross-sectional areas are optimized using IPOPT (Interior Point OPTimizer, [25]). The optimized design is reevaluated in FEDEM Windpower using a full transient multibody analysis with an integrated turbine and recalculated wave-loads. Nodal displacements from the integrated analysis are post-processed in JADOP such that SCFs can be used in the fatigue analysis.

To achieve fully optimized designs, the optimization process can be restarted using updated rotor and wave loads. At this stage, it is recommended to include more constraints such as ULS and manufacturing constraints. This is not a focus area in the present work. Thus, the presented work can be considered a benchmark of the three methods rather than an attempt to produce a fully optimized design.

Wind Energ. 0000; **00**:1–15 © 0000 John Wiley & Sons, Ltd.
DOI: 10.1002/we
Prepared using weauth.cls

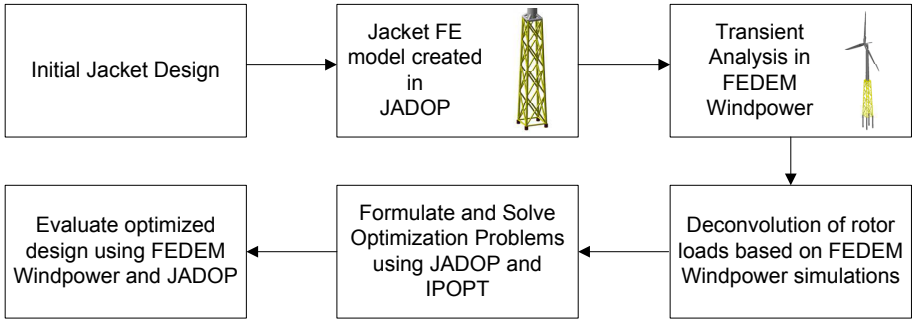

Figure 1. The applied design process.

2.1. Structural analysis

A linear elastic finite element analysis is used, and the jacket is modeled using two-node Timoshenko beam elements with six degrees-of-freedom in each node [26]. The equilibrium at time t is:

$$\boldsymbol{M}(\boldsymbol{x})\ddot{\boldsymbol{U}}(\boldsymbol{x},t) + \boldsymbol{C}(\boldsymbol{x})\dot{\boldsymbol{U}}(\boldsymbol{x},t) + \boldsymbol{K}(\boldsymbol{x})\boldsymbol{U}(\boldsymbol{x},t) = \boldsymbol{P}(t) \tag{1}$$

$\boldsymbol{x}$ is the vector of design variables (diameters and thicknesses), $\boldsymbol{M}$ is the mass matrix, $\boldsymbol{C}$ is the damping matrix, and $\boldsymbol{K}$ is the stiffness matrix. $\boldsymbol{P}$ is the load vector assumed independent of design changes. $\boldsymbol{U}, \dot{\boldsymbol{U}}$, and $\ddot{\boldsymbol{U}}$ are the vectors of global displacements, velocities and accelerations, respectively. In the quasi-static approach, the mass and damping terms are omitted. A consistent mass matrix $\boldsymbol{M}$ is applied. The α and β parameters of the Rayleigh damping matrix $\boldsymbol{C}$ is tuned to 1% critical damping at the first eigenfrequency of the structure without the Rotor-Nacelle-Assembly (RNA) attached. Time-integration is performed using Newmark-β with constant average acceleration. The soil-structure boundary is simplified as fixed. The analyses in JADOP and FEDEM Windpower have been compared and differences in displacements are generally $< 1\%$.

Jacket structures are dominated by normal stresses. Thus, the recommended practice for fatigue assessment in welded tubular joints combines normal stresses with SCFs [23]. SCFs are design-dependent scaling factors. There are separate SCFs to scale damage caused by normal stress from normal forces (N), from in-plane bending moments (MIP), and from out-of-plane bending moments (MOP). The normal stresses in each element e is:

$$\begin{bmatrix} \sigma_e^{\mathrm{N}}(\boldsymbol{x},\boldsymbol{U}(\boldsymbol{x},t)) \\ \sigma_e^{\mathrm{MIP}}(\boldsymbol{x},\boldsymbol{U}(\boldsymbol{x},t)) \\ \sigma_e^{\mathrm{MOP}}(\boldsymbol{x},\boldsymbol{U}(\boldsymbol{x},t)) \end{bmatrix} = \boldsymbol{E}\boldsymbol{B}_{\boldsymbol{xx}}(\boldsymbol{x})\boldsymbol{u}_e(\boldsymbol{x},t), \quad \forall e \tag{2}$$

$\boldsymbol{E}$ is the constitutive matrix, $\boldsymbol{B}_{xx}$ is the strain-displacement matrix including only terms regarding normal stresses, and $\boldsymbol{u}_e$ is the element displacement vector. Let x, y, z be local element coordinates, then the sampling locations must be located as shown in Figure 2. The scaled stress σ_i for location i is:

$$\sigma_i(\boldsymbol{x},\boldsymbol{U}(\boldsymbol{x},t)) = \begin{bmatrix} SCF_i^{\mathrm{N}}(\boldsymbol{x}) & SCF_i^{\mathrm{MIP}}(\boldsymbol{x}) & SCF_i^{\mathrm{MOP}}(\boldsymbol{x}) \end{bmatrix} \boldsymbol{E}\boldsymbol{B}_{\boldsymbol{xx}}(\boldsymbol{x})\boldsymbol{u}_e(\boldsymbol{x},t), \quad \forall i \tag{3}$$

Here $SCF_i^{\mathrm{N}}, SCF_i^{\mathrm{MIP}}$, and SCF_i^{MOP} are the SCFs for the stresses caused by axial forces, in-plane moments, and out-of-plane moments, respectively, for location i. The SCFs are explicit functions of the design variables, the connection type, and the loading type. The equations were derived using 3D shell finite element analyses [27, 28].

Restrictions must be enforced on the design variables to ensure reliable results using the HSS method. If a subscript b refers to a brace element, and a subscript c refers to a chord element, the diameters d and thicknesses t must for all relations

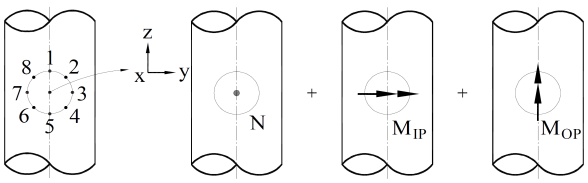

Figure 2. Stresses in the circumference of a weld are determined by superposition of stresses caused by the normal force N, the in-plane bending moment M_{IP}, and the out-of-plane bending moment M_{OP}. Figure adapted from [23].

DLC	v [m/s]	TI [%]	H_s [m]	T_p [s]	γ	Occurences/year [hrs]
1.2	6	17.5	1.18	5.76	1.0	4730.1
	14	14.2	1.91	6.07	1.0	3388.1
	22	13.3	3.09	7.40	1.0	647.8

Table I. Environmental loading conditions from [30]. v is the mean wind speed, TI is the turbulence intensity, H_s is the significant wave height, T_p is the wave period, and γ is the peak enhancement factor.

satisfy [23]:

$$\frac{d_c}{5} \leq d_b \leq d_c \tag{4}$$

$$\frac{t_c}{5} \leq t_b \leq t_c \tag{5}$$

Additionally, for each element:

$$16t_e \leq d_e \leq 64t_e, \qquad \forall e \tag{6}$$

These linear constraints are reformulated and collectively referred to as $\boldsymbol{Ax} \leq \boldsymbol{b}$.

2.2. Loading conditions

One Design Load Case (DLC) from IEC 61400-3 [29] is used, specifically the FLS power production DLC 1.2. Three ten minutes load series are included, see Table I. The three load series are linearly scaled to represent the lifetime using weather statistics of the K13 deep water site [30]. Accurate load reduction is not a focus area of this work and we instead refer to published literature on the subject, e.g. [31]. The loading conditions are assumed fixed in the optimization.

2.2.1. Aerodynamic loading

The application of aerodynamic loads differs among the three analyses. The dynamic analysis in FEDEM Windpower allows for an aero-elastic simulation under inflow turbulence environment, while the quasi-static and dynamic analyses in JADOP are performed with pre-computed force and moment time-series applied on tower top. The static analysis requires a DEL as described in Section 2.3. FEDEM Windpower is utilized to generate rotor loads (i.e. time-series for forces and moments that are applied in JADOP) that represent the time-dependent rotor loads from an integrated transient analysis. The precomputed rotor loads lead to the same structural response as the integrated analysis that was used to generate these force and moment time-series. An algorithm that is based on a discrete convolution method is used for this purpose.

The method is described for a single degree-of-freedom, but it is straightforward to apply to a multi degree-of-freedom system [32]. The effect of a general load time-history $f(t)$ on a linear system at an arbitrary point in time $t = \tau$ can be considered as the effect to an infinitesimal impulse load. The impulse load causes a response of the system for $t > \tau$ that is given by

$$du(t;\tau) = h(t-\tau)f(\tau)d\tau \tag{7}$$

$h(t)$ is the Impulse Response Function (IRF). The total response of the system $u(t)$ at time t can therefore be obtained by summing (integrating) all contributions to the response from the loads between times $\tau = 0$ to $\tau = t$. This leads to an integral expression for the response $u(t)$ that is often referred to as the Duhamel integral [33]:

$$u(t) = \int_0^t h(t-\tau)f(\tau)d\tau \tag{8}$$

The integral can also be written in a discretized version:

$$u_n = \sum_{i=0}^{n-1}(h_{n-i}f_i\Delta t) \tag{9}$$

Here u_n is the discretized displacement at time step n, h the discretized IRF, f the discretized excitation, and Δt the time step used in the dynamic simulation. Using the convolution integral in an inverse manner, a so-called deconvolution, allows for computing the input $f(t)$ (e.g. a load time-history applied on a certain degree of freedom) for a given response $u(t)$ (e.g. displacements at the same or a second degree-of-freedom). The transformed equation (9) is given by:

$$f_n = \frac{1}{h_1}\left(\frac{u_n}{\Delta t} - \sum_{i=1}^{n-1}(h_{n+1-i}f_i)\right) \tag{10}$$

Wind Energ. 0000; **00**:1–15 © 0000 John Wiley & Sons, Ltd.
DOI: 10.1002/we
Prepared using weauth.cls

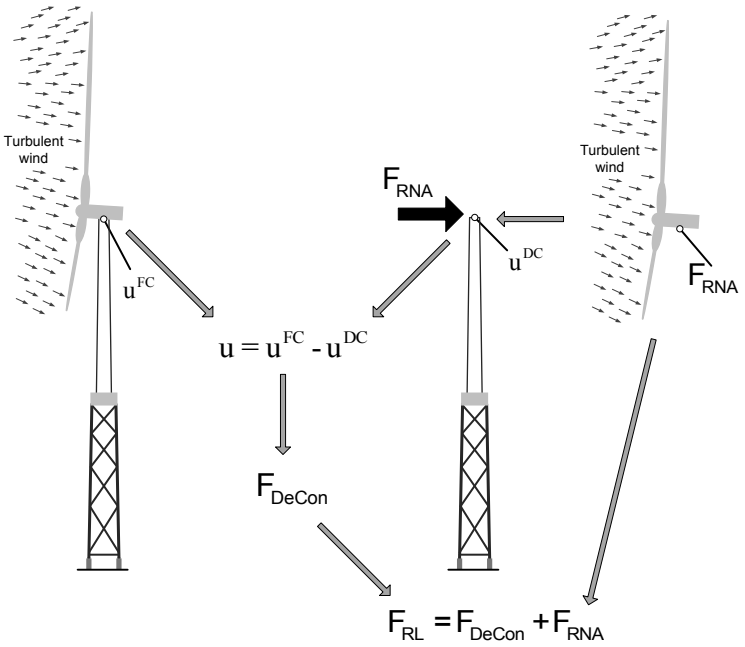

Figure 3. Deconvolution of rotor loads. The differences in tower top displacements from a dynamic analysis with the support structure fully-coupled (FC) to the rotor and from a decoupled (DC) model with precomputed loads (F_{RNA}) are used for the deconvolution. The sum of the deconvoluted loads (F_{DeCon}) and the precomputed loads (F_{RNA}) are applied as rotor loads (F_{RL}) in JADOP.

Equation (10) is prone to numerical issues, especially the minus sign and the fractions can lead to instability of the deconvolution algorithm. A possibility to overcome these numerical issues is used for this study.

A simulation of a standalone model of the RNA with fixed boundary conditions is performed using the same turbulent wind input as the dynamic analysis in FEDEM Windpower. Reaction forces and moments (F_{RNA}) are extracted from the bottom of the RNA and applied at tower top of the same numerical model that is used for the dynamic analysis. However, this second dynamic analysis is performed without aerodynamic calculations, but with the previously calculated forces and moments applied at tower top. The differences in tower top displacements between the dynamic analysis with aero-elastic simulation (fully-coupled) and the decoupled dynamic analysis using the precomputed rotor loads from a standalone turbine simulation ($u^{FC} - u^{DC}$) is afterwards used in equation (10) to calculate a corrective force (F_{DeCon}) that is added to the precomputed rotor loads from the standalone turbine simulation. A flow chart of this method is shown in Figure 3.

2.2.2. Hydrodynamic loading

In the quasi-static and dynamic approach it is possible to include hydrodynamic loading. Based on the wave kinematics for the JONSWAP spectrum [34], the wave forces f_w are determined using the Morison equation [35, 36]. Following offshore recommendations [29], Wheeler stretching is applied to extend the waves to above mean sea level. The wave forces are applied aligned with the main wind direction. For a fixed body the Morison equation is:

$$f_w(\boldsymbol{x}) = \rho_w C_m V \dot{u} + \frac{1}{2}\rho_w C_d A(\boldsymbol{x}) u|u| \tag{11}$$

ρ_w is the water density, C_m and C_d are coefficients for added mass and drag. In this work, the coefficients are assumed fixed and set conservatively to $C_m = C_d = 2$. V is the volume of the body and A is the reference area per unit cylinder length. Thus, for a circular cylinder $A = D$ and $V = \frac{1}{4}\pi D^2$.

The Morison equation assumes that the water particle velocity u and acceleration $\dot{u}$ are perpendicular to the center axis of the cylinder. However, the jacket members are oriented in a variety of ways, and thus the tangential contributions of the distributed wave forces are neglected.

2.3. Fatigue analysis

To simplify the notation, the dependencies on the design variables $\boldsymbol{x}$ and on the state variables $\boldsymbol{U}(\boldsymbol{x}, t)$ are no longer shown. In the quasi-static and dynamic approach, the fatigue analysis follows the recommended practice [23]. The accumulated

damage D_i in location i is determined using Palmgren-Miner's rule [37, 38] and a bilinear S-N relationship:

$$D_i = \sum_{j=1}^{3} c_j \sum_{k=1}^{n_k} \frac{n_{ijk}}{N_{ijk}} \leq \eta \tag{12}$$

$$\log(N_{ijk}) = \log(\bar{a}) - m\log(\Delta\sigma_{ijk}) \tag{13}$$

Here c_j is a scaling factor for each load case $j = 1, 2, 3$ to make the data represent 20 years, and is based on weather data in [30]. Traditional rainflow-counting is performed to determine the stress range $\Delta\sigma_{ijk}$ [39]. N_{ijk} is the expected cycles to failure at location i, load case j, and stress state k. Likewise, n_{ijk} is the number of load cycles. n_k is the number of stress cycles and $\eta = 1$ is the allowable damage, also referred to as the utilization factor. (12) constitutes the fatigue constraint equations in the quasi-static and dynamic approaches. Assuming that all steel members are submerged in seawater, the material parameters are [23]:

$$\log(\bar{a}) = \begin{cases} 11.764, & \text{if } \Delta\sigma_{ijk} \geq 83.41\text{MPa.} \\ 15.606, & \text{otherwise.} \end{cases} \qquad m = \begin{cases} 3.0, & \text{if } \Delta\sigma_{ijk} \geq 83.41\text{MPa.} \\ 5.0, & \text{otherwise.} \end{cases}$$

In the DEL approach, the structure is subject to a harmonic load with a frequency of 1 Hz and a load range of $\Delta P^{1\text{Hz}}$. The DEL accumulated damage $D_i^{1\text{Hz}}$ is:

$$D_i^{1\text{Hz}} = \frac{n_T}{N_i^{1\text{Hz}}} \tag{14}$$

$n_T = \sum_{j=1}^{3} c_j n_S$ is the total lifetime, with $n_S = 600$ s being the simulated time per load case. $N_i^{1\text{Hz}}$ is the expected number of cycles to failure for the DEL approach. Assuming one-degree-of-freedom loading and quasi-static structural response, the stresses scale linearly with the load, $\sigma_i = \alpha_i \boldsymbol{P}$. We set $D_i^{1\text{Hz}} = D_i$ and solve for the load range:

$$\frac{n_T(\alpha_i \Delta \boldsymbol{P}^{1\text{Hz}})^m}{\bar{a}} = \sum_{j=1}^{3} c_j \sum_{k=1}^{n_k} \frac{n_{jk}(\alpha_i \Delta \boldsymbol{P}_{jk})^m}{\bar{a}} \tag{15}$$

$$\Rightarrow \Delta \boldsymbol{P}^{1\text{Hz}} = \left(\frac{1}{n_T} \sum_{j=1}^{3} c_j \sum_{k=1}^{n_k} n_{jk} (\Delta \boldsymbol{P}_{jk})^m \right)^{\frac{1}{m}} \tag{16}$$

Note that the DEL approach does not allow for bilinear S-N relations. $\log(\bar{a}) = 11.764$ and $m = 3.0$ are conservatively chosen. The stress range $\Delta\sigma_i^{1\text{Hz}}$ from the harmonic load is the absolute value of the stress when $\Delta \boldsymbol{P}^{1\text{Hz}}$ is applied as a static load. Thus, the DEL accumulated damage is:

$$D_i^{1\text{Hz}} = \frac{n_T(|\sigma_i^{1\text{Hz}}|)^m}{\bar{a}} \leq \eta \tag{17}$$

This can be reformulated into a stress constraint bounded by a lower $\underline{\Delta\sigma}$ and an upper $\overline{\Delta\sigma}$ stress range limit:

$$\underline{\Delta\sigma} = -\left(\frac{\eta\bar{a}}{n_T}\right)^{\frac{1}{m}} \leq \sigma_i^{1\text{Hz}} \leq \left(\frac{\eta\bar{a}}{n_T}\right)^{\frac{1}{m}} = \overline{\Delta\sigma}, \tag{18}$$

This equation constitutes the DEL constraints.

Although the DEL is generally limited to one-degree-of-freedom loading, two load scenarios that include more load-components are applied based on recommendations in [40]. A thrust dominated load, which in theory should be design driving for the legs, and a torsion dominated load, which is expected to be design driving for the braces.

- Thrust-based: F_x, M_y, and $\frac{1}{2}M_z$
- Torsion-based: $\frac{1}{2}F_x$, $\frac{1}{2}M_y$ and M_z

Both load scenarios include all three load cases. As two load scenarios are used, there are twice the amount of fatigue constraints, $2 \cdot n_i$, in the DEL approach as compared with the other approaches.

2.4. Frequency analysis

The eigenfrequencies ω_l are determined by the finite element formulation of a real, symmetric eigenvalue problem:

$$\boldsymbol{K}\boldsymbol{\phi}_l = \lambda_l \boldsymbol{M}\boldsymbol{\phi}_l, \quad \omega_l = \sqrt{\frac{\lambda_i}{2\pi}}, \quad l = 1, 2, ..., n_l \tag{19}$$

DOI: 10.1002/we
Prepared using weauth.cls

Parameter	Value
mu stategy	'adaptive'
nlp scaling method	'none'
hessian approximation	'limited-memory'
tol	10^{-5}
max iter	100

Table II. IPOPT settings different from default.

Here ϕ_l and λ_l represent the eigenvector and eigenvalue, respectively. The eigenvalues have been sorted such that $\lambda_1 < \lambda_2 < ... < \lambda_{n_l}$. Distinct eigenvalues are assumed.

The initial jacket is designed to have the lowest eigenfrequencies in the soft-stiff region, i.e. between the rotor (1P) and blade passing (3P) frequency bands. In the optimization, the first fore-aft and side-to-side frequencies are constrained to lie within these limits with a ten percent safety-margin, i.e. 0.22 Hz $\leq f_l \leq 0.31$ Hz, $l = 1, 2$. Additionally, the third eigenfrequency is constrained to be above the 3P frequency. Thus, there are $n_l = 3$ frequency constraints.

2.5. Optimal design problems

The *minimization of mass* problem for the DEL approach is:

$$\begin{aligned}
\underset{\boldsymbol{x}\in\mathbb{R}^{n_v}}{\text{minimize}} \quad & f = \rho \sum_{e=1}^{n_e} A_e l_e \\
\text{subject to} \quad & \boldsymbol{A}\boldsymbol{x} \leq \boldsymbol{b} \\
& \underline{\Delta\sigma} \leq \Delta\sigma_i^{1Hz} \leq \overline{\Delta\sigma}, && i = 1, 2, ..., 2 \cdot n_i \\
& \underline{\omega_l} \leq \omega_l \leq \overline{\omega_l} && l = 1, 2, ..., n_l \\
& \underline{x_v} \leq x_v \leq \overline{x_v}, && v = 1, 2, ..., n_v
\end{aligned}$$

Here ρ is the material density of S355 steel, and A_e and l_e are the cross sectional area and length of element e, respectively. n_e is the total number of elements. $\underline{x_v}$ and $\overline{x_v}$ are the design variable bounds defined in (27), and n_v is the number of design variables. The optimization problem for the quasi-static and dynamic approach is:

$$\begin{aligned}
\underset{\boldsymbol{x}\in\mathbb{R}^{n_v}}{\text{minimize}} \quad & f = \rho \sum_{e=1}^{n_e} A_e l_e \\
\text{subject to} \quad & \boldsymbol{A}\boldsymbol{x} \leq \boldsymbol{b} \\
& D_i \leq \eta, && i = 1, 2, ..., n_i \\
& \underline{\omega_l} \leq \omega_l \leq \overline{\omega_l} && l = 1, 2, ..., n_l \\
& \underline{x_v} \leq x_v \leq \overline{x_v}, && v = 1, 2, ..., n_v
\end{aligned}$$

The optimization problems are solved using IPOPT. A few parameters have been altered from the default values, see Table II. A user-defined scaling is implemented, where the load, the structural matrices, and the objective functions are scaled with 10^{-5}. The Hessian is approximated using a limited-memory BFGS method. In addition to the convergence criteria in IPOPT, the optimization is set to stop if the relative design change $\Delta\boldsymbol{x}$ in an iteration (I) is below a limit:

$$\Delta\boldsymbol{x} = \frac{||\boldsymbol{x}^{(I-1)} - \boldsymbol{x}^{(I)}||}{||\underline{\boldsymbol{x}} - \overline{\boldsymbol{x}}||} \leq 10^{-5} \tag{20}$$

2.6. Design sensitivity analysis

The design sensitivity analysis of the DEL approach is performed using the direct differentiation method [41]. Using the chain rule, the stress sensitivity with respect to a design variable x_v is:

$$\frac{d\sigma_i^{1\text{Hz}}}{dx_v} = \frac{\partial\sigma_i^{1\text{Hz}}}{\partial x_v} + \frac{\partial\sigma_i^{1\text{Hz}}}{\partial \boldsymbol{U}^{1\text{Hz}}} \frac{d\boldsymbol{U}^{1\text{Hz}}}{dx_v} \tag{21}$$

The displacement sensitivity is found by differentiating (1) for the static case:

$$\boldsymbol{K} \frac{d\boldsymbol{U}^{1\text{Hz}}}{dx_v} = -\frac{d\boldsymbol{K}}{dx_v} \boldsymbol{U}^{1\text{Hz}} \tag{22}$$

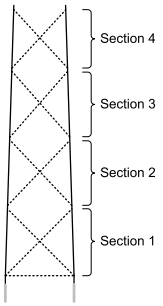

Figure 4. Design variables. Solid line represents legs and dotted line represents braces.

Section	Design Variable	d [mm]	t [mm]
4	Legs	800	20
4	Braces	200	35
3	Legs	800	20
3	Braces	300	35
2	Legs	800	20
2	Braces	300	35
1	Legs	800	20
1	Braces	300	50

Table III. Initial diameters and thicknesses.

The loading is assumed design independent, thus $\frac{d\boldsymbol{P}^{1\text{Hz}}}{dx_v} = 0$. The same assumption is made in the quasi-static and dynamic approaches.

Differentiating the quasi-static and dynamic constraint equation (12) with respect to a design variable gives:

$$\frac{dD_i}{dx_v} = \frac{\partial D_i}{\partial x_v} + \sum_{j=1}^{3}\sum_{k=1}^{n_k} \frac{\partial D_i}{\partial \Delta \boldsymbol{U}_{jk}} \frac{d\Delta \boldsymbol{U}_{jk}}{dx_v} \tag{23}$$

For the quasi-static approach, the full derivative of the displacement range for every load case j, and every stress state k, are found by:

$$\boldsymbol{K}\frac{d\Delta \boldsymbol{U}_{jk}}{dx_v} = -\frac{d\boldsymbol{K}}{dx_v}\Delta \boldsymbol{U}_{jk}, \qquad j = 1,2,3 \qquad k = 1,...,n_k \tag{24}$$

It can be seen that the computational cost of the quasi-static approach is much higher than the static approach as this equation needs to be solved many times.

The dynamic design sensitivities differ from the quasi-static approach in computational cost primarily for the displacement sensitivities. The design sensitivity is given by (23), and the displacement sensitivities are:

$$\boldsymbol{K}\frac{d\Delta \boldsymbol{U}_{jk}}{dx_v} = -\frac{d\boldsymbol{M}}{dx_v}\Delta \ddot{\boldsymbol{U}}_{jk} - \boldsymbol{M}\frac{d\Delta \ddot{\boldsymbol{U}}_{jk}}{dx_v} - \frac{d\boldsymbol{C}}{dx_v}\Delta \dot{\boldsymbol{U}}_{jk} - \boldsymbol{C}\frac{d\Delta \dot{\boldsymbol{U}}_{jk}}{dx_v} - \frac{d\boldsymbol{K}}{dx_v}\Delta \boldsymbol{U}_{jk},\ j = 1,2,3\ k = 1,...,n_k \tag{25}$$

In order to solve this differential equation, time integration is necessary. Thus, it is computationally more costly than the quasi-static counterpart. The derivative of the mass and stiffness matrices are computationally cheap. As Rayleigh damping is applied, the derivative of the damping matrix is a weighted sum of the derivative of the mass and stiffness matrices. From the above equations, it is clear that the computational costs of the design sensitivities follow (22) $\ll$ (24) $<$ (25). Note that mode superposition can be applied in the quasi-static and dynamic approach to increase computational efficiency.

Assuming real distinct eigenvalues, the frequency sensitivity is [42]:

$$\frac{d\lambda_i}{dx_j} = \boldsymbol{\phi}_i^T \left(\frac{d\boldsymbol{K}}{dx_j} - \lambda_i \frac{d\mathbf{M}}{dx_j} \right) \boldsymbol{\phi}_i \tag{26}$$

The computational effort involved in the frequency analysis and its sensitivities is negligible.

3. NUMERICAL EXAMPLES

This section is comprised of two parts. First, the overall modeling accuracy is investigated, and then optimized designs are evaluated. The numerical examples are based on the OC4 reference jacket [43] with the NREL 5MW turbine [44]. The jacket is discretized using $n_e = 524$ finite elements and the damage is evaluated in $n_i = 4192$ locations. The braces and legs are optimized in each section, resulting in $n_v = 16$ design variables, see Figure 4 and Table III. The design variable bounds are:

$$300\,\text{mm} \leq d \leq 2000\,\text{mm}, \quad 15\,\text{mm} \leq t \leq 120\,\text{mm} \tag{27}$$

DOI: 10.1002/we
Prepared using weauth.cls

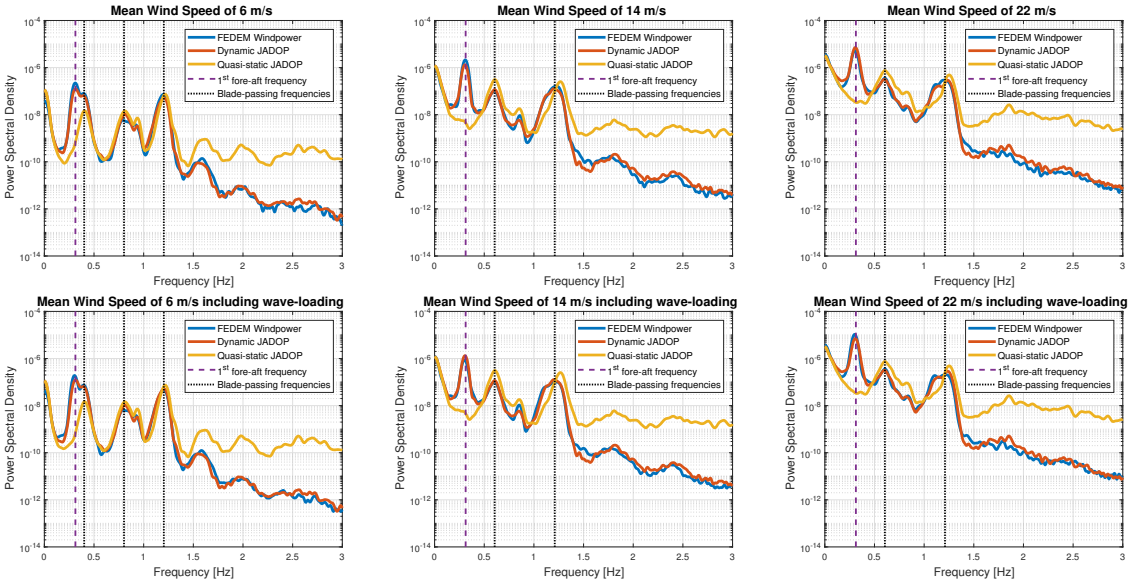

Figure 5. Power spectral densities of out-of-plane displacements in an X-brace in section 3. Very good agreement is seen between the dynamic analysis in JADOP using deconvoluted loads and the integrated analysis in FEDEM Windpower. Rotor frequencies are captured well by all methods, but structural frequencies cannot be captured by the quasi-static method as highlighted with the first fore-aft frequency.

3.1. Comparison of analyses

To ensure an optimization that presents reliable designs with accumulated damage near the utilization limit, a thorough understanding of the analyses is necessary. In the following, the accuracy of the damage estimates is investigated.

As seen in Table IV, the dynamic approach captures the maximum and mean damage values well. The static approach overpredicts the damage in two locations at section 4 in X-braces perpendicular to the wind-direction on either side of the jacket. Additionally, both the static and quasi-static analyses severely underestimate the damage in most X-braces, especially in X-braces aligned with the wind-direction.

The underestimates are primarily caused by the quasi-static analysis not correctly capturing all out-of-plane displacements in the X-braces. On Figure 5 a spectral analysis of the out-of-plane displacements in an X-brace aligned with the wind-direction in section 3 of the jacket is shown. It is clear that the errors are a direct result of excitations at a structural frequency which cannot be captured by quasi-static modeling. The rotor harmonics are captured well through the applied loading condition (see the 3P, 6P etc. peaks) for all analysis methods. Thus, quasi-static modeling should only be applied if fatigue damage from structural frequencies is negligible or otherwise accounted for. Lastly, note the very good agreement between the dynamic analysis with deconvoluted rotor loads and the integrated aero-elastic simulation in FEDEM Windpower.

Although investigations have shown that the modeling errors are design dependent (as they are primarily due to structural frequencies), a simple correction factor is proposed and tested in an optimization setting for the quasi-static and DEL approaches. The relationship between the mean damage of the applied method as compared with the integrated analysis can be used as a constant constraint scaling factor assumed fixed in all optimization iterations. The scaling values are taken directly from Table IV. In other words, the right-hand-side of the fatigue constraints are altered depending on the accuracy of the analysis of the initial design.

Method	Max Damage	Mean Damage
Dynamic JADOP	1.08	0.95
Quasi-static JADOP	0.86	0.49
Static JADOP	1.80	0.46

Table IV. Damage caused by aerodynamic loading in the static, quasi-static, and dynamic approach as compared with FEDEM Windpower. Values are normalized with respect to damage in the integrated analysis.

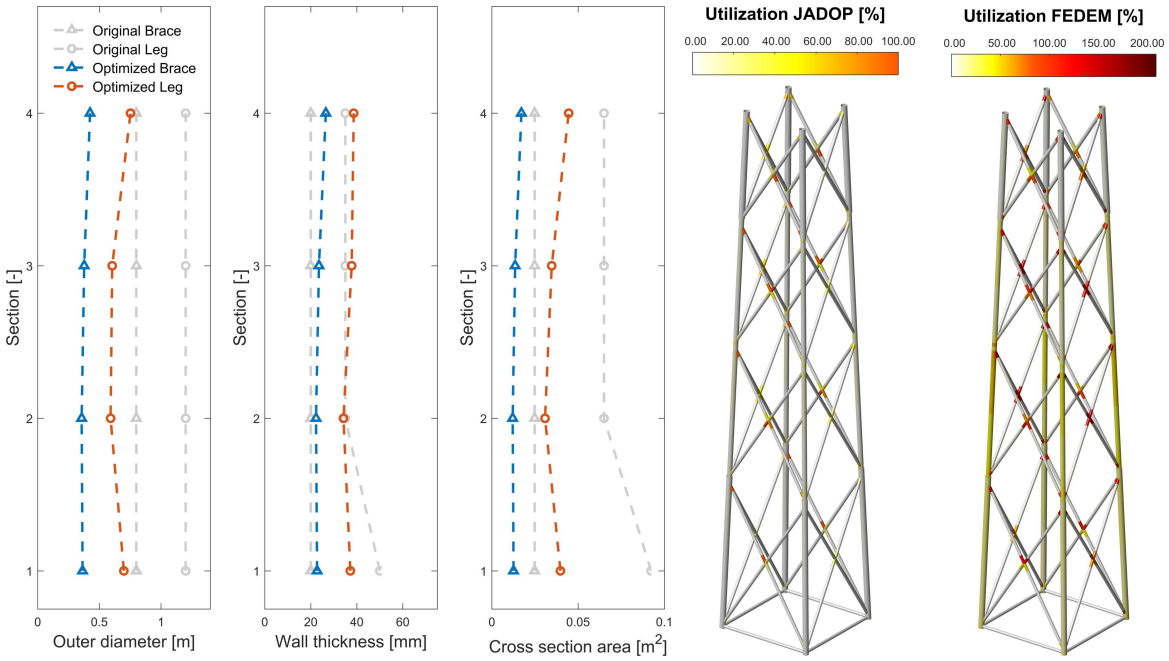

Figure 6. Jacket optimized using the DEL method. The same colormap is used for Figures 6-8.

A limitation of the DEL method is that wave-loads cannot be included. However, fatigue in jackets are in general not affected much by wave-loading. This claim is supported by the findings on Figure 5, as there is little difference in the power spectral densities with or without hydrodynamic loads.

3.2. Utilization of optimized designs

The DEL method achieved a reduction in mass of 48.17% in 42 iterations, see Table V and Figure 6. The highest damage is evaluated using FEDEM Windpower to be 2.09. The poor modeling accuracy in the static analysis in JADOP causes the design to become infeasible by a factor of two at the optimum. The quasi-static optimization reduces the mass by 51.86% in 53 iterations, with a highest damage of 2.81, see Figure 7. A light design is expected as the quasi-static analysis gives the lowest accumulated damage at the original design. The dynamic approach reduced the mass by 38.20% in 80 iterations, and has a highest accumulated damage of 0.75, see Figure 8. Thus, a feasible design is achieved without load recalculation. In Figure 9 the accumulated damage for each approach is illustrated. Due to the linear S-N curve in the DEL approach, the damage levels differ a lot from the quasi-static and dynamic approaches in JADOP. However, when the design is evaluated in FEDEM Windpower, the bilinear S-N curve is applied and the damage levels resemble the other methods more.

Using the constant constraint scaling as defined in Section 3.1, the performance of the DEL and quasi-static optimized designs are improved significantly. In fact, none of the two optimized designs have a highest fatigue damage more than 27% away from the optimal value. Considering the highly non-linear behaviour of fatigue, this is satisfactory.

All three optimization methods have been tested with a diagonal loading condition, i.e. rotated $45°$. It can be seen in Table V that load direction can have a significant influence on the design.

3.3. Influence of Stress Concentration Factors

As seen in Table V, the SCF values are decreased during the optimizations. In general, lowering the SCFs can be achieved by reducing the diameter to thickness ratios of the chords. In Figure 10, SCFs for all joint-types in the initial jacket are plotted with chord thickness $T = 0.0675m$ and brace thickness $t = T/2$, $t = T/3$, and $t = T/4$.

The amount of fatigue evaluations is prescribed in standards to be eight equally spaced locations in the circumference of the weld. However, previous studies show that the highest fatigue damage is not necessarily captured when using eight hotspots [45]. In this work the fatigue damage was captured within an acceptable level of accuracy using eight hotspots. Thus, this design-dependent issue is not further investigated.

Wind Energ. 0000; **00**:1–15 © 0000 John Wiley & Sons, Ltd.
DOI: 10.1002/we
Prepared using weauth.cls

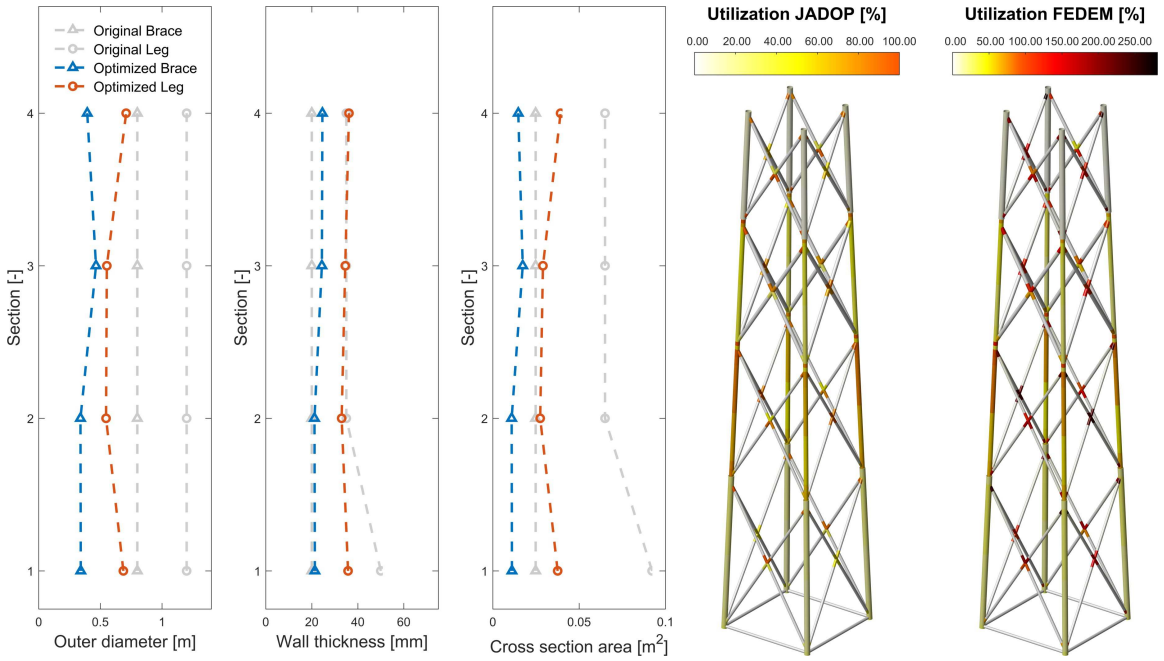

Figure 7. Jacket optimized using the quasi-static method. The same colormap is used for Figures 6-8.

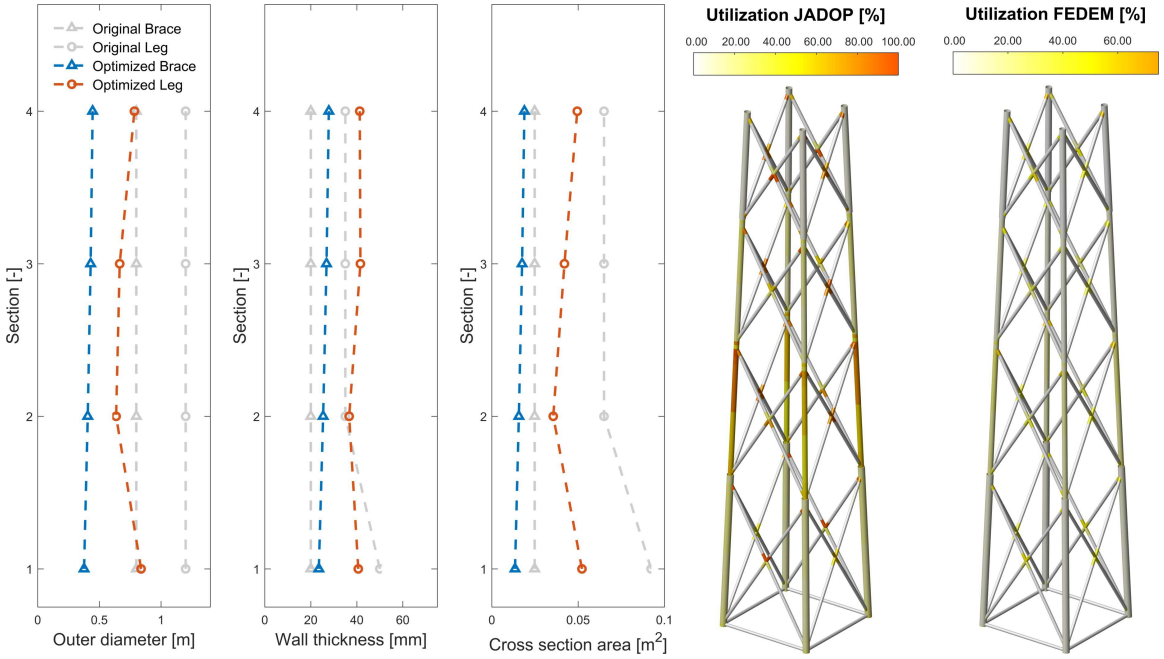

Figure 8. Jacket optimized using the dynamic method. The same colormap is used for Figures 6-8.

4. DISCUSSION

The accuracy of the analyses is reflected in the optimizations. The DEL method overestimates the damage significantly in a few hotspots. Thus, the method produces a design closer to feasibility than the quasi-static approach. However, the damage is better distributed in the quasi-static design. The dynamic approach generates a feasible design without a single load recalculation during the optimization.

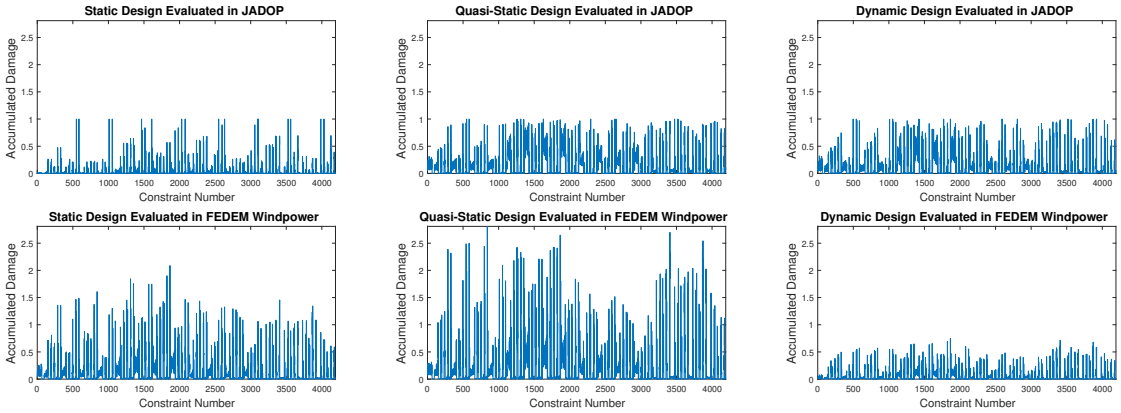

Figure 9. Fatigue damage values. JADOP optimized the quasi-static and dynamic design to a similar damage distribution. However, when evaluated in FEDEM Windpower, it is clear that the quasi-static approach produces an infeasible design.

	Optimization Settings				Optimization Results						
Method	Freq. constr.	Wave-loads	Load angle [°]	Constraint scaling	No of Iter.	Max dmg.	Max SCF	Mean SCF	Lowest freq. [Hz]	Mass red. [%]	Mass [ton]
Initial Design							6.54	3.21	0.31		540.21
DEL	Yes	No	0	-	42	2.09	3.63	2.23	0.26	48.17	279.97
	No	No	0	-	51	-	-	-	-	48.17	279.97
	Yes	No	45	-	35	1.88	3.75	2.36	0.27	45.29	295.53
	Yes	No	0	Yes	39	0.86	3.67	2.25	0.27	38.79	330.67
Quasi-static	Yes	Yes	0	-	53	2.81	3.56	2.24	0.25	51.86	260.04
	Yes	Yes	45	-	100	2.33	3.57	2.31	0.26	48.73	276.98
	Yes	No	0	-	42	3.09	3.48	2.19	0.25	54.02	248.39
	No	No	0	-	66	-	-	-	-	54.02	248.39
	Yes	Yes	0	Yes	55	1.27	3.51	2.26	0.26	44.04	302.28
Dynamic	Yes	Yes	0	-	80	0.75	3.57	2.25	0.27	38.20	333.88
	Yes	Yes	45	-	36	0.70	3.45	2.33	0.28	35.00	351.11
	Yes	No	0	-	53	0.83	3.58	2.19	0.27	39.96	324.36
	No	No	0	-	51	-	-	-	-	39.96	324.36

Table V. Different optimization scenarios run. Excluding frequency constraints did not affect the optimized structure. Including wave-loading does not add significant weight to the structure. Changing the load direction has a large influence on the overall mass. The dynamic approach is superior, but with constant constraint scaling, each method performs well.

Although the structures are reduced to almost half the total weight, the damage caused by the updated aero- and hydrodynamic loading is not changed significantly as compared with the damage caused by the initial loading conditions. This is key to an effective gradient-based optimization approach. Partly because recalculating loads in each design iteration is computationally expensive, and partly because it is not possible to determine the design sensitivity of the loading condition analytically. If loads are very sensitive to design changes, and load sensitivities are not provided, this can prevent the optimization from converging. It is possible to use finite differences to estimate the loading sensitivity, but this is very computationally costly.

Restarting the design process with an optimized design as initial guess and applying updated rotor and wave-loads can, ultimately, produce a design that has full utilization. The computational cost of this process is greatly reduced when the loading condition does not change significantly.

Hydrodynamic loading does not influence the optimized designs much. However, load direction is important for the design as seen in Table V. Therefore, it is recommended to include loads in different directions.

Using constraint scaling, better designs were achieved for both the DEL and quasi-static methods. The constant constraint scaling is an adjustment of the limit of Palmgren-Miner's damage rule and does not provide optimal designs. With the constant safety factor, the static and quasi-static approaches generate more realistic and less non-conservative designs, but the trends not captured by the simpler analyses may not be accounted for in the optimized design.

In the present work a strict convergence criterion is applied. When bilinear S-N curves are used, oscillations near optimum could be observed in some cases. Smoothing of the bilinear S-N curve can be applied to address this issue.

Wind Energ. 0000; **00**:1–15 © 0000 John Wiley & Sons, Ltd.
DOI: 10.1002/we
Prepared using weauth.cls

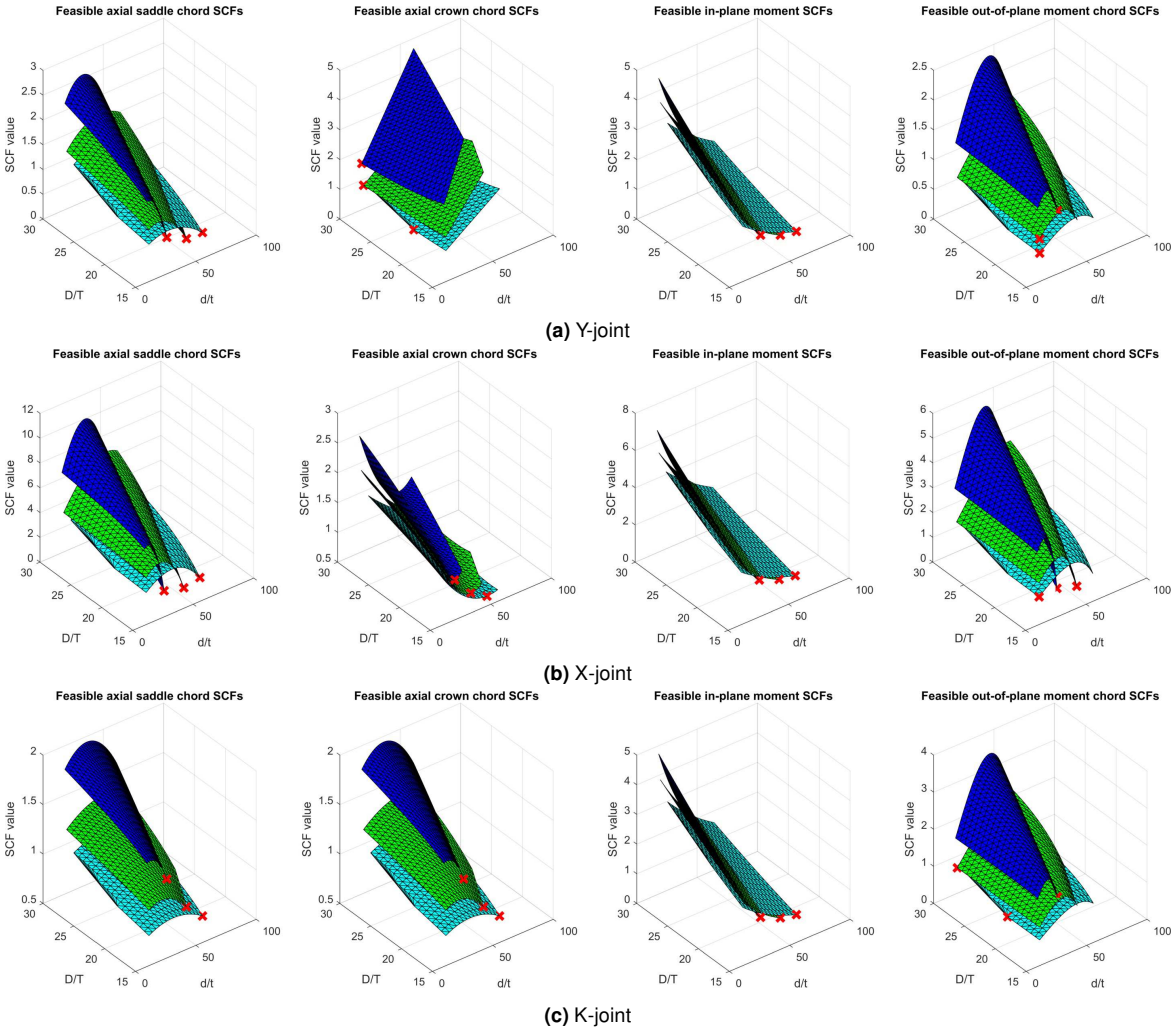

Figure 10. SCF values for three different thickness relationships between the chord thickness, T, and the brace thickness, t. In blue t = T/2, in green t = T/3, and in cyan t = T/4. The red cross represents the lowest SCF value for the given thickness relations.

None of the presented observations may be generic, and it is therefore important to have a deep knowledge of the mechanics of jackets even for conceptual and preliminary design optimizations. Many parameters such as yaw misalignment, wind speed, different jackets and turbines, soil-structure interaction etc. have not been investigated. Additionally, the study is limited to fatigue constraints, and thus the effects of ULS and manufacturing constraints are not investigated.

5. CONCLUSION

In this work, three different approaches to gradient based optimization of a jacket structure for offshore wind turbines are investigated. The optimizations are based on (i) damage equivalent loads, (ii) quasi-static analysis, and (iii) dynamic analysis. Based on the analyses and the optimizations, the following observations can be made:

- Hydrodynamic loading can be left out during the early design phases.
- It is not necessary to recalculate the loading conditions in the preliminary design phase.
- Load direction can have a significant influence on the optimized designs.
- Damage equivalent loads and quasi-static approaches can lead to large errors in the estimation of fatigue damage and should only be applied when fatigue caused by excitations of structural frequencies is negligible or when a

sufficient safety factor ensures a valid design. Using the mean error of the analysis in initial design as a safety factor works well.
- The optimized designs are to a large extent driven by reducing the stress concentration factors.
- To achieve the best preliminary design it is recommended to use the most accurate modeling approach.
- To produce designs with full fatigue utilization, it is necessary to recalculate loading conditions during the optimization.

ACKNOWLEDGEMENTS

This research is part of the project ABYSS - Advancing BeYond Shallow waterS - Optimal design of offshore wind turbine support structures, sponsored by the Danish Council for Strategic Research, Grant no. 1305-00020B. This support is gratefully acknowledged. Additionally, support by NOWITECH, the Norwegian Research Centre for Offshore Wind Technology, is gratefully acknowledged (Research council of Norway, Contract no. 193823). We thank in particular Fedem Technology AS for providing software licenses and quick and helpful feedback. Lastly, the authors would like to thank Alexander Verbart for his work on JADOP.

REFERENCES

1. Sun X, Huang D, Wu G. The current state of offshore wind energy technology development. *Energy* 2012; **41**(1):298–312.
2. International Energy Agency. Technology roadmap - Wind energy. *Technical Report*, Paris 2013.
3. Burton T, Sharpe D, Jenkins N, Bossanyi E. *Wind Energy Handbook*. 2nd editio edn., John Wiley & Sons, 2001.
4. The Carbon Trust. Offshore Wind Power: Big Challenge, Big Opportunity: Maximising the Environmental, Economic and Security Benefits. *Technical Report* 2008.
5. The Crown Estate. Offshore Wind Cost Reduction: Pathways Study. *Technical Report* 2012.
6. Yoshida S. Wind Turbine Tower Optimization Method Using a Genetic Algorithm. *Wind Engineering* 2006; **30**(6):453–470.
7. Uys PE, Farkas J, Jármai K, van Tonder F. Optimisation of a steel tower for a wind turbine structure. *Engineering Structures* jul 2007; **29**(7):1337–1342.
8. Thiry A, Bair L, Buldgen GR, Rigo P. Optimization of monopile offshore wind structures. *Proceedings of the 3rd international conference on marine structures*, 2011; 633–642.
9. Gentils T, Wang L, Kolios A. Integrated structural optimisation of offshore wind turbine support structures based on finite element analysis and genetic algorithm. *Applied Energy* 2017; **199**:187–204.
10. Long H, Moe G, Fischer T. Lattice towers for bottom-fixed offshore wind turbines in the ultimate limit state: variation of some geometric parameters. *Journal of Offshore Mechanics and Arctic Engineering* dec 2011; **134**(2):21 202.
11. Long H, Moe G. Preliminary design of bottom-fixed lattice offshore wind turbine towers in the fatigue limit state by the frequency domain method. *Journal of Offshore Mechanics and Arctic Engineering* feb 2012; **134**(3):31 902.
12. Zwick D, Muskulus M, Moe G. Iterative optimization approach for the design of full-height lattice towers for offshore wind turbines. *Energy Procedia* 2012; **24**(0):297–304.
13. Pasamontes LB, Torres FG, Zwick D, Schafhirt S, Muskulus M. Support structure optimization for offshore wind turbines with a genetic algorithm. *Proceedings of the ASME 2014 33rd Internation Conference on Ocean, Offshore and Arctic Engineering*, San Fransisco, 2014; 1–7.
14. Schafhirt S, Zwick D, Muskulus M. Reanalysis of Jacket Support Structure for Computer-Aided Optimization of Offshore Wind Turbines with a Genetic Algorithm. *Proceedings of the Twenty-fourth International Ocean and Polar Engineering Conference*, Busan, 2014; 234–241.
15. Schafhirt S, Zwick D, Muskulus M. Two-stage local optimization of lattice type support structures for offshore wind turbines. *Ocean Engineering* 2016; **117**:163–173.
16. Ashuri T, Zaaijer MB, Martins J, van Bussel GJW, van Kuik GAM. Multidisciplinary design optimization of offshore wind turbines for minimum levelized cost of energy. *Renewable Energy* 2014; **68**:893–905.
17. Ashuri T, Ponnurangam C, Zhang J, Rotea M. Integrated Layout and Support Structure Optimization for Offshore Wind Farm Design. *Journal of Physics: Conference Series*, vol. 753, 2016; 92 011.
18. Chew Kh, Muskulus M, Narasimalu S, Tai K, Ng EYK. Fatigue sensitivity analysis of offshore wind turbine structures. *Proceedings of WCSMO-11* 2015; :798–803.
19. Oest J, Sørensen R, Overgaard LCT, Lund E. Structural optimization with fatigue and ultimate limit constraints of jacket structures for large offshore wind turbines. *Structural and Multidisciplinary Optimization* 2017; **55**(3):779–793.

20. Chew KH, Tai K, Ng EYK, Muskulus M. Optimization of offshore wind turbine support structures using an analytical gradient-based method. *Energy Procedia* 2015; **80**:100–107.
21. Chew KH, Tai K, Ng EYK, Muskulus M. Analytical gradient-based optimization of offshore wind turbine substructures under fatigue and extreme loads. *Marine Structures* 2016; **47**:23–41.
22. Muskulus M, Schafhirt S. Design optimization of wind turbine support structures - a review. *Journal of Ocean and Wind Energy* 2014; **1**(1):12–22.
23. DNV. *RP-C203: Fatigue design of offshore steel structures*. Det Norske Veritas: Høvik, 2014.
24. Freebury G, Musial W. Determining equivalent damage loading for full-scale wind turbine blade fatigue tests. *2000 ASME Wind Energy Symposium*, 2000; 50.
25. Wächter A, Biegler LT. On the Implementation of a Primal-Dual Interior Point Filter Line Search Algorithm for Large-Scale Nonlinear Programming. *Mathematical Programming* 2006; **106**(1):25–57.
26. Cook RD, Malkus DS, Plesha ME, Witt RJ. *Concepts and applications of finite element analysis*. 4th ed. edn., John Wiley & Sons: New York, N.Y., 2002.
27. Efthymiou M, Durkin S. Stress concentrations in T/Y and gap/overlap K-joints. *Proceedings of the 4th International Conference on Behaviour of Offshore Structures* 1985; :1–12.
28. Efthymiou M. Development of SCF formulae and generalised influence functions for use in fatigue analysis. *Proceedings of the Offshore Tubular Joints Conference* 1988; :1–13.
29. IEC. *IEC 61400-3 Wind Turbines - Part 3: Design requirements for offshore wind turbines*. International Electrotechnical Commission: Geneva, 2009.
30. Fischer T, de Vries W, Schmidt B. UpWind Design Basis. *Technical Report* 2010.
31. Zwick D, Muskulus M. Simplified fatigue load assessment in offshore wind turbine structural analysis. *Wind Energy* 2015; **19**(2):265–278.
32. Passon P, Branner K. Load calculation methods for offshore wind turbine foundations. *Ships and Offshore Structures* 2013; **9**(4):433–449.
33. Clough RW, Penzien J. *Dynamics of Structures*. McGraw-Hill, 1975.
34. Hasselmann K, Barnett TP, Bouws E, Carlson H, Cartwright DE, Enke K, Ewing JA, Gienapp H, Hasselmann DE, Kruseman P, *et al.*. Measurements of Wind-Wave Growth and Swell Decay during the Joint North Sea Wave Project (JONSWAP). *Technical Report 8 0* 1973.
35. Morison JR, O'Brien MP, Johnson J, Schaaf S. The Force Exerted by Surface Waves on Piles. *Journal of Petroleum Technology* 1950; **2**(5):149–154.
36. Schløer S, Castillo LG, Fejerskov M, Stroescu E, Bredmose H. A model for Quick Load Analysis for monopile-type offshore wind turbine substructures. *Journal of Physics: Conference Series* 2016; **753**(9):92 008.
37. Palmgren AG. Die Lebensdauer von Kugellagern. *Zeitschrift des Vereines Deutscher Ingenieure* 1924; **14**:339–341.
38. Miner MA. Cumulative Damage in Fatigue. *Journal of Applied Mechanics* 1945; **12**(3):A159–A164.
39. Matsuishi M, Endo T. Fatigue of metals subjected to varying stress. *Japan Society of Mechanical Engineering* 1968; **68**(2):37–40.
40. Seidel M, Voormeeren S, van der Steen JB. State-of-the-art design processes for offshore wind turbine support structures. *Stahlbau* 2016; **85**(9):583–590.
41. Tortorelli D, Michaleris P. Design sensitivity analysis: Overview and review. *Inverse Problems in Science and Engineering* 1994; **1**(1):71–105.
42. Seyranian AP, Lund E, Olhoff N. Multiple eigenvalues in structural optimization problems. *Structural optimization* 1994; **8**(4):207–227.
43. Vorpahl F, Kaufer D, Popko W. Description of a basic model of the "Upwind reference jacket" for code camparison in the OC4 project under IEA Wind Annex 30". *Technical Report*, Institute for Wind Energy and Energy Systems Technology 2011.
44. Jonkman J, Butterfield S, Musial W, Scott G. Definition of a 5-MW reference wind turbine for offshore system development. *Technical Report February* 2009.
45. Hammerstad BH, Schafhirt S, Muskulus M. On Fatigue Damage Assessment for Offshore Support Structures with Tubular Joints. *Energy Procedia* 2016; **94**:339–346.

Paper III

K. Sandal, C. Latini, V. Zania, M. Stolpe, Integrated optimal design of jackets and foundations. To be submitted to *Marine Structures*.

Integrated optimal design of jackets and foundations

Kasper Sandal * Chiara Latini † Varvara Zania ‡ Mathias Stolpe §

July 25, 2017

Abstract

The article proposes a method for integrated design of jackets and foundations using numerical structural optimization. Both piles and suction caissons are considered in both clayey and sandy soil, and several design procedures are considered. The optimal design problem enables an automatic design process which minimizes the primary steel mass of the jacket and the foundations. The numerical results indicate that the jacket design is not very dependent on the foundation design, but that the foundation design can be quite dependent on the jacket design. In medium to stiff soils, the natural frequency of the full offshore wind turbine structure is only slightly overestimated when foundations are assumed to be rigid.

Keywords: structural optimization, foundation design, suction caisson, pile, jacket structure, integrated design.

1 Introduction

The main objective for the offshore wind industry nowadays is to reduce the cost of energy, in order to be competitive with respect to fossil-fuel-based energy sources. Support structures comprise as much as 20 percent of capital expenditures, and have been identified as areas with high potential for cost reduction [37]. The cost-reduction targets set by industry can be met either by using new technologies or by optimization of design methods and existing technologies. In that regards structural optimization appears as an attractive approach to investigate any potential cost benefits from the design optimization of the substructure and the foundation.

Optimization of wind turbine components has been well studied in the literature, and for example, a gradient based rotor optimization is presented in [17]. Integrated design of multiple components of the offshore wind energy turbine, such as of tower and rotor, have been done in the work of e.g. Ashuri [2]. Here it was showed that an integrated approach towards optimization

*DTU Wind Energy, Technical University of Denmark, Frederiksborgvej 399, 4000 Roskilde, Denmark. E-mail: kasp@dtu.dk

†DTU Civil Engineering, Technical University of Denmark, Brovej Building 108, 2800 Kgs. Lyngby, Denmark. E-mail: chila@byg.dtu.dk

‡DTU Civil Engineering, Technical University of Denmark, Brovej Building 108, 2800 Kgs. Lyngby, Denmark. E-mail: vaza@byg.dtu.dk

§DTU Wind Energy, Technical University of Denmark, Frederiksborgvej 399, 4000 Roskilde, Denmark. E-mail: matst@dtu.dk

can considerably reduce the cost of energy, which often implicates compromises between rotor and support structure design. However, the foundation was not optimized, since all degrees of freedom of the monopile at the seabed were constrained. Terminology of the main components of the support structures for offshore wind turbines are given in Figure 1. Detailed design of support structures according to rules and guidelines [21] implies that a large number of load cases must be assessed, which is a computationally expensive and time-consuming task. Many design approaches therefore uses a reduced number of load cases [40].

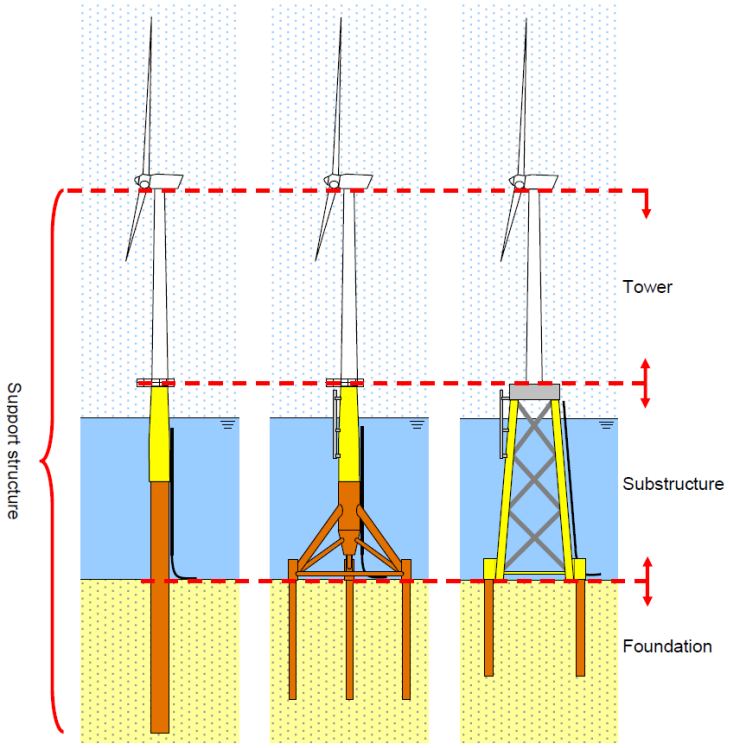

Figure 1: Definition of the main components of the support structure for offshore wind turbines. The jacket substructure can be further diveded into the actual jacket, and the transition piece which connects it to the tower. Figure credit: [12].

Optimal design of support structures for offshore wind turbines has developed from gradient-free approaches where an aero-elastic software is used as a black-box for the function evaluations [41], towards the use of gradient-based methods [28]. The advantage of the black-box approach is that the analysis can be state-of-the-art. With gradient-based methods one has so far been forced to decouple the rotor from the structure and assume design independent loading. However, due to the nature of the industry, where turbine designers are unwilling to share models with the support structure designer, a decoupled load model is actually industrially relevant. Gradient-based optimization of jacket substructures is presented in [29] and [9] with quasi-static and dynamic analysis, respectively. In these works, the fatigue and ultimate limit states were assessed during multiple 10-minute load cases. For conceptual design of jacket substructures, a load

analysis with static damage equivalent loads, and static extreme loads can be sufficient [34].

Contrary to the mechanical engineering field, in the geotechnical sector numerical optimization methods have been only scarcely investigated in the literature. Few studies have been conducted on the dimension optimization of shallow foundations [23] and pile groups [8]; while the topology optimization of foundations in granular soils was addressed in the work of Pucker and Grabe [30] and Seitz and Grabe [35]. In the latter ones, a combined method of topology and shape optimization was implemented and linked up to a finite element program. The study [35] proved that the optimized foundation topologies are more efficient due to the significant improvement of the deformation behaviour when compared to quadratic surface foundations. It is worth mentioning the work of Barakat et al. [4], in which a general approach to the reliability-based analyses was performed to optimize designs of laterally loaded piles. For a monopile, Thiry et al [38] used a genetic algorithm to design a monopile in the frequency domain. Furthermore, a preliminary investigation of pile foundation design using structural optimization was performed in the work of Sandal and Zania [33]. The main conclusion derived from the abovementioned study was that the total mass of the piles was considerably influenced by the soil strength characteristics.

For an offshore wind turbine structure, the support structure design typically has some global requirements, e.g. frequency [12] [5]. These global constraints are influenced by both the soil properties, the foundation design, as well as the substructure design. The foundation and substructure designs will in turn have their own design requirements. An integrated design approach would include all the design constraints for both the foundation, the substructure, and the full support structure in one design procedure. This can rapidly become too complex for it to be manually handled, but is well within the limits of computer-aided design approaches. One computer-aided design approach can be based on the principle of fully utilized design. The principle here is to establish limits for e.g. the maximum stress, and then adjust the structural dimensions iteratively until all design members are fully utilized with respect to this limit. However, a fully utilized design is generally not the same as an optimal design. A simple example which illustrates this is a thin-walled pipe subjected to bending loads. The pipe can be fully utilized and still have potential for lowering the mass by increasing the diameter and lower the wall thickness. An approach which is often better in dealing with such problems is numerical structural optimization, where the design problem is modelled as a mathematical program.

The advantage of the integrated design approach is that interaction effects between the foundation and support structure are properly accounted for. This way, one avoids a situation where new loads and designs are sent back and forth between the foundation designer and the support structure designer. The disadvantage of the integrated design approach is of course that it requires a more complex model, especially if variable soil conditions, foundation types and design procedures are included.

Integrated optimal design of foundation and jacket design has to the authors knowledge not been performed yet. The aim of this paper is to investigate interaction effects between soil properties, foundation design, and support structure design for offshore wind turbines. This is achieved by automating six different design procedures for two different types of foundations and two different soil conditions with numerical structural optimization. The integration of the analysis models and sensitivity analyses with an existing framework for jacket design optimization

allows for integrated design of foundations and jackets. The structural optimization problem is formulated in such a way to minimize the combined mass of jacket and foundation with requirements on fatigue, frequency, buckling, and foundation capacities. Additionally the design trends for varying jacket leg distance and soil stiffness are analysed. Moreover a comparison between the sequential and integrated optimization allows for estimation of the benefit from an integrated approach.

2 Modelling methodology

The structural design and analysis model is used to formulate an integrated optimal design problem for both the jacket and the foundation. The foundation models and capacities are explained, and the implementation details are given.

2.1 Model and design parametrization

The model is assembled by a design dependent foundation, a design dependent jacket, and a non-design dependent transition piece, tower, and rotor-nacelle-assembly (RNA). The jacket design is described by

$$\mathbf{x} = \begin{pmatrix} d_1^l & t_1^l & d_1^b & t_1^b & \dots & d_{n_s}^l & t_{n_s}^l & d_{n_s}^b & t_{n_s}^b \end{pmatrix}^T \in \mathbb{R}^{4n_s}$$

where d and t are the outer diameter and wall thickness of the members in the jacket. The superscript l and b refers to legs and braces, and the subscripts $1, \dots, n_s$ refers to the section number. Alas, there are four design variables per section of the jacket, as shown in Figure 2.

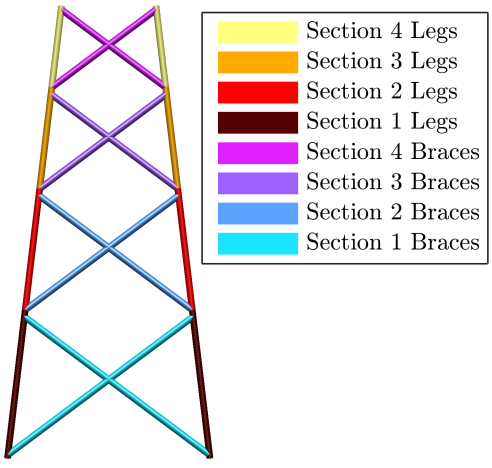

Figure 2: Overview of the jacket design parametrization.

The foundation design is described by

$$\mathbf{y} = \begin{pmatrix} d^f, t^f, l^f \end{pmatrix}^T \in \mathbb{R}^3$$

where d^f ,t^f, and l^f are the outer diameter, wall thickness, and length of the foundation. There is one foundation connected to each of the four jacket legs, and all the foundation designs are identical. The design parametrization is the same for both piles and suction caissons.

Finally, the non-design part of the model consists of the transition piece, tower, and a simplified rotor-nacelle-assembly. The non-design dependent part of the structure is necessary in the structural analysis because it is at the tower top the loads are applied, and it also influences the natural frequencies of the structure.

2.2 Structural analysis

The structural model is built from two types of two-noded finite elements. The jacket, transition piece and tower are modelled with Timoshenko beam elements [11] for linear elasticity. The foundation is modelled with specialized foundation elements described in section 2.3.

The global stiffness matrix $\mathbf{K}(\mathbf{x}, \mathbf{y}) \in \mathbb{R}^{n \times n}$ is assembled as

$$\mathbf{K}(\mathbf{x}, \mathbf{y}) = \mathbf{K}_0 + \sum_{i=1}^{n_j} \mathbf{K}_i(\mathbf{x}) + \sum_{i=1}^{n_f} \mathbf{K}_i^f(\mathbf{y})$$

where n_j and n_f are the number of elements in the jacket and foundation, respectively, and n is the number of unconstrained degrees of freedom. The stiffness matrices of elements in the non-design dependent part (tower, transition piece, and RNA) are collected in $\mathbf{K}_0$, and the stiffness of the elements in the foundation and jacket are assembled as functions of the design variables. The assembly also distributes the element stiffness matrices to the appropriate degrees of freedom in the global stiffness matrix.

Static equilibrium is now given as

$$\mathbf{K}(\mathbf{x}, \mathbf{y})\mathbf{u}^\ell = \mathbf{f}^\ell(\mathbf{x}).$$

where $\mathbf{f}^\ell(\mathbf{x}, \mathbf{y})$ is the ℓth applied static load. The load is design dependent, because gravity forces on the jacket are included.

In the described structural model, the boundary conditions are applied on the foundation elements. Since the displacement field is a function of both foundation and jacket design, we refer to this model as the integrated model. A common assumption in analysis of jacket structures is that the bottom of the jacket is clamped, i.e., that there is no displacement or rotation in the foundation. This assumption can easily be applied to this model as well, by fixing the six degrees of freedom at the top node of the foundation. This model, from here referred to as the clamped model, will be used as a reference in the numerical simulations.

The global mass matrix $\mathbf{M}(\mathbf{x}) \in \mathbb{R}^{n \times n}$ is assembled as

$$\mathbf{M}(\mathbf{x}) = \mathbf{M}_0 + \sum_{i=1}^{n_j} \mathbf{M}_i(\mathbf{x})$$

where $\mathbf{M}_0$ contains the mass matrices of the elements in the transition piece, tower, and rotor-nacelle-assembly. Whereas the global stiffness matrix is a function of both the foundation and

jacket design variables $\mathbf{x}$ and $\mathbf{y}$, the mass matrix is here only a function of the jacket design variables $\mathbf{x}$. In this definition the contribution of the foundations to the mass matrix is neglected. This assumption disregards the frequency dependency of the foundation stiffness (impedance functions) due to the inertial response of the soil-foundation system which is commonly taken into consideration in dynamic soil-structure-interaction problems [5]. The abovementioned simplification is considered appropriate for the current study since the natural eigenfrequencies of the superstructure (wind turbine and jacket) are smaller than the eigenfrequencies corresponding to most of the considered soil conditions. The generalized eigenvalue problem is computed as

$$\left(\mathbf{K}(\mathbf{x},\mathbf{y}) - \lambda_i \mathbf{M}(\mathbf{x})\right) \boldsymbol{\phi}_i = 0, \quad i = 1, \ldots, n$$

where λ_i and $\boldsymbol{\phi}_i$ are the ith eigenvalue and eigenmode. We assume the eigenvalues to be distinct and sorted, $\lambda_1 <, \ldots, < \lambda_n$, and compute the eigenfrequency in Hz as

$$\omega_i = \frac{\sqrt{\lambda_i}}{2\pi}.$$

The eigenvalues of a jacket structure is generally not distinct, as the structure is often symmetric. However, the model of the rotor-nacelle-assembly of the wind turbine is non-symmetric, and this ensures distinct eigenvalues, at least for the first ones which are considered in this article.

2.3 Joint connection between jacket legs and foundations

We solve for the global displacement vector for a given load case as $\mathbf{u}(\mathbf{x},\mathbf{y}) = \mathbf{K}(\mathbf{x},\mathbf{y})^{-1}\mathbf{f}(\mathbf{x},\mathbf{y})$, which illustrates that the displacement field is a function of both foundation and jacket design variables. The top node of the foundation is from here referred to as the *joint*, and it is the connection between the jacket legs and the foundations. From the global displacement vector $\mathbf{u}(\mathbf{x},\mathbf{y}) \in \mathbb{R}^n$ we can extract the displacement vector for each joint, $\mathbf{u}_i^f(\mathbf{x},\mathbf{y}) \in \mathbb{R}^6$, $i = 1, \ldots, 4$. The reaction forces at the joints can now be computed as

$$\mathbf{f}_i^f(\mathbf{x},\mathbf{y}) = \mathbf{K}_i^f(\mathbf{y})\mathbf{u}_i^f(\mathbf{x},\mathbf{y})$$

where $\mathbf{K}_i^f(\mathbf{y})$ is now only given for the joint degrees of freedom, so that

$$\mathbf{f}_i^f(\mathbf{x},\mathbf{y}) = \begin{pmatrix} F_{x,i}(\mathbf{x},\mathbf{y}) \\ F_{y,i}(\mathbf{x},\mathbf{y}) \\ F_{z,i}(\mathbf{x},\mathbf{y}) \\ M_{x,i}(\mathbf{x},\mathbf{y}) \\ M_{y,i}(\mathbf{x},\mathbf{y}) \\ M_{z,i}(\mathbf{x},\mathbf{y}) \end{pmatrix}, \quad \mathbf{u}_i^f(\mathbf{x},\mathbf{y}) = \begin{pmatrix} u_i(\mathbf{x},\mathbf{y}) \\ v_i(\mathbf{x},\mathbf{y}) \\ w_i(\mathbf{x},\mathbf{y}) \\ \theta_{x,i}(\mathbf{x},\mathbf{y}) \\ \theta_{y,i}(\mathbf{x},\mathbf{y}) \\ \theta_{z,i}(\mathbf{x},\mathbf{y}) \end{pmatrix},$$

$$\mathbf{K}_i^f(\mathbf{y}) = \begin{pmatrix} K_{su}(\mathbf{y}) & 0 & 0 & 0 & 0 & 0 \\ 0 & K_{su}(\mathbf{y}) & 0 & 0 & 0 & -K_{sc}(\mathbf{y}) \\ 0 & 0 & K_v(\mathbf{y}) & 0 & K_{sc}(\mathbf{y}) & 0 \\ 0 & 0 & 0 & K_{mc}(\mathbf{y}) & 0 & 0 \\ 0 & 0 & K_{sc}(\mathbf{y}) & 0 & K_{mc}(\mathbf{y}) & 0 \\ 0 & -K_{sc}(\mathbf{y}) & 0 & 0 & 0 & K_t(\mathbf{y}) \end{pmatrix},$$

and $\mathbf{K}_i^f(\mathbf{y})$ is the same for all four joints. The stiffness entries K_{su}, K_{sc}, and K_{mc} are different for piles and suction caissons, and are given in sections 2.6 and 2.7. The vertical and torsional stiffness coefficients K_t and K_v are evaluated according to the suggested expressions for piles by Randolph [31] and these expressions are also used for suction caissons:

$$K_t(d,l) = Gd^3\left(\frac{2}{3} + \frac{\pi l}{d}\right)$$
$$K_v(d,l) = \frac{2Gd}{1-\nu}\left(1 + \frac{(1-\nu)\pi\tanh(\xi(d,l))l}{\zeta(d,l)d\xi(d,l)}\right)$$

where

$$\zeta(d,l) = \ln\left(\frac{5(1-\nu)l}{d}\right), \quad \text{and} \quad \xi(d,l) = \sqrt{\frac{2G}{\zeta E_p}}\frac{2l}{d},$$

and ν and G are the Poisson's ratio and shear stiffness of the soil.

2.4 Optimal design problem

We consider the optimal design problem, for now described in general terms,

$$\begin{array}{ll} \underset{\mathbf{x}\in\mathbb{R}^{4n_s},\mathbf{y}\in\mathbb{R}^3}{\text{minimize}} & f(\mathbf{x},\mathbf{y}) \\ \text{subject to} & \mathbf{A}_x\mathbf{x} + \mathbf{A}_y\mathbf{y} \le \mathbf{b} \\ & g_j(\mathbf{x},\mathbf{y}) \le 0, \qquad j = 1,..,,n_c \\ & \underline{\mathbf{x}} \le \mathbf{x} \le \overline{\mathbf{x}} \\ & \underline{\mathbf{y}} \le \mathbf{y} \le \overline{\mathbf{y}}, \end{array} \tag{P}$$

where $\underline{\mathbf{x}}$, $\overline{\mathbf{x}}$, $\underline{\mathbf{y}}$, and $\overline{\mathbf{y}}$ are lower and upper bounds on the design variables. The nonlinear contraint functions $g_j(\mathbf{x},\mathbf{y})$ are used to model design requirements. This includes structural frequencies, and local design requirements such as fatigue and buckling in the jacket, and load capacities for the foundation. The linear constraints model geometrical restrictions on the jacket and foundation designs (see below).

The optimal design problem (P) is a non-convex optimization problem in the variables $\mathbf{x}$ and $\mathbf{y}$. The objective is to minimize the mass of the combined substructure

$$f(\mathbf{x},\mathbf{y}) = \rho^j\sum_{i=1}^{n_j} V_i(\mathbf{x}) + \rho^f n_f V^f(\mathbf{y})$$

where V_i is the volume of element number i in the jacket, V^f is the volume of one foundation, and ρ^j and ρ^f is the material density in the jacket and the foundation, respectively. All elements are modelled as thin walled cylinders so that

$$V_i(d_i,t_i,l_i) = \frac{\pi}{4}\left(d_i^2 - (d_i - 2t_i)^2\right)l_i, \quad \text{and} \quad V^f(d^f,t^f,l^f) = \frac{\pi}{4}\left(d^{f\,2} - (d^f - 2t^f)^2\right)l^f.$$

The mass of the structural connection between the foundation and the jacket leg is thus not modelled. For suction caissons there is a flat lid with stiffeners which can account for a significant part of the suction caisson mass. The objective function does not consider this part of the mass of the suction caisson, therefore the comparison between the mass of the suction caisson and the pile should be treated with caution.

Linear constraints, $\mathbf{A}_x\mathbf{x}+\mathbf{A}_y\mathbf{y} \leq \mathbf{b}$ are placed on both jacket and foundation design to ensure manufacturability and compliance with design requirements. For the pile foundation there is a wall thickness constraint $t^f \geq 6.3 + d^f/100$ which is assumed to avoid buckling during the pile driving procedure [1]. The same constraint is also applied to the suction caisson, although the installation procedure here is different there is still the risk of buckling due to the suction. Furthermore, in order to distinguish the capacity functions of piles and suction caissons the slenderness ratio (diameter over skirt length) is used as a criterion and this slenderness ratio is enforced in the linear constraints. For the jacket structure there is a validity range [14] which must be enforced when the design methodology for stress concentrations in welded joints are applied. For joints where braces b are welded onto legs l, the brace dimension should lie between 20 and 100 percent of the leg dimension. This results in the linear inequalities

$$\frac{d_i^l}{5} \leq d_i^b \leq d_i^l, \quad i = 1, \ldots, n_s$$
$$\frac{t_i^l}{5} \leq t_i^b \leq t_i^l, \quad i = 1, \ldots, n_s.$$

The diameter to thickness ratio in all elements should satisfy

$$16t_i^l \leq d_i^l \leq 64t_i^l, \quad i = 1, \ldots, n_s$$
$$16t_i^b \leq d_i^b \leq 64t_i^b, \quad i = 1, \ldots, n_s.$$

The constraints $g_j(\mathbf{x}, \mathbf{y})$ include design requirements on the jacket as well as the foundations. Since the displacements are functions of the both jacket and foundation design variables $\mathbf{x}$ and $\mathbf{y}$, most of the design requirements on the jacket and foundation are also functions of both $\mathbf{x}$ and $\mathbf{y}$.

The nonlinear constraints on the jacket design include stress and buckling constraints. Stress constraints are computed in eight hot spots h in every finite element for all load cases. In the ultimate limit state load cases, local shell buckling and column buckling are considered according to the offshore standard [15] and the recommended practice [13]. Shell buckling is formulated as a design dependent stress constraint in compression,

$$\sigma_i^b(\mathbf{x}) - \sigma_{ih}(\mathbf{x}, \mathbf{y}) \leq 0, \quad i = 1, \ldots, n_e, \; h = 1, \ldots, 8$$

for all finite elements i in the jacket. Here $\sigma_{ih}(\mathbf{x}, \mathbf{y})$ is the stress in element i at position h along the outer circumference of the element. The shell buckling capacity $\sigma_i^b(\mathbf{x})$ is defined as

$$\sigma_i^b(\mathbf{x}) = \frac{-\sigma_y}{\gamma_M \sqrt{1 + \left(\frac{\sigma_y}{f_i}\right)^2}}, \qquad f_i = C_i \frac{\pi^2 E}{12(1-\nu^2)} \left(\frac{t_i}{L_i}\right)^2, \qquad C_i = \sqrt{1 + (\tilde{\rho}_i \tilde{\xi}_i)^2}$$
$$\tilde{\rho}_i = \frac{1}{2\sqrt{1 + \frac{d_i}{600 t_i}}}, \qquad \tilde{\xi}_i = 1.404 \frac{L_i^2}{d_i t_i} \sqrt{1-\nu^2},$$

where L_i is the length of the member, from one joint to the next, to which element i belongs, σ_y is the material yield strength, ν is the Poisson's ratio, and $\gamma_M = 1.25$. Column buckling need only be assessed for element i if

$$\frac{(kL_i)^2 A_i(d_i, t_i)}{I_i(d_i, t_i)} \geq \frac{2.5E}{\sigma_y} \tag{1}$$

where $k = 0.7$ is the effective column length. To avoid assessing column buckling, the inverse of equation (1) is formulated as a non-linear constraint

$$\sqrt{\frac{3.2\sigma_y}{E}} kL_i - d_i^2 + 2d_i t_i - 2t_i^2 \leq 0, \quad i = 1, \ldots, n_j.$$

Since the buckling assessment is load independent, it is only a function of the jacket design variables.

All the constraint functions are implemented as smooth, differentiable analytical functions. The nonlinear constraints on the foundation design are based on standard design procedures, and vary depending on the type of foundation and soil conditions. Details for the design requirements of these design cases are given in sections 2.6 and 2.7. Variable bounds are placed on both jacket and foundation variables, to ensure that the optimized designs are manufacturable.

2.5 Load cases

The static load cases applied in this study are listed in Table 1. The fatigue loads are damage equivalent 1 Hz loads based on aeroelastic simulations of a rotor, assuming a perfectly rigid support structure. The ultimate loads are taken from the design report of the DTU 10 MW wind turbine [3]. No safety factors have been applied. The fatigue loads are applied as two different weighted combinations of damage equivalent loads in thrust, overturning moment, and torsion degrees of freedom. The two fatigue loads are then applied from two directions, 45 degrees apart, to increase the probability that the worst case is captured. The ultimate loads are also applied from two directions.

The fatigue loads are assumed to be design driving for the jacket, and the extreme loads are assumed to be design driving for the foundations. This means that in the optimal design problem, the constraints on the jacket are applied for the fatigue load cases, and the constraints on the foundations are applied in the extreme load cases. The use of damage equivalent loads for the fatigue constraints in the jacket is not perfectly accurate, but is a recommended approach for conceptual design [34]. The use of extreme static loads for the ultimate design of the piles is also a simplification.

Table 1: Static design loads.

Load case	Limit state	Angle [deg]	Thrust force [MN]	Overturning moment [MNm]	Torsion [MNm]	Tower top mass [tons]
DEL00thrust	Fatigue	0	0.142	5.69	3.10	0
DEL45thrust	Fatigue	45	0.142	5.69	3.10	0
DEL00torsion	Fatigue	0	0.071	2.85	6.21	0
DEL45torsion	Fatigue	45	0.071	2.85	6.21	0
ULT00	Ultimate	0	4.61	17.9	0	677
ULT45	Ultimate	45	4.61	17.9	0	677

2.6 Pile stiffness and capacity formulation

The stiffness coefficients of the soil-pile system have been estimated according to the expressions suggested by Randolph [31] for slender piles:

$$K_{su}(d,t) = 6.29 G_s \left(\frac{E_c(d,t)}{G_s}\right)^{\frac{1}{7}} \left(\frac{d}{2}\right)$$

$$K_{sc}(d,t) = 2.21 G_s \left(\frac{E_c(d,t)}{G_s}\right)^{\frac{3}{7}} \left(\frac{d}{2}\right)^2$$

$$K_{mc}(d,t) = 1.97 G_s \left(\frac{E_c(d,t)}{G_s}\right)^{\frac{5}{7}} \left(\frac{d}{2}\right)^3$$

where G_s is given in [31], E_c is the equivalent Young's modulus

$$E_c(d,t) = \frac{E_p I_p(d,t) + E_s I_s(d,t)}{I_p(d,t) + I_s(d,t)},$$

and E_s, I_s, E_p, and I_p are the Young's modulus and inertias of soil and pile.
Design requirements on the axial and lateral ultimate capacities of the piles are computed according to the current state of practice for offshore foundations [1]. Axial pile resistance is given by two separate contributions: shaft resistance acting along the pile length and end bearing resistance at the pile tip. In this study both plugged and unplugged capacities have been estimated and the minimum of the two is taken as the final axial pile capacity.

The axial capacity constraints for piles in clay and sand are

$$-(Q_f(\mathbf{y}) + Q_b(\mathbf{y})) \leq F_{z,i}(\mathbf{x},\mathbf{y}) \leq Q_f(\mathbf{y}), \quad i = 1,\ldots,n_f, \tag{2}$$

where Q_f is the friction capacity and Q_b is the end bearing capacity. Positive F_z equals tension force in the pile. Detailed formulas of the the friction capacity and Q_b is the end bearing capacity adopted in the analyses are given in Appendix A for both sandy and clayey soil.

For clay profiles the shaft resistance can be formulated as a function of the effective overburden pressure at each given depth adopting the α–method formulated in [1], while the β–method [1] is used for the estimation of the shaft resistance in sands. The end bearing resistance of piles embedded in clay is governed by the maximum bearing strength of the soil, usually defined

as $9s_u$, where s_u is the undrained shear strength of the soil. While in sands the end bearing behaviour of piles is defined by the effective vertical stress in the soil and a non-dimensional bearing factor N_q, which is dependent on the angle of friction ϕ. It is important mentioning that bearing capacity theory applied to estimate base resistance in cohesionless soils involves a rather approximate ϕ-N_q relationship which originates from Meyerhoff [27] coupled with the difficulty of determining a reliable and representative in-situ value of the ϕ angle and the assumption of a proper shear failure surface around the pile tip [10]. While CPT-based methods have shown statistically closer predictions of pile load test results and hence, their use is recommended by design codes [1]. In the proposed study the optimization of the pile foundation was also assessed by adopting the UWA [25] CPT-based method for the estimation of the friction and end bearing contribution to pile capacity in cohesionless soil (sand). The expression of the axial capacity is given by:

$$-\left(\frac{3}{100}Q_f(\mathbf{y})+Q_b(\mathbf{y})\right)\leq F_{z,i}(\mathbf{x},\mathbf{y})\leq\frac{11}{500}Q_f(\mathbf{y}),\quad i=1,\ldots,n_f, \tag{3}$$

where Q_f and Q_b also are function of the CPT-data set. The CPT-data are given as $q_c(z)$, which is the soil cone resistance at depth z below the seabed. The data set is interpolated in Matlab such that it is smooth and differentiable. The friction capacity function Q_f is calculated as reported in Appendix A. Finally, the lateral capacity of piles can be expressed as follows, considering Brom's theory [7] for flexible piles:

- in clay

$$-Q_l(\mathbf{y})\leq\frac{F_{x,i}(\mathbf{x},\mathbf{y})|F_{x,i}(\mathbf{x},\mathbf{y})|}{9s_ud}+\frac{3F_{x,i}d}{2}+M_{y,i}\leq Q_l(\mathbf{y}),\quad i=1,\ldots,n_f$$

- in sand

$$-Q_l(\mathbf{y})\leq\frac{0.544F_{x,i}(\mathbf{x},\mathbf{y})|F_{x,i}(\mathbf{x},\mathbf{y})|^{\frac{1}{2}}}{(dK_p\gamma)^{\frac{1}{2}}}+M_{y,i}(\mathbf{y})\leq Q_l(\mathbf{y}),\quad i=1,\ldots,n_f,$$

where $K_p=\tan^2(45+\frac{\phi}{2})$. Note that $Q_l(\mathbf{y})$ is computed as:

$$Q_l(\mathbf{y})=\frac{2I(d,t)\sigma_y}{d},$$

which is only a function of the pile design, and not the soil properties. The sensitivity of the lateral capacity is the same for the pile in clay and sand. The absolute value is non-differential at zero, but since $F_{x,i}(\mathbf{x},\mathbf{y})$ does not approach zero in the numerical experiments, this is not a problem.

2.7 Suction caisson stiffness and capacity formulation

Suction caisson is a novel foundation concept for jacket structures in offshore wind engineering. Detailed design guidelines are not well established for this type of foundation and hence, state-of-art formulations in the framework of API provisions [1] were adopted in the current work.

The stiffness components of the soil-suction caisson system have been defined according to the expressions proposed by Latini and Zania [24]:

$$K_{su}(d,l) = \frac{G_s d}{0.560}\left(\frac{E_c(d,l)}{G_s}\right)^{0.18}\left(\frac{l}{d}\right)^{0.156}$$
$$K_{sc}(d,l) = \frac{G_s d^2}{7.10}\left(\frac{E_c(d,l)}{G_s}\right)^{0.52}\left(\frac{l}{d}\right)^{0.656}$$
$$K_{mc}(d,l) = \frac{G_s d^3}{2.29}\left(\frac{E_c(d,l)}{G_s}\right)^{0.40}\left(\frac{l}{d}\right)^{0.730}.$$

In regards with the optimization of the suction caisson, a fully encompassing yield surface in vertical load $F_{z,i}(\mathbf{x},\mathbf{y})$, horizontal load $F_{x,i}(\mathbf{x},\mathbf{y})$ and bending moment $M_{y,i}(\mathbf{x},\mathbf{y})$ space is taken into account. The magnitude of the uniaxial capacity and the shape of the yield surface depend on the soil response to loading (undrained and drained), the soil strength profile, foundation shape, foundation embedment and inclusion of tension between the foundation and the soil. In the case of undrained soil conditions, the bearing capacity of suction caissons subjected to combined vertical, horizontal and moment loading is estimated by deploying the failure envelopes expressions suggested by [19] and [36]. Two different capacity functions were used for suction caissons in order to distinguish between slenderness ratios lower and larger than 1. In such ultimate limit states the soil medium was modelled as linear elastic – perfectly plastic material and Tresca criterion was used to define the failure conditions. For the tensile capacity, API provisions [1] suggest that uplift capacity should be analyzed as a reverse bearing capacity problem with a minimum recommended factor of safety factor equal to 2.0. Note that different formulations must be adopted based on the soil conditions.

Particularly, the ultimate bearing capacity of suction caissons in clay with slenderness ratio $0 \leq l/d \leq 1$ is estimated according to Gouvernec [19] as follows:

$$\frac{F_{z,i}(\mathbf{x},\mathbf{y})}{V_c(\mathbf{y})} - \left(1 - \frac{F_{x,i}(\mathbf{x},\mathbf{y})}{H(\mathbf{y})}\right)^{p(\mathbf{y})} \leq 0, \quad i = 1,\ldots,n_f,$$

where

$$V_c(\mathbf{y}) = \frac{6.05 s_u \pi}{4}(d^2 + 0.86ld - 0.16l^2), \quad H(\mathbf{y}) = s_u\left(d + 4.46l - 1.52\frac{l^2}{d}\right), \tag{4}$$
$$\text{and} \quad p(\mathbf{y}) = \begin{cases} 0.18 + 0.14\frac{l}{d}, & \text{for } \frac{l}{d} \leq \frac{1}{2} \\ \frac{1}{4}, & \text{for } \frac{l}{d} \geq \frac{1}{2} \end{cases}$$

There are two issues with this capacity function which can cause problems in the numerical examples. One is that $p(\mathbf{y})$ is non-differentiable at $l/d = 1/2$. The second is the case where $F_{x,i}(\mathbf{x},\mathbf{y}) \geq H(\mathbf{y})$, as this produce a complex number. Neither caused any problems in the numerical experiments.

In regards with suction caissons with slenderness ratio less than 1 and embedded in clayey soils, the maximum tensile design load must not exceed the design tensile capacity, given as the

sum of the caisson weight, external shaft friction and reverse end bearing. Hence, the tensile capacity for suction foundation in clay can be estimated as

$$F_{z,i}(\mathbf{x},\mathbf{y}) - \frac{1}{2}V_t(\mathbf{y}) \leq 0, \quad i = 1,\ldots,n_f, \tag{5}$$

where

$$V_t(\mathbf{y}) = \frac{\pi\rho g}{200}d^3 + \pi\rho^f g(dt - t^2)l + \frac{9s_u\pi}{4}d^2 + \frac{s_u\pi}{5}dl \tag{6}$$

and ρ^f and g are the pile density and the gravitational constant, respectively. Here it is assumed that the thickness of the caisson lid is equal to $d/50$.

When the slenderness ratio is greater than 1, the expression of Supachawarote et al. [36] can be applied:

$$\left(\frac{F_{x,i}(\mathbf{x},\mathbf{y})}{H(\mathbf{y})}\right)^{a(\mathbf{y})} + \left(\frac{F_{z,i}(\mathbf{x},\mathbf{y})}{V_c(\mathbf{y})}\right)^{b(\mathbf{y})} - 1 \leq 0 \quad i = 1,\ldots,n_f, \tag{7}$$

where

$$H(\mathbf{y}) = 4dls_u, \quad V_c(\mathbf{y}) = \frac{9s_u\pi}{4}d^2, \quad a(\mathbf{y}) = \frac{l}{2d} + 4.5, \quad \text{and} \quad b(\mathbf{y}) = -\frac{l}{4d} + 3.5.$$

When the suction caisson undergoes to tensile loads, a similar failure envelope as described in equation (7) is assumed with the difference that $V_c(\mathbf{y})$ is substituted by the tensile capacity given by equation (6).

Due to the absence in the literature of mathematical formulations on the ultimate resistance of suction caissons embedded in sands, the closed-form expression suggested by Gottardi et al. [18] for circular footing on dense sand based on the concept of plasticity theory was adopted in this study:

$$\left(\frac{M_{y,i}(\mathbf{x},\mathbf{y})}{Q_i(\mathbf{x},\mathbf{y})}\right)^2 + \left(\frac{F_{x,i}(\mathbf{x},\mathbf{y})}{H_i(\mathbf{x},\mathbf{y})}\right)^2 + \frac{F_{x,i}(\mathbf{x},\mathbf{y})M_{y,i}(\mathbf{x},\mathbf{y})}{C_i(\mathbf{x},\mathbf{y})} - 1 \leq 0, \quad i = 1,\ldots,n_f,$$

where

$$Q_i(\mathbf{x},\mathbf{y}) = 0.36F_{z,i}(\mathbf{x},\mathbf{y})\left(1 - \frac{F_{z,i}(\mathbf{x},\mathbf{y})}{V_c(\mathbf{y})}\right)d, \quad H_i(\mathbf{x},\mathbf{y}) = 0.48F_{z,i}(\mathbf{x},\mathbf{y})\left(1 - \frac{F_{z,i}(\mathbf{x},\mathbf{y})}{V_c(\mathbf{x},\mathbf{y})}\right),$$

$$C_i(\mathbf{x},\mathbf{y}) = 0.39F_{z,i}(\mathbf{x},\mathbf{y})^2\left(1 - \frac{F_{z,i}(\mathbf{x},\mathbf{y})}{V_c(\mathbf{y})}\right)^2 d, \quad V_c(\mathbf{y}) = c_{ult}d^3,$$

$$\text{and} \quad c_{ult} = 0.11\gamma\pi\tan\phi\left(e^{\pi\tan\phi}\tan\left(45 + \frac{\phi}{2}\right) - 1\right)$$

On the other hand, the tensile capacity of suction caissons in sands is calculated according to the equation (5), where V_t is calculated as proposed by Houlsby et al. [20]:

$$V_t(\mathbf{y}) = \frac{\pi\rho g}{200}d^3 + \pi\rho g(dt - t^2)L + P_\gamma(d - t)L^2, \quad \text{and} \quad P_\gamma = \gamma\pi\left(1 - \sin\phi\right)\tan\frac{\phi}{3}$$

2.8 Design sensitivities of the joint reaction forces

The design sensitivities of the reaction forces $\mathbf{f}_i^f(\mathbf{x},\mathbf{y})$ with respect to jacket variables $\mathbf{x}$ and foundation variables $\mathbf{y}$ can be computed as

$$\begin{aligned}\frac{\mathrm{d}\mathbf{f}_i^f(\mathbf{x},\mathbf{y})}{\mathrm{d}\mathbf{x}} &= \mathbf{K}_i^f(\mathbf{y})\frac{\mathrm{d}\mathbf{u}_i^f(\mathbf{x},\mathbf{y})}{\mathrm{d}\mathbf{x}} \\ \frac{\mathrm{d}\mathbf{f}_i^f(\mathbf{x},\mathbf{y})}{\mathrm{d}\mathbf{y}} &= \mathbf{K}_i^f(\mathbf{y})\frac{\mathrm{d}\mathbf{u}_i^f(\mathbf{x},\mathbf{y})}{\mathrm{d}\mathbf{x}} + \frac{\mathrm{d}\mathbf{K}_i^f(\mathbf{y})}{\mathrm{d}\mathbf{y}}\mathbf{u}_i^f(\mathbf{x},\mathbf{y})\end{aligned} \tag{8}$$

where the sensitivities of the pile head displacements are found by solving the full system

$$\mathbf{K}(\mathbf{x},\mathbf{y})\frac{\mathrm{d}\mathbf{u}(\mathbf{x},\mathbf{y})}{\mathrm{d}v_k} = \frac{\mathrm{d}\mathbf{f}(\mathbf{x},\mathbf{y})}{\mathrm{d}v_k} - \frac{\mathrm{d}\mathbf{K}(\mathbf{x},\mathbf{y})}{\mathrm{d}v_k}\mathbf{u}(\mathbf{x},\mathbf{y})$$

for each variable v_k in $\mathbf{x}$ and $\mathbf{y}$.

2.9 Implementation

The structural analysis model and sensitivity analysis are implemented in a Matlab package called JADOP (JAcket Design OPtimization), and interfaces the optimizer IPOPT [39]. JADOP is an analysis and optimization software developed for optimal design of jacket structures, and this paper documents the extension to foundation modelling and design. IPOPT is an open source software package for large-scale nonlinear optimization. It uses a primal-dual interior point method with filters to promote global convergence. The tolerance is set to 10^{-5}, and the nlp scaling is turned off. Instead a user-defined scaling of 10^{-5} is applied to the stiffness and mass matrix, the load, the stresses, and the objective function.

3 Numerical study

The optimal design problem is solved to propose foundation and jacket designs for an offshore wind turbine at 50 m water depth. Piles and suction caissons are considered as foundation types, while different soil conditions are investigated as described in the following.

3.1 Definition of design parameters

A structural finite element model with piles, jacket, transition piece, and tower is built in JADOP, see Figure 3. All cross sections are assumed to be thin-walled pipes with constant cross section along the element length, and with a shear correction factor of 0.5 [11]. The material is steel, and the density and yield stress is set to 7800 kg/m^3 and 355 MPa for both jacket and foundation.

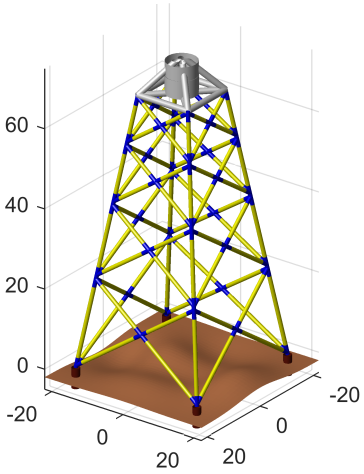

Figure 3: Describe the structure.

The jacket has four straight legs, and four levels of X-braces. The leg distance is 30 meters at the bottom, and 14 meters at the top. The structure is symmetric, and the footprint is square. The transition piece, tower, and RNA is modelled to be a close replica of the DTU 10 MW reference wind turbine, see [3] and [6].
In order to cover a broad spectrum of soil conditions, different sets of soil profiles have been taken into account, representing both cohesive (clay) and cohesionless (sand) soil. The definition of the soil profiles was based on the soil categorization scheme suggested in EC8 ([16]−part 1). The optimal design problem is solved where feasible for ten different soil properties described in Table 2. The Young modulus of the soil was estimated based on the elastic shear wave velocity, thus it is representative of small strain stiffness. Unless otherwise specified, soil-type B is used in the numerical studies.

Table 2: Soil profiles considered in the optimization study.

Soil Profile	Shear wave velocity [m/s]	Youngs modulus [MPa]	Angle of friction [deg]	Undrained shear strength [kPa]	Unit weight [kN/m3]
A	600	2138	45	300	22
B	400	864	40	250	20
C	250	287	35	150	17
D	100	44.6	33	50	16.5
E	50	10.8	30	20	16

Moreover five different CPT records from offshore sites were analysed. The tip resistance is plotted in Figure 4 along with the results of the classification analysis which was carried out according to Robertson et al. [32]. The strength properties of the cohesionless layers were evaluated by first calculating the relative densities D_r [22] and then the angle of shearing resistance (friction) ϕ, while for the cohesive layers N_{kt} was assumed to be 15 [26]. As shown in Figure 4 the first CPT is characterized by a homogeneous sand layer of D_r equal to 80% and angle of shearing resistance between 39° and 42°. Three different soil layers are found at the second

CPT, starting from silt (from clayey to sandy), to alternating layers of sand and gravelly sand. The undrained shear strength was estimated for the silt layer to 200kPa, while the cohesionless layers had D_r between 77% and 87% with angles of friction 38.5° to 43.7° respectively. At the third CPT 4 layers were identified namely silty sand, sand, silty sand and gravelly sand. The relative density increases from the silty sand layers to the sand and the gravelly sand, and the same holds for the angle of friction as expected. The first 18m of the fourth CPT provided a very scattered trend in Robertson's classification chart [32] ranging from silty clay to silty sand without a clear pattern with increasing depth. The deeper layers are gravelly sand and sand with mean D_r 89% and 73% respectively. The last CPT is characterized by alternating sand and gravelly sand layers with very high D_r values ranging between 84% and 94%. Concluding it was found that most of the CPT profiles were characterized by cohesionless soil layers with relative densities D_r varying between 73% and 94% and angles of friction between 38° and 44°. Therefore the CPT data are appropriate for the implementation of the UWA method [25] for estimation of the axial pile capacity. Unless otherwise specified, the CPT−data named CPT4 is used in the numerical studies.

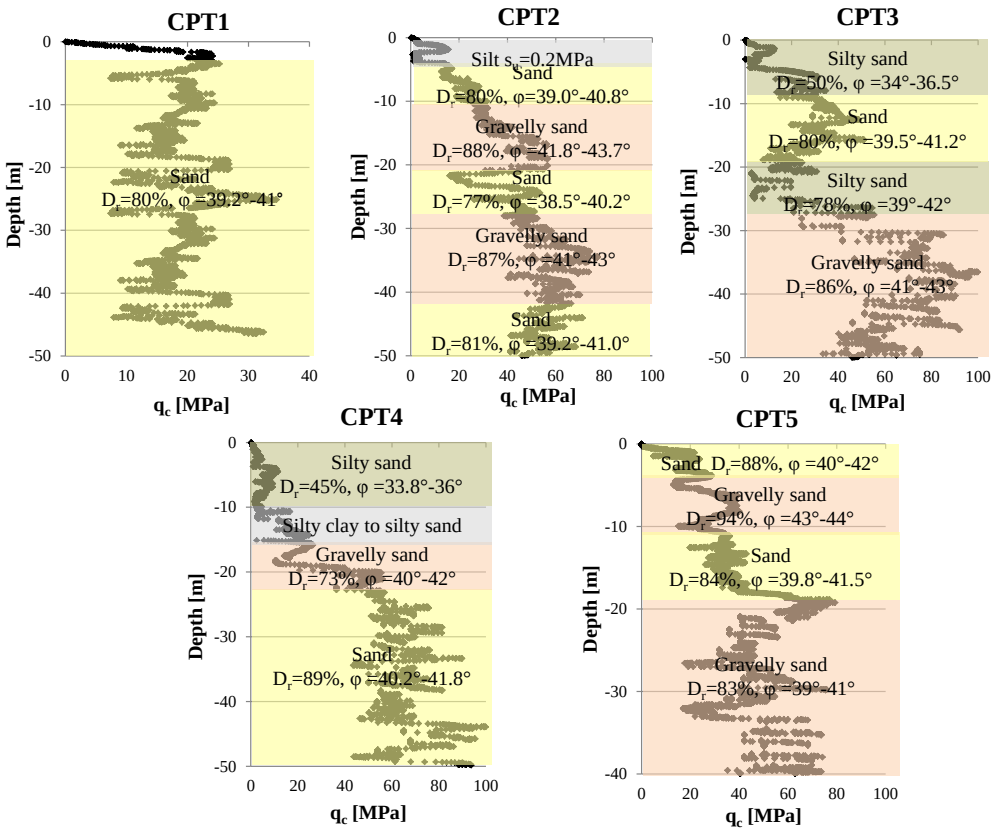

Figure 4: Five CPT data sets.

In the fatigue limit state load cases the stress constraints are bounded by an equivalent fatigue limit, which is the stress corresponding to 20 years of fatigue life when the 1 Hz damage equivalent load is applied. In addition, the stresses in the elements connected to a tubular joint are multiplied with stress concentration factors according to [14]. Bounds on the jacket and foundation design variables, natural frequency, as well as stress constraints in ultimate and fatigue load cases are given in Table 3. Note that the foundation capacity constraints and linear constraints are not included in Table 3.

Table 3: Soil profiles considered in the optimization study.

Bounds	Jacket	Pile	Suction caisson	Full structure
Lower diameter	0.4 m	1 m	2 m	-
Upper diameter	1.4 m	6 m	11 m	-
Lower thickness	15 mm	15 mm	15 mm	-
Upper thickness	120 mm	120 mm	400 mm	-
Lower length	-	10 m	2 m	-
Upper length	-	60 m	20 m	-
Lower frequency	-	-	-	0.178 Hz
Upper frequency	-	-	-	0.270 Hz
Yield stress	355 MPa	355 MPa	355 MPa	-
Equivalent fatigue limit	11.5 MPa	-	-	-

3.2 Integrated optimal designs of jacket and foundations

The optimal design problem is solved for suction caissons and piles in both sand and clay, and the results are shown in Table 4. All jacket designs converge to approximately the same mass and the same design. This indicates that jacket design is fairly decoupled from the design of the foundation for the soil conditions and jacket leg distance considered here.

The different foundation design cases lead to very different masses. It can be observed that the piles in clay are heavier than the ones designed for a sand site. Moreover for a clay site the best foundation solution, in terms of mass appears to be the suction caisson with slenderness ratio equal to 1. However the opposite trend is observed in sand, where the suction caisson is more than an order of magnitude heavier than the piles. As the pull-out force is design-driving for most of the foundation design cases, the suction caisson in sand becomes extremely heavy due to the poor tensile capacity. Additionally the CPT based method provides a more economic pile design in the sand site. Note that CPT4 can be grossly characterized as soil type B listed in Table 4, therefore the comparison of the pile designs is consistent. An alternative solution to make the use of suction caissons attractive would be to increase the mass of the structure, for example with a transition piece made by concrete. In the following numerical simulations the suction caisson in sand design case is excluded, as the design can be hardly comparable to the other design cases.

Table 4: Optimization results for integrated optimal design of jackets and foundations with two foundation types and two soil types.

Soil profile	Foundation design case	Jacket mass [tons]	Foundation mass [tons]	Foundation diameter [m]	Foundation wall thickness [mm]	Foundation length [m]
Clay	Pile	631	87.4	1.89	25.2	18.9
	Caisson	635	49.8	4.18	48.1	2.56
	Caisson (l/d >1)	634	35.6	3.12	37.6	3.13
Sand	Pile	633	73.5	1.24	18.7	32.8
	Pile (CPT)	633	51.8	1.13	17.6	27.1
	Caisson	636	1727	9.13	97.6	20.0

3.3 Sequential optimal designs of jacket and foundations

In the previous example the design of foundation and jacket was done in an integrated optimization. A simpler approach is to do the designs sequentially. First the jacket design is optimized with clamped boundary conditions. Secondly, the jacket design is kept fixed, and the foundation design is optimized. The results are shown in Table 5.

Table 5: Optimization results for all two foundation types and two soil types, using pre-designed jacket.

Soil profile	Foundation design case	Jacket mass [tons]	Foundation mass [tons]	Foundation diameter [m]	Foundation wall thickness [mm]	Foundation length [m]
Clay	Pile	637	91.5	1.20	18.3	43.3
	Caisson	637	49.8	4.20	48.3	2.53
	Caisson (l/d >1)	637	35.6	3.13	37.6	3.13
Sand	Pile	637	74.1	1.25	18.8	32.6
	Pile (CPT)	637	69.4	1.50	21.3	22.5
	Caisson	637	1726	9.12	97.5	20.0

The optimized jacket mass is of course the same for all foundation design cases, since it was designed without a foundation model. The jacket mass is heavier than in all of the integrated design cases, but the difference is less than one percent. This indicates that sequential design works well for the jacket, at least for the stiff soil conditions as is soil profile B.

The optimized suction caissons obtained from the sequential design procedure are practically identical with the designs obtained from the integrated design procedure. This might be either because the caissons are very stiff in rotation, and thus act similarly as a clamped boundary condition, or because the mass of the jacket is only marginally decreased in the integrated optimization with suction caissons.

The optimized piles obtained from the sequential design procedure are also comparable with the designs obtained from the integrated design procedure. Regarding the sand site, the pile design according to the CPT−based method, has 34% higher mass. However, it is still more economic than the traditional pile in sand design from the integrated design procedure. The

CPT design has also become less slender. The pile in clay becomes 5% heavier, and increases its slenderness ratio.

3.4 Influence of leg distance on foundation design

The loads on the foundation change when the leg distance of the jacket varies. Figures 5 and 6 show how the jacket and foundation change when the leg distance is varied between 18m and 38m.

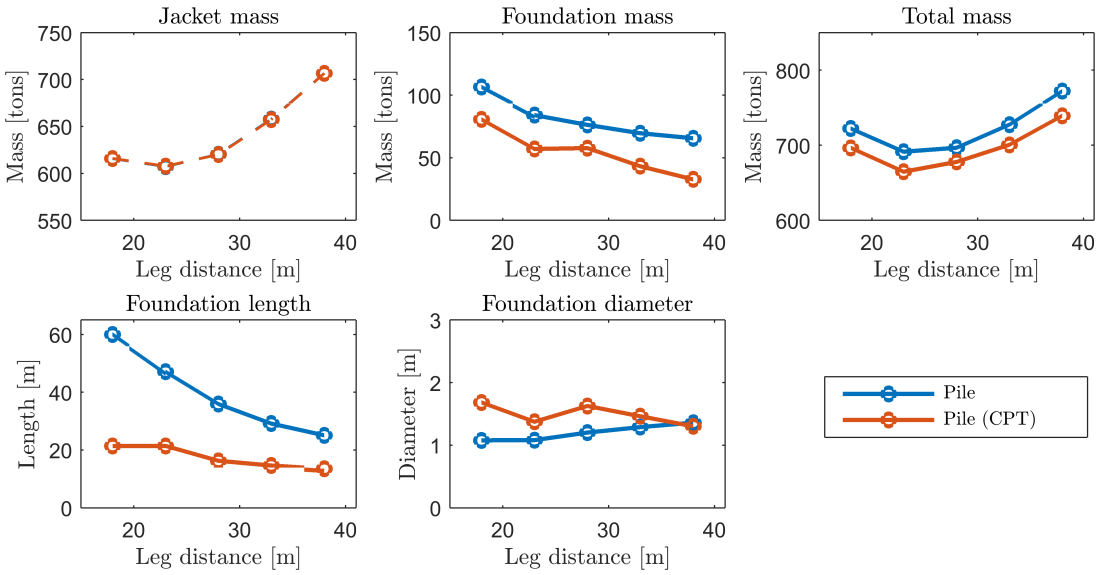

Figure 5: Variation of the jacket, foundation and total masses, foundation length and diameter with respect to the leg distance in sand soil profile.

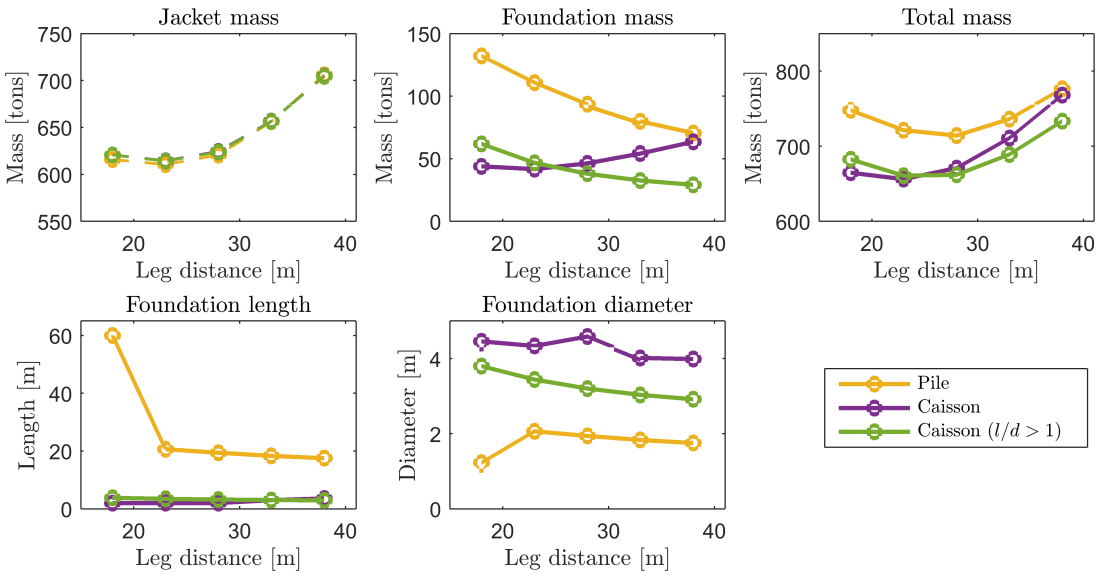

Figure 6: Variation of the jacket, foundation and total masses, foundation length and diameter with respect to the leg distance in clayey soil profile.

The integrated optimization for the jackets installed in sand profiles results in increased mass of the jacket as the leg distance increases. On the contrary the foundation (pile) mass decreases mainly due to the decrease of the pile length. The fact that the foundation mass reduces as the leg distance increases is determined by the redistribution of the axial forces among the single foundations. The total mass exhibits an increasing trend, as the foundation mass comprises a smaller portion with increasing leg distance. The pile design is influenced by the applied design method, and consistently the CPT based method provides shorter piles with larger diameters and smaller total mass. The jacket mass increases with increasing leg distance, and therefore the total substructure mass (left) is lowest at an intermediate leg distance between 23m and 28m, depending on foundation type.
The general trends in the jacket and foundation mass observed in the sand profile are also valid for the clay profile. Exception to this is the caisson with the slenderness ratio (L/d) smaller than 1, which appears to increase in mass with increasing leg distance of the jacket. This could be mean that the combined failure due to vertical and horizontal load becomes more critical as the pull out force decreases with increasing leg distance. It is also worth noticing that the suction caissons result always in lower foundation mass compared to the piles. Additionally the design of suction caisson in clayey soil with slenderness ratio $L/d > 1$ showed that the foundation diameter doubled as the leg distance reduces; while this increasing pattern is less apparent for the suction caisson with slenderness ratio $L/d \leq 1$.

3.5 Influence of soil properties on jacket and foundation design

Figures 7 and 8 show how the foundation design varies as a function of soil stiffness, where A and E represent the stiffest and the softest soil deposit, respectively. The CPT-pile design case is based on a medium to stiff soil profile, and is therefore only solved for soil types A, B and C.

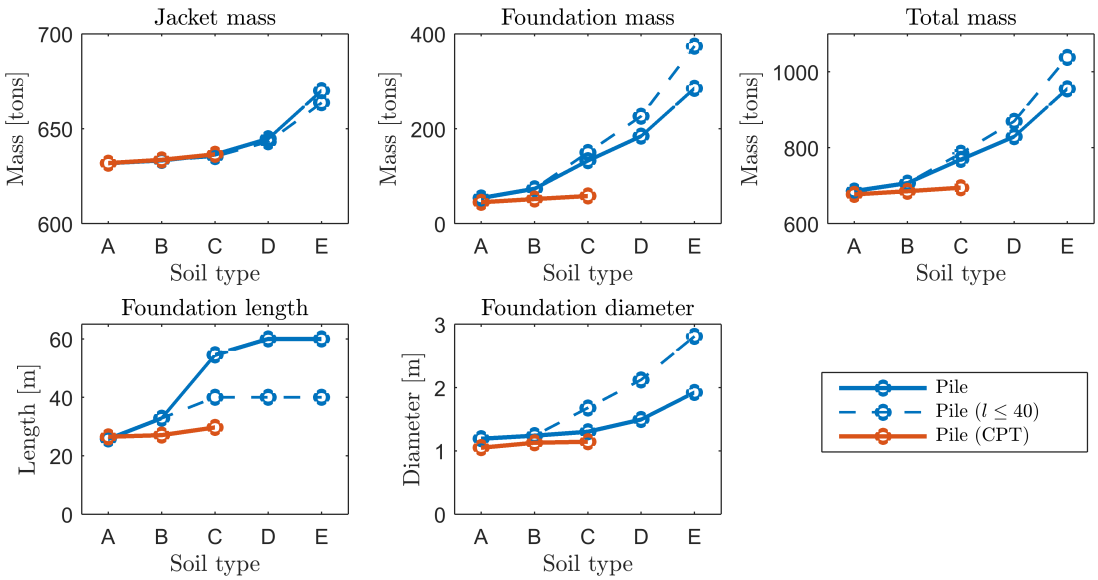

Figure 7: Effect of the soil type on the jacket, foundation and total masses, foundation length and diameter in sand soil profile.

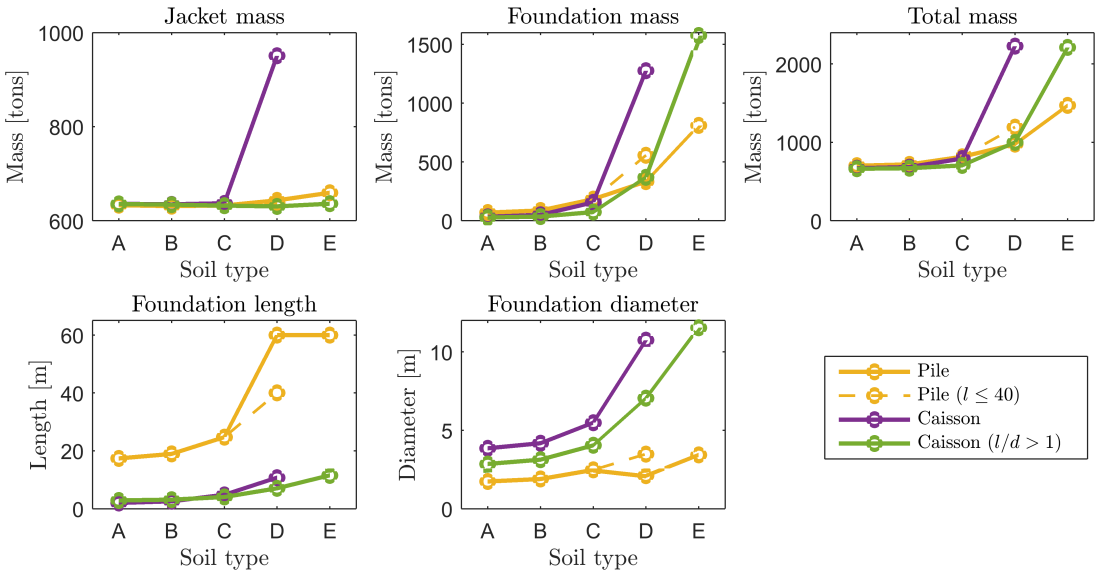

Figure 8: Effect of the soil type on the jacket, foundation and total masses, foundation length and diameter in clay soil profile.

The CPT based design was performed for the soil stiffness reported as soil type A, B and C, which is representative for the measured tip resistance of CPT 4. The investigation of the soil type effect on the optimization of the design in sand profiles demonstrates that the mass of the jacket is influenced by the foundation stiffness, especially for medium dense to loose sand

deposits (type D and E). As expected the foundation mass increases also as the stiffness and strength of the sand decreases. It is interesting to observe that the length is the preferred optimization parameter compared to the diameter. This is evident by comparing the results of the pile design with maximum length constraint set to 60m and 40m. It is shown that in the first case the length of the pile increases more rapidly compared to the diameter, while the opposite holds for the latter case. In regards with the CPT based method it is seen that the foundation mass is always smaller than the one provided by the traditional design approach, with the design diameter being always smaller and the pile length substantially reduced.
The jacket mass appears to increase with decreasing soil stiffness also for the foundation designs in clay, where particularly high mass is obtained for suction caissons with small slenderness ratio. On the contrary suction caissons with large slenderness ratio affect to a minor extent the design of the jacket, which could be attributed to their larger rotational and coupling stiffness components. When it comes to the foundation optimization the caisson with the larger slenderness ratio is the foundation type with the lower mass for soil types up to C, however for soil type D and E the long pile results in smaller mass.

3.6 Influence of CPT data on pile design

In the optimal design problem, the maximum pile length was set to 60m. To comply with such piles, the CPT data sets were linearly extrapolated. However, none of the CPT-piles in the numerical simulations exceeded 30m. The optimal design problem was solved for all five CPT data sets, and the results are shown in Table 6.

Table 6: Optimization results for all five CPT data sets.

Foundation design case	Pile mass [tons]	Diameter [m]	Wall thickness [mm]	Length [m]	Mean q_c [MPa]
Pile in sand (CPT1)	102	1.98	26.1	20.5	18.2
Pile in sand (CPT2)	44.7	1.22	18.5	20.5	26.7
Pile in sand (CPT3)	54.4	1.59	22.2	15.9	23.4
Pile in sand (CPT4)	51.8	1.13	17.6	27.1	21.4
Pile in sand (CPT5)	52.2	1.49	21.2	17.0	27.8

The foundation mass obtained after the optimization with the CPT records $2-5$ is very similar, indicating that the sensitivity of the pile design to variations of the tip resistance is not significant. On the other hand the pile design according to the first CPT record resulted in a foundation mass double than the other records. As shown in Table 5, the mean tip resistance over the pile length for CPT1 is lower than the corresponding of CPTs $2-5$. This can be explained by the lower tip resistance values. Comparing the CPT based design with the traditional approach the first record would be closer to soil type C, which resulted in mass slightly higher than 100tons according to Figure 7. It can be concluded that regardless of slight variations in the CPT data the CPT based method provides more economic pile designs.

3.7 Influence of leg distance and soil type on structural frequency

The first natural frequency of an offshore wind turbine structure should lie in the range between the 1P and 3P frequencies of the rotor to avoid resonance problems. For the DTU 10 MW reference wind turbine this range is from 0.16 to 0.30 Hz. A safety margin of 10 percent is often included, which means that the allowable frequency range is actually from 0.176 to 0.27 Hz, as shown in Table 3. While the frequency is dominated by the tower and turbine, the soil, foundation type, and jacket has some small influence on the natural frequency.

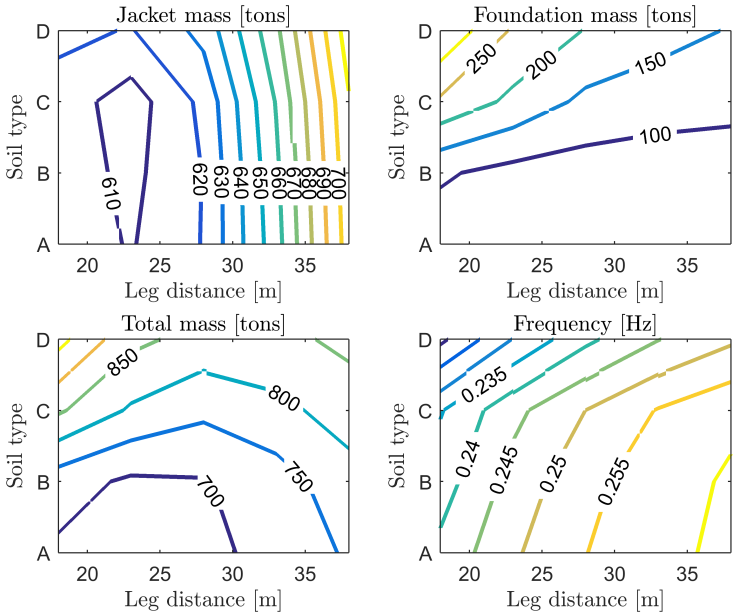

Figure 9: Variation of the frequency, jacket and foundation masses with respect to the leg distance and soil stiffness for pile foundation in sand.

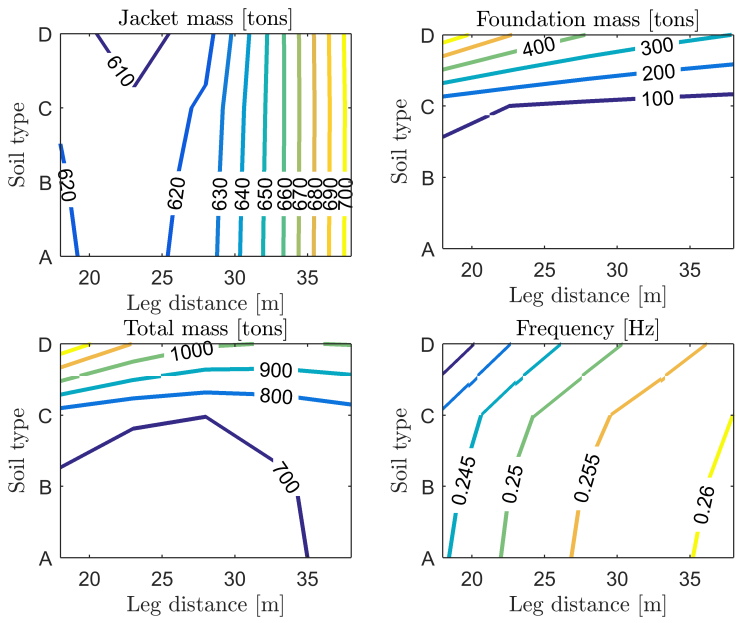

Figure 10: Variation of the frequency, jacket and foundation masses with respect to the leg distance and soil stiffness for suction caisson foundation ($l/d > 1$) in clay.

In Figures 9 and 10, the jacket mass, foundation mass, total mass, and the lowest natural frequency of the full structure is plotted as a function of both leg distance and soil type. All data points are the result of an integrated optimization as described previously. First of all, the jacket mass is mostly a function of the leg distance, though for leg distances below 30 meters the mass is also varying with soil type. The mass of the piles in sand increase with softer soil and smaller leg distance, as observed earlier. The mass of the suction caisson in clay, however, is almost exclusively dependent on the soil type. Finally, the frequency plots show how the frequency decreases with smaller leg distance and softer soil. Note that with softer soils, the foundation mass increases while the frequency drops. This means that even though the foundation mass increases, the stiffness of the foundation actually decreases.

Based on this numerical study, it seems that the foundation and jacket design are quite decoupled, especially for suction caissons, and at least for medium to stiff soils. However, with small leg distance, soft soils, and piled foundation, the interaction is too large to be ignored. Notice for example that the frequency of the pile in sand for a 20 meter leg distance decreases from 0.245 Hz to 0.225 Hz when the soil type is changed from A to D. This drop in frequency of 8 percent can have significant implications for the structural response, and should be considered throughout the design process.

4 Conclusion

In this paper we have demonstrated that numerical optimization can be applied to automate several of the standard procedures for foundation design. This is not only beneficial because new foundation designs can be generated quickly when the design conditions are changed. It also

allows for integrated design of the jacket and the foundation. Integrated design optimization of jacket and foundation for two different foundation types, a range of different leg distances, and ten soil profiles revealed some trends:

- The jacket design is not very dependent on foundation design. The exception is for very soft soils when jacket mass can increase by 10%.
- The foundation design is very dependent on the jacket mass. This is because the pull-out force is often design driving.
- The jacket mass depends mostly on leg distance, while the foundation mass depends mostly on the soil stiffness. It appears that there is an optimal leg distance where the support structure mass becomes minimum. This is only marginally increased for suction caissons in clay, else it is independent of the foundation design. The natural frequency of the full structure depends on both.
- The natural frequency of the full structure is overestimated when the jacket is clamped at the seabed, but for stiff soils the error is smaller than one percent. For piled foundations in soft soil, the error can be up to ten percent.
- Sequential design works better for design of suction caissons than it does for piles. This is because suction caissons are stiffer in rotation than piles.

These observations are based only on extreme static loads with linear elastic soil models. Dynamic loads and more complex soil models might give other insights. It should also be noted that the objective function was steel mass. Cost drivers such as manufacturing, transportation and installation were not taken into account. However it should be noted that the manufacturing costs are also dependent on the mass, and together with the material costs they comprise the largest part of the costs for construction of support structures. Also, the lid and stiffeners of the foundations were not included in the mass function. This leads to a non-conservative estimate of the mass, especially for the suction caissons.
Future work on design optimization of foundations should focus on more realistic load cases and more advanced soil models, ideally including the effects of cyclic loading and nonlinear response. Another interesting aspect is to include the foundation installation as a design variable, since pile driving costs depend on the sizing of the piles.

5 Acknowledgements

The research presented in this manuscript is part of the strategic research project ABYSS: Advancing BeYond Shallow waterS (www.abyss.dk) sponsored by the Danish Council for Strategic Research, Grant no. 1305-00020B. The funding is gratefully acknowledged.

References

[1] API. Geotechnical and foundation design considerations. ANSI/API RP 2GEO 1st edition Petroleum and natural gas industries: Specific requirements for offshore structures, Part 4. Technical report, API, 2011.

[2] T. Ashuri. *Beyond Classical Upscaling : Integrated Aeroservoelastic Design and Optimization of Large Offshore Wind Turbines*. PhD thesis, Technische Universiteit Delft, 2012.

[3] C. Bak, F. Zahle, R. Bitsche, T. Kim, A. Yde, L. C. Henriksen, A. Natarajan, and M. Hansen. The DTU 10 MW reference wind turbine. Technical report, DTU Wind Energy, 2013.

[4] S. A. Barakat, A. I. Malkawi, and R. H. Tahat. Reliability-based optimization of laterally loaded piles. *Structural Safety*, 21(1):45 – 64, 1999.

[5] S. Bhattacharya. Challenges in design of foundations for offshore wind turbines. *Engineering & Technology Reference*, 1(1), 2014.

[6] T. Borstel. Design report - reference jacket. Technical Report D4.3.1, DTU Wind Energy, 2013.

[7] B. Broms. Methods of calculation for laterally loaded piles. *Royal Swedish Geotechnical Institute – Reprints and Preliminary Reports*, (9), 1965.

[8] C. M. Chan, L. M. Zhang, and J. T. Ng. Optimization of Pile Groups Using Hybrid Genetic Algorithms. *Journal of Geotechnical and Geoenvironmental Engineering*, 135(4):497–505, apr 2009.

[9] K. H. Chew, K. Tai, E. Y. K. Ng, and M. Muskulus. Analytical gradient-based optimization of offshore wind turbine substructures under fatigue and extreme loads. *Marine Structures*, 47:23–41, 2016.

[10] C. Clausen, P. Aas, and K. Karlsrud. Bearing capacity of driven piles in sand, the NGI approach. In *Proceedings of Proceedings of International Symposium. on Frontiers in Offshore Geotechnics, Perth*, pages 574–580, 2005.

[11] R. D. Cook, D. S. Malkus, M. E. Plesha, and R. J. Witt. *Concepts and Applications of Finite Element Analysis*. John Wiley & Sons, fourth edition, 2007.

[12] W. de Vries. Final report WP 4 . 2 Support Structure Concepts for Deep Water Sites. Technical report, Delft University of Technology, 2011.

[13] DNV. RP-C202: Buckling Strength of Shells. Technical Report January, DNV, 2013.

[14] DNVGL. RP-C203 Fatigue design of offshore steel structures. Technical report, DNVGL, 2014.

[15] DNVGL. OS-C101 Design of Offshore Steel Structures, general - LRFD method. Technical Report July, DNVGL, 2015.

[16] C. Eurocode. 8: Design of structures for earthquake resistance—part 1: General rules, seismic actions and rules for buildings (en 1998-1: 2004). *European Committee for Normalization, Brussels*, 2004.

[17] P. Fuglsang and H. A. Madsen. Optimization method for wind turbine rotors. *Journal of Wind Engineering and Industrial Aerodynamics*, 80(1-2):191–206, 1999.

[18] G. Gottardi, G. Houlsby, and R. Butterfield. Plastic response of circular footings on sand under general planar loading. *Géotechnique*, 49(4):453–470, 1999.

[19] S. Gourvenec. Effect of embedment on the undrained capacity of shallow foundations under general loading. *Géotechnique*, 58(3):177–186, 2008.

[20] G. T. Houlsby, R. B. Kelly, and B. W. Byrne. The tensile capacity of suction caissons in sand under rapid loading. In *Proceedings of the international symposium on frontiers in offshore geomechanics, Perth*, pages 405–410, 2005.

[21] IEC. IEC 61400-3: Wind turbines - Part 3: Design requirements for offshore wind turbines. Technical Report 300 V, IEC, 2009.

[22] M. Jamiolkowski, D. Lo Presti, and M. Manassero. Evaluation of relative density and shear strength of sands from cpt and dmt. In *Soil behavior and soft ground construction*, pages 201–238. 2003.

[23] C. H. Juang and L. Wang. Reliability-based robust geotechnical design of spread foundations using multi-objective genetic algorithm. *Computers and Geotechnics*, 48:96 – 106, 2013.

[24] C. Latini and V. Zania. Dynamic lateral response of suction caissons. *Soil Dynamics and Earthquake Engineering*, 100:59–71, 2017.

[25] B. Lehane, J. Schneider, and X. Xu. The UWA-05 method for prediction of axial capacity of driven piles in sand. *Frontiers in Offshore Geotechnics: ISFOG*, pages 683–689, 2005.

[26] T. Lunne, P. Robertson, and J. Powell. Cone penetration testing. *Geotechnical Practice*, 1997.

[27] G. Meyerhof. Compaction of sands and bearing capacity of piles. *Transactions of the American Society of Civil Engineers*, 126(1):1292–1322, 1961.

[28] M. Muskulus and S. Schafhirt. Design Optimization of Wind Turbine Support Structures — A Review. *Journal of Ocean and Wind Energy*, 1(1):12–22, 2014.

[29] J. Oest, R. Sørensen, L. C. T. Overgaard, and E. Lund. Structural optimization with fatigue and ultimate limit constraints of jacket structures for large offshore wind turbines. *Structural and Multidisciplinary Optimization*, 55(3):779793, 2017.

[30] T. Pucker and J. Grabe. Structural optimization in geotechnical engineering: Basics and application. *Acta Geotechnica*, 6(1):41–49, 2011.

[31] M. F. Randolph. The response of flexible piles to lateral loading. *Geotechnique*, 31(2):247–259, 1981.

[32] P. Robertson. Soil classification using the cone penetration test. *Canadian Geotechnical Journal*, 27(1):151–158, 1990.

[33] K. Sandal and V. Zania. Optimization of pile design for offshore wind turbine jacket foundations. In *12th EAWE PhD seminar on Wind Energy in Europe*, 2016.

[34] M. Seidel, S. Voormeeren, and J. van der Steen. State-of-the-art design processes for offshore wind turbine support structures. *Stahlbau*, 85(9):583–590, 2016.

[35] K.-F. Seitz and J. Grabe. Three-dimensional topology optimization for geotechnical foundations in granular soil. *Computers and Geotechnics*, 80:41–48, 2016.

[36] C. Supachawarote, M. Randolph, and S. Gourvenec. Inclined pull-out capacity of suction caissons. In *The Fourteenth International Offshore and Polar Engineering Conference*. International Society of Offshore and Polar Engineers, 2004.

[37] The Crown Estate. Offshore wind cost reduction-Pathways study. Technical report, The Crown Estate, 2012.

[38] A. Thiry, F. Bair, L. Buldgen, B. G. Raboni, and P. Rigo. Optimization of monopile offshore wind structures. *Advanced Marine Structures*, pages 633–642, 2011.

[39] A. Waechter and L. T. Biegler. On the Implementation of a Primal-Dual Interior Point Filter Line Search Algorithm for Large-Scale Nonlinear Programming. *Mathematical Programming*, 106(1):25–57, 2006.

[40] D. Zwick and M. Muskulus. The simulation error caused by input loading variability in offshore wind turbine structural analysis. *Wind Energy*, 18(8):1421–1432, 2014.

[41] D. Zwick, M. Muskulus, and G. Moe. Iterative Optimization Approach for the Design of Full-Height Lattice Towers for Offshore Wind Turbines. *Energy Procedia*, 24:297–304, jan 2012.

A Appendix

This appendix describes the friction, end bearing, and lateral capacity functions for the piles in sand and clay, as well as for the pile design using the CPT approach. Note that the foundation variable is $\mathbf{y} = \begin{pmatrix} d & t & l \end{pmatrix}^T$, where the superscript f is omitted for brevity.

A.1 Pile in clay

The friction capacity Q_f for piles in clay, as used in equation (2), is according to the α–method formulated in [1] computed as

$$Q_f(d,t,l) = \frac{2}{5}\pi d s_u^{\frac{3}{4}} \gamma^{\frac{1}{4}} z_{1c}^{\frac{5}{4}} + \frac{1}{3}\pi d s_u^{\frac{1}{2}} \gamma^{\frac{1}{2}} (l - z_{1c})^{\frac{3}{2}},$$

where

$$z_{1c}^c = \min\left(\frac{s_u}{\gamma}, l\right)$$

The non-differentiability of z_1 can potentially cause problems in the optimization, but this has not been observed in the numerical experiments. There are two alternatives for the end bearing capacities Q_b, and the lowest value shall be used. In practice that means that both alternatives can be applied as separate constraints, i.e.

$$-(Q_f(\mathbf{y}) + Q_{b_k}(\mathbf{y})) \leq F_{z,i}(\mathbf{x},\mathbf{y}) \leq Q_f(\mathbf{y}), \quad i = 1,\ldots,n_f, \quad k = 1,2$$

where

$$Q_{b_1}(\mathbf{y}) = \frac{9 s_u \pi d^2}{4}$$
$$Q_{b_2}(\mathbf{y}) = \frac{9 s_u \pi}{4}\left(d^2 - (d-2t)^2\right) + Q_{fi}(\mathbf{y}),$$

and $Q_{fi}(\mathbf{y})$ is the same as $Q_f(\mathbf{y})$, except with $d - 2t$ instead of d.

A.2 Pile in sand

The friction capacity Q_f for piles in sand, as used in equation (2), is according to the β–method formulated in [1] computed as

$$Q_f(d,t,l) = \frac{\pi}{2} d\beta\gamma z_{1s}^2 + \pi d f_{max}(l - z_{1s}),$$

where

$$z_{1s} = \min\left(\frac{f_{max}}{\beta\gamma}, L\right).$$

There are four alternatives for the end bearing capacity Q_b, and the lowest value shall be used. In practice that means that all alternatives can be applied in separate constraints, i.e.

$$-(Q_f(\mathbf{y}) + Q_{b_k}(\mathbf{y})) \leq F_{z,i}(\mathbf{x},\mathbf{y}) \leq Q_f(\mathbf{y}), \quad i = 1,\ldots,n_f, \quad k = 1,\ldots,4 \tag{9}$$

where

$$
\begin{aligned}
Q_{b_1}(\mathbf{y}) &= \frac{N_q \gamma \pi d^2 l}{4} \\
Q_{b_2}(\mathbf{y}) &= \frac{N_q \gamma \pi (d^2 - (d-2t)^2) l}{4} + Q_{fi}(\mathbf{y}) \\
Q_{b_3}(\mathbf{y}) &= \frac{q_{b,max} \pi d^2}{4} \\
Q_{b_4}(\mathbf{y}) &= \frac{q_{b,max} \pi (d^2 - (d-2t)^2)}{4} + Q_{fi}(\mathbf{y}).
\end{aligned}
$$

A.3 UWA-CPT based method

The friction capacity Q_f for piles in a soil described by CPT data, as used in equation (3), is according to the UWA-CPT method [25] computed as

$$
Q_f(\mathbf{y}) = P_\phi d \left(\frac{4t(d-t)}{d^2} \right)^{0.3} \left(\sqrt{d} f(d, L) + 2 g(d, L) \right)
$$

where

$$
P_\phi = \pi \tan(0,75\phi), \quad f(d, L) = \int_0^{L-2d} \frac{q_c(z)}{\sqrt{L-z}} \mathrm{d}z \quad \text{and} \quad g(d, L) = \int_{L-2d}^{L} q_c(z) \, \mathrm{d}z.
$$

The end bearing capacity is computed as

$$
Q_b(d, t, L) = \frac{\pi}{40} \left(d + \frac{6t(d-t)}{d} \right) k(d, L)
$$

where

$$
k(d, L) = \int_{L-1.5d}^{L+1.5d} q_c(z) \, \mathrm{d}z.
$$

Paper IV

M. Stolpe, K. Sandal, Structural optimization with several discrete design variables per part by outer approximation. To be submitted to *Structural and Multidiciplinary Optimization*.

Structural optimization with several discrete design variables per part by outer approximation

Mathias Stolpe * Kasper Sandal †

July 14, 2017

Abstract

The article proposes an optimal design approach to minimize the mass of load carrying structures with discrete design variables. The design variables are chosen from catalogues, and several variables are assigned to each part of the structure. This allows for more design freedom than only choosing parts from a catalogue. The problems are modelled as mixed 0–1 nonlinear problems with nonconvex continuous relaxations. An algorithm based on outer approximation is proposed to find optimized designs. The capabilities of the approach are demonstrated by optimal design of a space frame (jacket) structures for offshore wind turbines, with requirements on natural frequencies, strength, and fatigue lifetime.

Keywords: Structural optimization, outer approximation, offshore wind turbines, jacket structures, discrete variables

1 Introduction

Computer-aided optimal structural design procedures can explore a large set of designs much faster than a classical design process. Numerical structural optimization is thus popular in design processes in for example automotive and aeroplane industries. However, these applications often consider continuous design variables, and the methods are not directly applicable to design problems with discrete design variables. The aim of this paper is to propose a heuristic and a method to solve optimal design problems with several discrete design variables per part and to illustrate their capabilities on industrially relevant design problems.

Optimal design of structures is often focused on minimizing mass by allowing large design freedom by continuous design variables. In practice the cost benefit is often larger if the structural components can be picked from a catalogue instead of being tailor-made. One such example is the offshore wind turbine support structure. In one wind farm, there can be as much as one hundred structures with a steel mass of more than a thousand tons each. To avoid high manufacturing costs, it is important that these designs are mass-manufacturable. This can be achieved for example by assembling mass-manufactured parts which are available in product catalogues.

*DTU Wind Energy, Technical University of Denmark, Frederiksborgvej 399, 4000 Roskilde, Denmark. E-mail: matst@dtu.dk

†DTU Wind Energy, Technical University of Denmark, Frederiksborgvej 399, 4000 Roskilde, Denmark. E-mail: kasp@dtu.dk

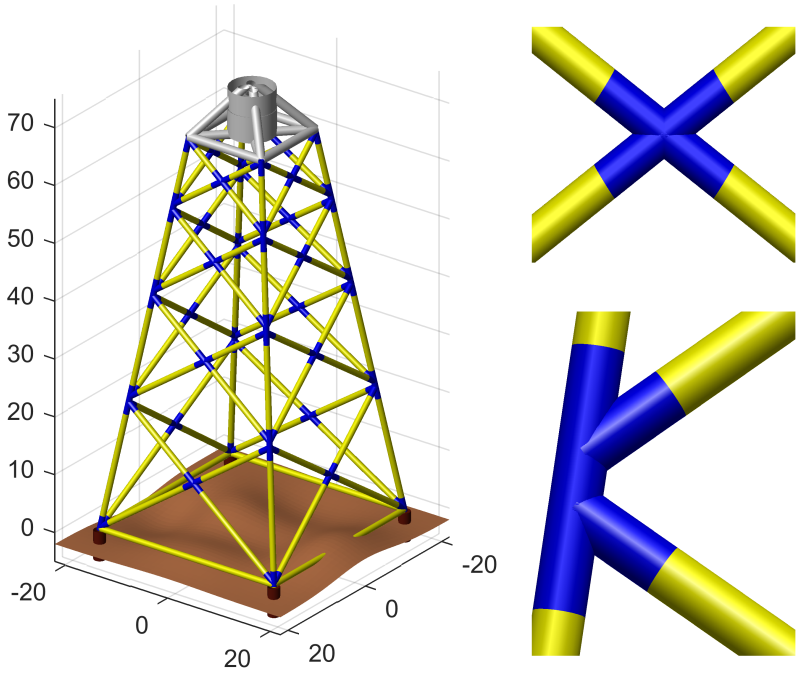

Figure 1: The jacket support structure. To the left is a jacket support structure for an offshore wind turbine at 50 m water depth. To the right is a close-up of welded X- and K-joints. The figure is made in the in-house software JADOP.

The specific example which illustrates the modelling and is the basis for the numerical experiments is design of a jacket support structure, as illustrated in Figure 1. The jacket structure under consideration is a four-legged space frame structure welded together from steel pipes in X- and K-joints. Here the tubular members are considered as parts, and the outer diameter and wall thickness are the two variables associated with each part. The number of degrees of freedom can be kept reasonable low since Timoschenko beam elements can be used for the structural analysis. The main issue in optimization is the size of the catalogues from which the dimensions of the parts should be chosen. These catalogues are in general rather large for the considered application. This difficult situation can partly be resolved by adding constraints on the geometric variation of the structure. Examples of such geometric constraints include that dimensions in braces must be smaller than dimensions in legs, and the diameter to thickness ratio is also limited.

Numerical structural optimization of frames is an extension of truss optimization, and many of the same methods and challenges are encountered. The mathematical properties of truss optimization with discrete design variables are discussed in [47], and the complexity of finding an optimal solution is emphasized. The segmental method presented in [45] avoids the combinatorial problem, but also gives no guarantee for a global optimal solution. Structural optimization with continuous design variables has seen a variety of applications. Optimization of truss structures with continuous design variables as well as joint position variables is applied to practical problems in [35]. Minimum mass of a frame is presented in [36], where Euler-Bernoulli and Timoshenko elements are shown to yield different solutions for non-slender beams. Emphasis on joint modelling and optimization in frame structures is given in [12] and [23]. Optimal design of frame structures for crash-worthiness in transient

analysis is given in [34]. Using the solution to the continuous problem to find an optimal design in discrete variables, however, is certainly not easy [44]. The review article [6] discusses problem formulations for structural optimization problems and emphasizes that while most formulations are focused on the truss element, they need to be extended to other complex structures.

Optimal design of support structures for offshore wind turbines is a non trivial task [31]. This is mainly due to the the advanced simulations required to obtain the structural response. Specialized aero-servo-elastic software are necessary to obtain accurate results, and these do not yet provide analytical design sensitivities. Several approaches to support structural design optimization are therefore based on gradient-free methods, using the specialized analysis software as a black box [48]. A ground structure approach with frame elements was used in [27] to perform topology optimization of a jacket with a genetic algorithm. A genetic algorithm was also used in [33] for combined joint-location and sizing optimization of a jacket. It is argued that this method can also be used for discrete dimensions, but this is not demonstrated. Improvements to [33] are presented in [39], but without the joint location variables. Another approach is to use simplified function evaluations, for example by assuming the rotor loads to be design independent, so that a regular finite element analysis can be used to compute the structural response. An offshore jacket sizing tool using simplified loads and limit states is developed at NREL and described in [17, 16]. Design of a jacket structure with gradient based optimization was performed in [32] and [13] with quasi-static and dynamic analysis, respectively. Constraints were placed on the natural frequencies, ultimate stresses, and fatigue in the welded joints.

Fatigue in the welded joints is considered the most important design constraint for the jacket structure. Due to the cyclic nature of the loading from the rotor, fatigue limit state is more often the design driver than ultimate limit states. Welded joints are the most critical locations, as stress concentrations in the weld significantly impact the fatigue performance. A method for fatigue stress evaluation in welded joints, called the hot spot method, is given in [18]. Only axial stresses are assumed to be contributing, and the fatigue is computed for eight evenly spaced locations, or hot spots, along the perimeter of the pipe. A design dependent stress concentration factor (SCF) is multiplied with the stress prior to the fatigue computation. The SCF factors for these structures are in the range 1-6. A geometric validity range is given for the hot spot method, as explained in Remark 2.

In some situations, structural optimization problems with discrete design variables can be reformulated as mixed 0-1 linear or convex quadratic problems. These reformulation techniques are especially well-developed for truss and frame structures, see e.g. [43], [41], [20], and [29]. Many type of structural requirements fit into this modelling approach, including limits on stresses, displacements, mass, etc. The main advantage is that the problems can be solved to global optimization using e.g. branch-and-cut methods. These reformulation techniques are however not always possible. This is for example the case when the problem includes limits on eigenfrequencies or if the the nonlinearities coupling the discrete design- and the continuous state-variables are too complicated. In these situations it is therefore necessary to resort to methods and heuristics for mixed 0-1 nonlinear optimization. This field is covered in e.g. the review articles [5] and [24].

One possible method for mixed integer nonlinear optimization is Outer Approximation (OA) which was introduce in [19] for problems which are linear in the integer variables. Outer approximation is further developed and analyzed in [22] for problems with nonlinearities in the integer variables. Outer approximation techniques have been used for applications in

structural optimization. Two- and three-dimensional truss topology optimization problems with discrete variables are solved to global optimality by outer approximation in [42]. The objective function was mass of the truss while the constraints limited the compliances under several load cases. The design variable were discrete and indicated choices of cross-section areas from catalogues. Outer approximation was also used to solve minimum compliance truss topology optimization problems in [30].

Outer approximation is chosen for optimal design of offshore support structures for several reasons. First, it is relatively easy to implement on top of a software which is capable of performing structural optimization with continuous design variables and which is capable of computing analytical design sensitivities. Second, outer approximation generates a sequence of designs which satisfies the linear constraints and which are taken from the catalogue of values. This implies that the nonlinear functions are only called when the structure satisfies necessary requirements (e.g. from standards and recommended practices) to be well-defined. Thirdly, outer approximation solves a sequence of mixed 0-1 linear problems and therefore generates a sequence of designs that satisfy the requirements that the design variables should be from catalogues. Although these sub-problems are difficult to solve in general there are robust and in practice often efficient global optimization methods and heuristics implemented with parallel computation capabilities allowing for problems of industrially relevant size to be solved. Finally, the strong theoretical properties from the convex case suggests that it could behave very well as a heuristic for nonconvex problems.

The overall purpose is proposing mass-manufacturable designs by structural optimization. The continuous problem is used to find a good starting point for the discrete problem, and then an outer approximation algorithm is used to propose designs in the discrete variables. The presented method is then used to propose designs of an offshore wind turbine jacket based on four different catalogues of available diameters and thicknesses.

This article is organized as follows. The next section presents the general problem formulation and a reformulation which is suitable for numerical optimization. The section additionally presents modelling of the application in optimal design of offshore support structures for wind turbines. Section 4 presents the outer approximation techniques for the optimal design problem and additionally suggests a heuristic technique for finding candidate designs satisfying the requirements on discrete design variables. The following two sections describe the implementation of the algorithms and the numerical experience obtained in designing offshore jacket structures. The article ends in Section 7 with conclusions and lists future possible generalizations.

2 Problem formulations

The problem formulations are classical in structural optimization in the sense that the structural analysis is based on the assumptions of linear elasticity coupled with the finite element method applied to frame structures. The objective and constraint functions model limitations on mass (or cost), local stresses, and fundamental eigenfrequencies. For problems with continuous design variables, these classes of problems are well-studied and the literature is rich, ranging from fundamental mathematical theory to industrial applications, see e.g. the textbook [10]. The situation that the design variables are associated with dimensions of parts and that several discrete design variables are associated with the parts is however much less studied. The design parametrization imposes enormous challenges on the optimization algorithms but do also provide possibilities of advanced modelling.

2.1 Design parametrization

In the design parametrization it is assumed that the design variable vectors $\mathbf{v}_i \in \mathbb{R}^{n_i}$, related to part (member or module) i of the structure, have the form

$$\mathbf{v}_i = \begin{pmatrix} v_{i,1} & \cdots & v_{i,n_i} \end{pmatrix}^T$$

where n_i is the number of design variables related to member i. The elements of $\mathbf{v}_i \in \mathbb{R}^{n_i}$ are to be chosen from catalogues of values, i.e.

$$v_{i,j} \in W_j = \{w_j^1, \ldots, w_j^{m_j}\}, \quad \text{for } j = 1, \ldots, n_i.$$

For simplicity it is assumed that $W_j \neq \emptyset$ and that the values in the sets W_j are unique and ordered, i.e.

$$0 < w_j^1 < w_j^1 < \cdots < w_j^{m_j} < +\infty \text{ for all } j.$$

The member design variables are collected into the (structural) design variable vector $\mathbf{v} \in \mathbb{R}^N$

$$\mathbf{v} = \begin{pmatrix} \mathbf{v}_1^T & \cdots & \mathbf{v}_n^T \end{pmatrix}^T$$

where n is the total number of parts considered in the optimal design problem and

$$N = \sum_i^n n_i.$$

It is also assumed that the catalogues are the same for all parts and that the number of design variables per part is also the same. These situations can of course be generalized, but will complicate both the notation and the presentation.

Remark 1. *The application presented is sizing optimization of jacket support structures for offshore wind turbines, see Figure 1. The wall thickness of the members in part i in the jacket design example is given by t_i and the outer diameter is given by d_i. Associated with each part is the variable vector*

$$\mathbf{v}_i = \begin{pmatrix} t_i \\ d_i \end{pmatrix} \in \mathbb{R}^2.$$

We assume that the variables must be chosen from a finite set of catalogues of available values, i.e.

$$t_i \in \{t^1, t^2, \ldots, t^{m_1}\}$$

and

$$d_i \in \{d^1, d^2, \ldots, d^{m_2}\}$$

for all $i = 1, \ldots, n$. Identification thus gives that

$$W_1 = \{t^1, t^2, \ldots, t^{m_1}\}, \text{ and } W_2 = \{d^1, d^2, \ldots, d^{m_2}\}$$

for the considered application.

2.2 Structural analysis

The structural analysis is herein done by the finite element method (see e.g. [15]). In the application Timoschenko beam elements are used. Other analysis methods (or finite elements) are of course possible if they comply with the format described below. The section outlines the structural analysis used in the numerical experiments but other, more advanced, models could also be used.

2.2.1 Static and dynamic analysis

The stiffness $\mathbf{K}(\mathbf{v})$ and mass $\mathbf{M}(\mathbf{v})$ matrices for the structure described by the design variables $\mathbf{v}$ are assumed to be in the form[1]

$$\mathbf{K}(\mathbf{v}) = \mathbf{K}_0 + \sum_{i=1}^{n} \mathbf{K}_i(\mathbf{v}_i)$$

and

$$\mathbf{M}(\mathbf{v}) = \mathbf{M}_0 + \sum_{i=1}^{n} \mathbf{M}_i(\mathbf{v}_i)$$

where $\mathbf{K}_0 = \mathbf{K}_0^T \in \mathbb{R}^{d\times d}$ and $\mathbf{M}_0 = \mathbf{M}_0^T \in \mathbb{R}^{d\times d}$ are given positive semidefinte matrices (possibly equal to the zero matrix) that do not depend on the design variables, and d is the number of non-fixed degrees of freedom. Each of the $\mathbf{K}_i(\mathbf{v}_i) \in \mathbb{R}^{d\times d}$ and $\mathbf{M}_i(\mathbf{v}_i) \in \mathbb{R}^{d\times d}$ are in turn (and for a fixed variable vector) assembled by the element stiffness and mass matrices for the finite elements belonging to the part. The matrices $\mathbf{K}_i(\mathbf{v}_i)$ and $\mathbf{M}_i(\mathbf{v}_i)$ are all assumed to be both symmetric and positive semidefinite for given values on the design variables which are within the bound constraints. It is throughout assumed that the sensitivity analysis of mass and stiffness matrices can be provided, i.e. that

$$\frac{\partial \mathbf{K}(\mathbf{v})}{\partial v_{i,j}}, \frac{\partial \mathbf{M}(\mathbf{v})}{\partial v_{i,j}}$$

can be stated analytically and efficiently computed. This assumption is certainly satisfied for the application presented in Remark 1 if the finite element model is based on Timoschenko beam elements. It is additionally assumed that the matrix values functions $\mathbf{K}(\mathbf{v})$ and $\mathbf{M}(\mathbf{v})$ are at least once continuously differentiable.

The nodal displacements $\mathbf{u}_l$ satisfy the equilibrium equations

$$\mathbf{K}(\mathbf{v})\mathbf{u}_l - \mathbf{f}_l = \mathbf{0}, \text{ for } l = 1, \ldots, L$$

where $\mathbf{f}_l$ is some static external load and L is the number of loads.

Limits on natural eigenfrequencies are modelled through inequality constraints in the form

$$\lambda_k^{\min} \leq \lambda_k(\mathbf{K}(\mathbf{v}), \mathbf{M}(\mathbf{v})) \leq \lambda_k^{\max}$$

where λ_k is the kth lowest natural eigenvalue of the structure described by the design variables. The eigenfrequency ω_k in Hz is found from the eigenvalue λ_k

$$\omega_k = \frac{\sqrt{\lambda_k}}{2\pi}.$$

The eigenvalues satisfy the the generalized eigenvalue problem

$$\mathbf{K}(\mathbf{v})\mathbf{z}_k = \lambda_k \mathbf{M}(\mathbf{v})\mathbf{z}_k$$

where $\mathbf{z}_k \in \mathbb{R}^d$ is the kth eigenvector.

The above mentioned assumptions are sufficient to ensure that it is possible to compute sensitivities of static displacements, compliance, local stresses, eigenfrequencies, and eigenmodes.

[1] This assumption is by no means critical for the optimal design approach in this article. It is commonly encountered for similar modelling situations in structural optimization e.g. for multi-material topology optimization [9] and discrete material optimization, see e.g. [26] and [40].

2.2.2 Cost and mass

The cost and the mass of the structure are assumed to have forms similar to those of the stiffness and mass matrices, i.e. the cost is given by

$$c(\mathbf{v}) = c_0 + \sum_{i=1}^{n} c_i(\mathbf{v}_i)$$

while the mass is given by

$$m(\mathbf{v}) = m_0 + \sum_{i=1}^{n} m_i(\mathbf{v}_i)$$

where $c_i(\mathbf{v}_i)$ and $m_i(\mathbf{v}_i)$ are the cost and mass of the ith part, respectively. Again it is assumed that sensitivity analysis of the mass and cost functions can be computed analytically.

2.3 Problem formulation

Geometrical constraints on the design variables are modelled through the linear constraint $\mathbf{b}_l \leq \mathbf{A}\mathbf{v} \leq \mathbf{b}_u$, where $\mathbf{A}$ is a given matrix and $\mathbf{b}_l, \mathbf{b}_u$ are a given vectors. Similarly, requirements imposed by limitations in design standards and recommended practices are also assumed to be modelled by linear constraints.

Remark 2. *Relevant geometric constraints for the jacket sizing problem mentioned in Remark 1 are the SCF-validity ranges [18]. For a joint where a brace member, b, is welded onto a leg member, l, the dimensions should satisfy the linear inequalities*

$$\frac{d_l}{5} \leq d_b \leq d_l$$
$$\frac{t_l}{5} \leq t_b \leq t_l,$$

and that for all parts, the following should hold

$$16t_i \leq d_i \leq 64t_i, \quad i = 1, ..., n.$$

The considered structural optimization problem is

$$\begin{array}{lll} \underset{\mathbf{v}}{\text{minimize}} & f(\mathbf{v}) & \\ \text{subject to} & \mathbf{l} \leq \mathbf{g}(\mathbf{v}) \leq \mathbf{u} & \\ & \mathbf{b}_l \leq \mathbf{A}\mathbf{v} \leq \mathbf{b}_u & \\ & v_{i,j} \in W_j & \forall\ (i,j) \end{array} \tag{P}$$

where $f(\mathbf{v})$ is the objective function (such as mass or cost), and $\mathbf{g}(\mathbf{v})$ is the functions defining the nonlinear constraints (e.g. stiffness and strength requirements). It is throughout assumed that these functions are at least continuously differentiable. This assumption is satisfied for the structural models outlined above. The lower and upper bounds on the nonlinear constraints are defined by the given vectors $\mathbf{l}$ and $\mathbf{u}$ of appropriate dimensions, respectively. If $l_i = u_i$ for some i then the ith constraint is viewed as an equality constraint. The situation that the inequality constraints are one-sided (i.e. either $l_i = -\infty$ or $u_i = +\infty$) is also allowed.

With the assumptions stated on the catalogues W_j problem (P) becomes a sizing problem, i.e. no parts are allowed to vanish from the structure. This restriction has some positive side-effects. First of all, the stiffness and mass matrices are positive definite for all designs suggested by the algorithm. Secondly, modelling of e.g. stress constraints is simplified compared to the situation that the topology is allowed to change. For sizing problems, stress constraints are no longer design-dependent[2] [1] and issues with the so-called singularity problem, see e.g. [37] and [38], are thus avoided.

Note that (P) can, after reformulation, be classified as a mixed integer nonlinear program. The natural continuous relaxation of (P) is obtained if the discrete variables are replaced by continuous variables with lower and upper bounds, i.e. the problem

$$\begin{array}{ll} \underset{\mathbf{v}}{\text{minimize}} & f(\mathbf{v}) \\ \text{subject to} & \mathbf{l} \leq \mathbf{g}(\mathbf{v}) \leq \mathbf{u} \\ & \mathbf{b}_l \leq \mathbf{A}\mathbf{v} \leq \mathbf{b}_u \\ & w_j^1 \leq v_{i,j} \leq w_j^{m_j} \quad \forall\,(i,j). \end{array} \tag{R}$$

Both the discrete problem (P) and the continuous relaxation (R) are in general non-convex. Additionally, both problems can be infeasible if the technical requirements are too stringent.

3 Problem reformulations

There are several possibilities to reformulate problem (P) to a form which is acceptable for modern optimization methods and heuristics. The first step is to model the problem with binary variables. This can be achieved in more than one way. We focus on only one of the possible reformulations. The reformulation technique is chosen to keep the number of binary variables relatively low, for its ease in implementation, and since we anticipate to be able to solve the continuous relaxation (R). We first introduce the binary variables $x_{ijk} \in \{0,1\}$ with the interpretation

$$x_{ijk} = \begin{cases} 1 & \text{if value } k \text{ is chosen from list } W_j \text{ for part } i, \text{ and} \\ 0 & \text{otherwise.} \end{cases}$$

This definition of the new variables together with the generalized upper bound constraints

$$\sum_k x_{ijk} = 1 \text{ for all } (i,j)$$

ensure that exactly one of the catalogue values are chosen for each part and design variable. The design variables $v_{i,j}$ can thus be replaced by the linear expression

$$v_{i,j}(\mathbf{x}) = \sum_k x_{ijk} w_j^k \text{ for all } (i,j).$$

In short, we write

$$\mathbf{v}(\mathbf{x}) = \mathbf{V}\mathbf{x}$$

for some appropriately chosen matrix $\mathbf{V}$. Note that the introduction of the binary variables x_{ijk} "absorb" many of the nonlinearities that potentially exist in the functions $c(\mathbf{v})$, $m(\mathbf{v})$, $\mathbf{K}(\mathbf{v})$, and $\mathbf{M}(\mathbf{v})$.

[2] This term refers to constraints which should be removed from the problem formulation if the corresponding part is not in the structure described by the current design variables.

The set X is introduced to model the linear constraints and the 0-1 requirements on the variables, i.e.

$$X = \{\mathbf{x} \in \{0,1\}^J \mid \sum_k x_{ijk} = 1,\ \forall\ (i,j), \mathbf{b}_l \leq \mathbf{AVx} \leq \mathbf{b}_u\}$$

where J is the total number of 0-1 variables.

Problem (P) is equivalent to the mixed 0-1 nonlinear problem

$$\begin{array}{ll} \underset{\mathbf{x}}{\text{minimize}} & f(\mathbf{v}(\mathbf{x})) \\ \text{subject to} & \mathbf{l} \leq \mathbf{g}(\mathbf{v}(\mathbf{x})) \leq \mathbf{u} \\ & \mathbf{x} \in X. \end{array} \tag{P_x}$$

Note that the objective function and the displacements constraints in (P_x) are in general nonlinear functions in the binary variables $\mathbf{x}$ and that (P_x) in general is a non-convex 0-1 problem. The continuous relaxation of (P_x) has both more variables and more constraints compared to (R) and therefore (R) is favoured in the implementation and numerical experiments.

4 Outer approximation method

For pure nonlinear 0-1 problems an outer approximation algorithm is similar to sequential linear programming (SLP) (see e.g. [14]) for continuous problems. The sub-problem in outer approximation, from now on called the master problem, is however a mixed 0-1 linear problem. Another difference between SLP and outer approximation is that the approximations of the objective and constraint functions generated at each iteration are saved in outer approximation.

The master problem in a basic outer approximation algorithm applied to (P_x) becomes

$$\begin{array}{lll} \underset{\mathbf{x},\eta}{\text{minimize}} & \eta & \\ \text{subject to} & f(\mathbf{Vx}^k) + (\nabla f(\mathbf{Vx}^k))^T\mathbf{V}(\mathbf{x} - \mathbf{x}^k) \leq \eta & k \in \mathcal{T}^l \\ & \mathbf{l} \leq \mathbf{g}(\mathbf{Vx}^k) + \nabla\mathbf{g}(\mathbf{Vx}^k)\mathbf{V}(\mathbf{x} - \mathbf{x}^k) \leq \mathbf{u} & k \in \mathcal{T}^l \\ & \mathbf{l} \leq \mathbf{g}(\mathbf{Vx}^k) + \nabla\mathbf{g}(\mathbf{Vx}^k)\mathbf{V}(\mathbf{x} - \mathbf{x}^k) \leq \mathbf{u} & k \in \mathcal{S}^l \\ & \mathbf{x} \in X & \end{array} \tag{M_x}$$

where the set $\mathcal{T}^l$ contains the outer approximation iterations for which the found design is feasible with respect to both the linear and the nonlinear constraints, i.e.

$$\mathcal{T}^l = \{k \mid k \leq l, \mathbf{l} \leq \mathbf{g}(\mathbf{v}(\mathbf{x}^k)) \leq \mathbf{u}\}.$$

The set $\mathcal{S}^l$, on the other hand, contains the iterations for which at least one of the nonlinear constraints is violated, i.e.

$$\mathcal{S}^l = \{k \mid k \leq l, g_i(\mathbf{v}(\mathbf{x}^k)) > u_i \text{ or } g_i(\mathbf{v}(\mathbf{x}^k)) < l_i \text{ for some } i\}.$$

The master problem (M_x) can of course be infeasible or unbounded. The considered objective functions, i.e. mass or cost, are bounded from below by zero and (M_x) can correctly be augmented with $\eta \geq 0$. Unboundedness of the objective function is, with this modelling, not an issue.

A standard outer approximation[3] algorithm for (P_x) takes the form described in Algorithm 1. The algorithm is adopted from [22]. Note that since (P_x) is a pure 0–1 problem there is no need for a feasibility problem as is used in the outer approximation methods outlined in e.g. [22].

Algorithm 1: Vanilla outer approximation algorithm for (P_x).

Let $\mathbf{x}^1 \in X$ be given. Set $k = 1$, $\mathcal{T}^0 = \emptyset$, $\mathcal{S}^0 = \emptyset$, $\eta^0 = -\infty$, and $ub = +\infty$.
Initialize the absolute optimality tolerance $\epsilon > 0$.
repeat
  Linearize the nonlinear constraints around $\mathbf{x}^k$.
  Set $\mathcal{T}^k \leftarrow \mathcal{T}^{k-1} \cup \{k\}$ or $\mathcal{S}^k \leftarrow \mathcal{S}^{k-1} \cup \{k\}$ as suitable.
  if $\mathbf{x} = \mathbf{x}^k$ *is feasible to* (P_x) *and* $f(\mathbf{v}(\mathbf{x}^k)) < ub$ **then**
    Update the incumbent, i.e. set $\mathbf{x}^* = \mathbf{x}^k$ and $ub = f(\mathbf{x}^k)$.
  end
  Solve the current master problem (M_x).
  if (M_x) *is infeasible* **then**
    Stop, outer approximation algorithm completed.
  else
    Denote the solution $(\mathbf{x}^{k+1}, \eta^{k+1})$.
  end
  Set $k \leftarrow k + 1$.
until (M_x) *is infeasible or* $ub - \eta^k < \epsilon$;

If (M_x) is infeasible in Algorithm 1 then one of two possible events occur. Either the upper bound is $< +\infty$ in which case at least one design feasible to (P_x) has been found, or no feasible point has been found. The latter situation does, due to non-convexity, however not guarantee that (P_x) is infeasible.

Our computational experience shows that the outer approximation method behaves better if it is supplied with a reasonably good starting point which is feasible to the original problem. This point and the optimal solution from the continuous relaxation are used to generate the first set of linear inequalities in the master problem (M_x). We propose a heuristic which is relatively easy to implement and which is based on rounding of the design obtained from the continuous relaxation. Similar rounding heuristics have proven to work well on truss topology optimization problems with discrete design variables in e.g. [2, 3]. The idea is to use the optimal design found by solving the continuous relaxation and then apply rounding to satisfy the linear constraints and the requirements on the 0-1 variables. This is achieved by solving a least-square problem modelled as a mixed 0-1 linear problem. Chances to find feasible designs increase if the design is rounded to values upwards in the catalogues and we therefore introduce a scaling parameter α which is set to a value greater than one. In the implementation $\alpha = 1.2$.

[3]The outer approximation property is generally not maintained for non-convex problems such as (P_x). The algorithm should therefore be considered as a heuristic.

Algorithm 2: A heuristic for finding a starting point $\mathbf{x} \in X$ satisfying the linear constraints in (P_x).

Initialize the parameter $\alpha > 0$.
Solve[a] the continuous relaxation (R).
if *(R) is deemed infeasible* **then**
| Stop, the heuristic is unsuccessful.
else
| Denote the found design $\mathbf{v}^*$.
end
Solve the least-squares problem

$$\begin{aligned} \underset{\mathbf{x}}{\text{minimize}} \quad & \|\mathbf{V}\mathbf{x} - \alpha\mathbf{v}^*\|_1 \\ \text{subject to} \quad & \mathbf{x} \in X. \end{aligned} \tag{H}$$

if *(H) is infeasible* **then**
| Stop, (P_x) is infeasible.
else
| Denote the solution of (H) by $\mathbf{x}$.
end
Since $\mathbf{x} \in X$ it is a starting point for Algorithm 1.

[a]Solve should, in this context, be interpreted as finding a point numerically satisfying the first-order optimality conditions.

Problem (H) in Algorithm 2 does not need to be solved to optimality. Finding a feasible point to (H) is sufficient for the heuristic in Algorithm 2 to be successful. In the implementation problem (H) is modelled as mixed 0-1 linear program and solved to global optimality to within the default tolerances of the solver.

5 Implementation

The user provides the catalogues for the design variables, the type of constraints and associated bounds, the matrix and vector defining the geometric constraints, and routines for structural analysis and sensitivity analysis.

A software called JADOP for solving the considered problems with continuous design variables has been developed at DTU Wind Energy. This software implements both structural analysis and sensitivity analysis required for the applications. JADOP is implemented in Matlab [28] and includes interfaces to several modern methods for nonlinear optimization. The continuous relaxation (R) is solved using the open source interior point solver IPOPT version 3.11.8 [46], where non-default parameters are listed in Table 3. IPOPT is compiled with the MUMPS library [4].

The outer approximation implementation is called YAOAM (Yet Another Outer Approximation Method). This collection of Matlab scripts and functions is the main driver of the optimization process and calls the user supplied analysis and sensitivity analysis routines when required. The outer approximation algorithm and associated heuristics and the finite elements are implemented in Matlab. The most important parameters and tolerances used in the outer approximation method are listed in Table 1. The mixed 0-1 linear programs are solved by the commercial branch-and-cut solvers in IBM ILOG CPLEX [25]. The non-

differentiable problem (H) is modelled as a mixed 0-1 linear problem and solved by IBM ILOG CPLEX. IBM ILOG CPLEX is assigned 20 threads for all problems. The non default parameters and tolerances used in IBM ILOG CPLEX are listed in Table 2.

Table 1: Parameters and tolerances used in the outer approximation algorithm.

Description	Value
Feasibility tolerance	10^{-6}
Integrality tolerance	10^{-6}
Relative optimality gap	10^{-4}
Absolute optimality gap	10^{-4}

Table 2: Parameters and tolerances used in IBM ILOG CPLEX.

Description	Value
Max computation time [s]	36000
Relative optimality gap	10^{-4}
Absolute optimality gap	10^{-4}

Table 3: Parameters and tolerances when solving the continuous jacket sizing problem by IPOPT.

Description	Notation	Value
Barrier update strategy	`mu_strategy`	`'adaptive'`
Technique for scaling	`nlp_scaling_method`	`'none'`
Hessian information	`hessian_approximation`	`'limited-memory'`
Convergence tolerance	`tol`	10^{-5}

6 Numerical results

The outer approximation algorithm is applied to sizing optimization problems of four legged jacket structures for offshore wind turbines as illustrated in Figure 1. We first apply the rounding procedure form Algorithm 2 and then attempt to solve the discrete problem by the outer approximation method described in Algorithm 1. The optimized design from the discrete problem is compared to the optimized design from the continuous problem for four different catalogue sizes. The problems are solved on a machine with two Intel Xeon E5-2680v2 ten-core CPUs running at 2.8 GHz, with 64 GB memory.

6.1 Structural model

The analysis model consists of jacket, transition piece and tower, modelled as a frame structure. Moreover, the analysis assumes thin-walled tubular elements. A two-noded Timoshenko 3D beam finite element with constant shear correction factor of 0.52 is used throughout the structure [15]. Nodal displacements of element e in load case l is described in the element displacement vector $\mathbf{u}_{el} \in \mathbb{R}^{12}$. The element rotation matrix $\mathbf{T}_e \in \mathbb{R}^{12\times d}$ maps from global to local coordinates, $\mathbf{u}_{el} = \mathbf{T}_e\mathbf{u}_l$. The axial stress in element e is computed as $\sigma_e(\mathbf{v}, \boldsymbol{\gamma}_h) = E\mathbf{b}(\mathbf{v}, \boldsymbol{\gamma}_h)\mathbf{u}_{el}$, where $\boldsymbol{\gamma}_h = (\xi_h, \eta_h, \zeta_h)$ is the location in the element expressed in

element coordinates and $\mathbf{b}(\mathbf{v}, \boldsymbol{\gamma}_h)$ is the strain-displacement vector for axial stress. In fatigue load cases, stress concentration factors are implemented in the strain-displacement vector.

The jacket is meshed with 524 finite elements, and at least six finite elements in each member. The number of elements and unconstrained degrees of freedom in the full structure are 580 and 3087, respectively. The stiffness and mass matrices of the tower and transition piece constitute the main part of the non-zero entries of the constant matrices $\mathbf{K}_0$ and $\mathbf{M}_0$. The whole structure is modelled as steel with material properties as listed in Table 4.

Table 4: Material properties

Description	Notation	Value	Unit
Density	ρ	7800	$\mathrm{kg/m^3}$
Modulus of elasticity	E	210	GPa
Poisson's ratio	ν	0.3	–
Yield strength	σ_y	355	MPa

At the top of the tower is a non-structural mass matrix which includes the masses and inertias of the rotor-nacelle-assembly (RNA). Although the RNA does not contribute with stiffness to the structure, it is necessary to model the mass and inertia in order to get correct natural frequencies. The non-structural mass matrix $\mathbf{M}_{RNA} \in \mathbb{R}^{6\times6}$ contains only diagonal terms and is included in the constant mass matrix $\mathbf{M}_0$. Along the displacement degrees of freedom are the combined mass of the whole RNA, and along the rotation degrees of freedom are the equivalent moments of inertia around the tower top node, I_{xx}, I_{yy}, and I_{zz}. Furthermore, the density of the tower elements is increased with eight percent to account for secondary steel and equipment, which will also influence the frequency. These modelling approaches are adopted from the DTU 10 MW Reference wind turbine report [8] and the INNWIND.EU Reference jacket report [11]. The hub heigh, and tower dimensions are taken from [8], and the RNA properties, and the overall dimensions of the jacket and transition piece are taken from [11].

6.2 Load computations and fatigue model

The loads used for the numerical examples are based on the DTU 10 MW reference wind turbine in a turbulent wind field. The simulations are performed with a clamped tower top in the specialized aero-elastic software Flex5 for a sample of wind speeds in the operational range, $w = 4 : 2 : 24m/s$. The time series are $600s$ long, with a constant time step of $0.02s$. A 1 Hz damage equivalent load $P \in \mathbb{R}$ is computed independently for thrust, overturning moment, and torsion. The load is found from

$$n_s P^m = \sum_{w=1}^{n_w} p_w \sum_{i=1}^{q} n_{wi} \Delta P_{wi}^m,$$

where n_{wi} is the number of cycles at load amplitude ΔP_{wi}. A standard rainflow-counting algorithm [7] is used to compute n_{wi} and ΔP_{wi} based on the load time series. The wind speed probability distribution $p_1, ..., p_{n_w}$ [21] represents north sea conditions, and the material parameter m is the slope of the high-cycle SN-curve for tubular steel joints in seawater with cathodic protection [18]. The procedure is repeated for each degree of freedom in the load. The advantage of using a damage equivalent load, is that an approximated structural

response can be obtained from only one static load case. This is at least three orders of magnitudes faster than solving the equations of motions in the time-domain, and gives comparable estimation of fatigue damage for these types of structures.

6.3 Jacket sizing optimization

The jacket is partitioned into four sections which are stacked on top of each other, see Figure 2. The design parametrization follows Remark 1, and the geometric constraints follow Remark 2.

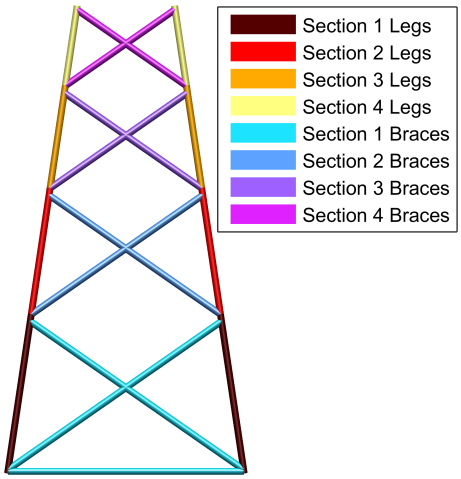

Figure 2: Illustration of the design parametrizations used in this article.

The objective function is the mass of the jacket

$$f(\mathbf{v}) = \rho \sum_{i=1}^{n} a_i(\mathbf{v}_i) l_i \tag{1}$$

where $a_i(\mathbf{v}_i)$ and l_i are the length and cross sectional area of part i, and ρ is the density of steel, as given in Table 4. Nonlinear constraints include global frequencies and local stresses, with bounds given in Table 5. There are three load cases for modelling the ultimate limit state, and four load cases for modelling the fatigue limit state. All seven load cases are static, and include an applied load at the thrust, overturning moment, and torsion degrees of freedom at the tower top. Ultimate limit state (ULS) stress is constrained in eight locations of each finite element in the design domain for each of the three ULS load cases. Fatigue limit state (FLS) stress is constrained in eight locations of each finite element in the design domain for each of the four FLS load cases. The diameter and thickness of all members are also bounded from below and above, as shown in Table 5.

Table 5: Constraint limits used in the jacket optimization examples.

Description	Notation	Lower bound	Upper bound
First bending eigenfrequencies	ω_1, ω_2	0.18 Hz	0.27 Hz
First twisting eigenfrequency	ω_3	0.54 Hz	∞
ULS stress	σ_i^u	-350 MPa	350 MPa
FLS stress	σ_i^f	-11.5 MPa	11.5 MPa
Diameter	D	400 mm	1400 mm
Thickness	T	15 mm	65 mm

The discrete problem was solved for four different catalogue sizes, ranging from small to extra large. The catalogues are defined as

$$W_1 = \{15, 15 + \Delta t, \ldots, 65\}$$

and

$$W_2 = \{400, 400 + \Delta d, \ldots, 1400\}.$$

The small catalogues have diameter and thickness steps of $\Delta d = 100$ and $\Delta t = 10$ mm, respectively, and the extra large catalogue has steps of only $\Delta d = 10$ and $\Delta t = 1$ mm, respectively. The upper and lower bound on the diameter and thickness is the same for all catalogues and all members. The characteristics of the problem is given in Table 6.

Table 6: Optimal design problem characteristics.

Descriptions	Value
Number of elements	580
Number of unconstrained DOF	3078
Number of variables	16
Number of nonlinear constraints	42444
Number of linear constraints	32

6.4 Results and discussion

Figure 3 illustrates how the optimized designs from the discrete problem (P_x) compares with the optimized design from the continuous problem (R). From a visual inspection, it seems that the solution to the discrete problem approaches the solution to the continuous problem when the catalogue size increases.

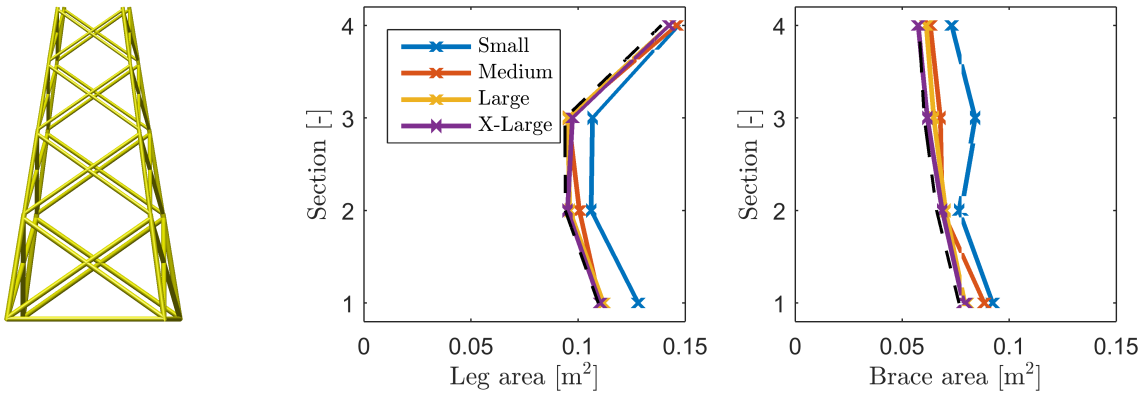

Figure 3: Optimized cross section areas from the discrete problems compared with the optimized cross sections from the continuous problem (dashed).

Table 7 summarises the statistics of the four discrete jacket sizing problems, and compares the optimized masses with the one from the continuous problem. All problems successfully met the tolerances placed on the relative optimality gap in the outer approximation algorithm. As expected, a problem instance with a larger catalogue size gives lower mass than a small one. Actually, the designs found to the discrete problems (P_x) seem to approach the design found from the continuous problem (R) when the catalogue size becomes sufficiently large.

Table 7: Convergence study on catalague size.

Catalogue size:	Small	Medium	Large	X-Large	Continuous
Number of choices for D	7	14	33	66	-
Number of choices for T	9	17	41	81	-
Number of OA iterations	3	3	4	4	-
CPU-time [hrs:mins]	0:08	0:27	7:33	20:47	0:09
Optimized mass [tons]	929	843	806	790	773

The interior point method used to solve the continuous relaxation requires 57 iterations and 63 objective and constraint function evaluations. The number of objective gradient and constraint Jacobian evaluations is 58. The outer approximation method on top of that requires as many function and gradient evaluations as iterations. The computation time for solving the mixed 0-1 linear problem (H) is very modest. The main bulk of computation time is instead spent in solving the mixed 0-1 linear programs (M_x), i.e. the outer approximation master problems. Partly this is because of the large number of constraints which additionally increases with the number of iterations and partly because of the problem class and the requirement to solve the problem to global optimality. The latter requirement can in fact be relaxed since the branch-and-cut methods provide correct lower bounds on the objective function value. This value could replace the optimal value and the optimality tolerances could be increased substantially leading to much less computational efforts for the master problems.

The numbers of outer approximation iterations reported in Table 7 are remarkably low. This is due to several reasons. First, the objective function value from the continuous relaxation is not too far away from the final objective value found by outer approximation.

Second, the heuristic outline in Algorithm 2 finds designs which are feasible for all problem instances. Finally, the problem instances have many more local constraints than design variables which generates many linearizations and hence convergence is promoted.

7 Conclusions and future work

A method for structural optimization with multiple discrete variables per part has been presented and demonstrated. The initial feasible point is found by a rounding procedure of the solution to a related continuous problem, and an outer approximation algorithm is used to propose improved designs for the discrete problem.

As industrial design often is based on a discrete catalogue of products, the presented method can improve the way structural optimization is used in practice. An application for sizing optimization of the tubular members in an offshore wind turbine jacket support structure is presented. When the catalogue size is very large, the solution to the discrete problem closely resembles the solution to the continuous problem, and good results are found for smaller catalogue sizes as well.

Future work includes extension of the modelling and the methods to include transient analysis to better capture fatigue. This leads to much more expensive analysis and sensitivity analysis and problems with very many constraints. If the observation from the outer approximation approach from this manuscript is still valid then also these problems will also require just a handful of iterations which is favourable.

The computational time of outer approximation can potentially be reduced if the number of constraints in the master problems could be decreased. Introducing an elaborate working-set approach could prove advantageous for the practical performance of the algorithm. However, the very efficient pre-processing routines which are included in modern software for mixed 0-1 linear problems prove very efficient in reducing the problem size and the effect of an working-set approach might therefore be limited. An alternative to reduce the computational time in outer approximation is to relax the requirement that the master problem is solved to global optimality and use the lower bound estimates by the solver rather then the optimal objective function value. This can be achieved by relaxing the optimality tolerances in the branch-and-cut solvers. Care must be taken to ensure that this approach generates sequences of improving upper and lower bounds. This approach will without any doubt increase the number of outer approximation iterations but likely reduce the computational time per master problem drastically.

8 Acknowledgements

The research presented in this manuscript is part of the strategic research project ABYSS: Advancing BeYond Shallow waterS - Optimal design of offshore wind turbine support structures (`www.abyss.dk`). The project is funded by the Danish Council for Strategic Research, Grant no. 1305-00020B. The funding is gratefully acknowledged.

References

[1] W. Achtziger and C. Kanzow. Mathematical programs with vanishing constraints: optimality conditions and constraint qualifications. *Mathematical Programming*, 114:69–99,

2008.

[2] W. Achtziger and M. Stolpe. Truss topology optimization with discrete design variables guaranteed global optimality and benchmark examples. *Structural and Multidisciplinary Optimization*, 34(1):1–20, 2007.

[3] W. Achtziger and M. Stolpe. Global optimization of truss topology with discrete bar areas-part ii: Implementation and numerical results. *Computational Optimization and Applications*, 44(2):315–341, 2009.

[4] P.R. Amestoy, I.S. Duff, J. Koster, and J.-Y. L'Excellent. A fully asynchronous multifrontal solver using distributed dynamic scheduling. *SIAM Journal on Matrix Analysis and Applications*, 23(1):15–41, 2001.

[5] J.S. Arora, M.W. Huang, and C.C. Hsieh. Methods for optimization of nonlinear problems with discrete variables - A review. *Structural Optimization*, 8(2–3):69–85, 1994.

[6] J.S. Arora and Q. Wang. Review of formulations for structural and mechanical system optimization. *Structural and Multidisciplinary Optimization*, 30(4):251–272, 2005.

[7] ASTM. Standard Practices for Cycle Conting in Fatigue Analysis. Technical Report E1049, ASTM, 2013.

[8] C. Bak, F. Zahle, R. Bitsche, T. Kim, A. Yde, L.C. Henriksen, A. Natarajan, and M. Hansen. The DTU 10 MW reference wind turbine. Technical report, DTU Wind Energy, 2013.

[9] M.P. Bendsøe and O. Sigmund. Material interpolation schemes in topology optimization. *Archive of Applied Mechanics*, 69(9–10):635–654, 1999.

[10] M.P. Bendsøe and O. Sigmund. *Topology Optimization: Theory, Methods and Applications*. Springer, 2003.

[11] T. Borstel. Design report - reference jacket. Technical Report D4.3.1, Ramboll, 2013. `www.innwind.eu/publications/deliverable-reports`, accessed on 2017-02-13.

[12] T.M. Cameron, A.C. Thirunavukarasu, and M.E.M. El-Sayed. Optimization of frame structures with flexible joints. *Structural and Multidisciplinary Optimization*, 19(3):204–213, 2000.

[13] K.H. Chew, K. Tai, E.Y.K. Ng, and M. Muskulus. Analytical gradient-based optimization of offshore wind turbine substructures under fatigue and extreme loads. *Marine Structures*, 47:23–41, 2016.

[14] C.M. Chin and R. Fletcher. On the global convergence of an SLP-filter algorithm that takes EQP steps. *Mathematical Programming*, 96(1):161–177, 2003.

[15] R.D. Cook, D.S. Malkus, M.E. Plesha, and R.J. Witt. *Concepts and Applications of Finite Element Analysis*. John Wiley & Sons, fourth edition, 2007.

[16] R. Damiani. JacketSE : An Offshore Wind Turbine Jacket Sizing Tool Theory Manual and Sample Usage with Preliminary Validation. Technical Report NREL/TP-5000-65417, National Renewable Energy Laboratory (NREL), 2016.

[17] R. Damiani, A. Ning, B. Maples, A. Smith, and K. Dykes. Scenario analysis for techno-economic model development of U.S. offshore wind support structures. *Wind Energy*, 20:731–747, 2017.

[18] DNVGL. RP-C203 Fatigue design of offshore steel structures. Technical report, DNVGL, 2014.

[19] M.A. Duran and I.E. Grossmann. An outer-approximation algorithm for a class of mixed-integer nonlinear programs. *Mathematical Programming*, 36(3):307–339, 1986.

[20] A.M. Faustino, J.J. Judice, I.A. Ribeiro, and A. Serra Neves. An integer programming model for truss topology optimization. *Investigação Operacional*, 26:111–127, 2006.

[21] T. Fischer, W. de Vries, and B. Schmidt. Upwind Design Basis. Technical report, Project Upwind, 2010.

[22] R. Fletcher and S. Leyffer. Solving mixed integer nonlinear programs by outer approximation. *Mathematical Programming*, 66(1–3):327–349, 1994.

[23] H. Fredricson, T. Johansen, A. Klarbring, and J. Petersson. Topology optimization of frame structures with flexible joints. *Structural and Multidisciplinary Optimization*, 25(3):199–214, 2003.

[24] I.E. Grossmann. Review of nonlinear mixed-integer and disjunctive programming techniques. *Optimization and Engineering*, 3(3):227–252, 2002.

[25] IBM Corporation. IBM ILOG CPLEX Optimization Studio V12.6.0 documentation. Technical report, IBM Corporation, 2014. `www-01.ibm.com/support/knowledgecenter/SSSA5P_12.6.0`.

[26] E. Lund and J. Stegmann. On structural optimization of composite shell structures using a discrete constitutive parametrization. *Wind Energy*, 8(1):109–124, 2005.

[27] J.H. Martens, D. Zwick, and M. Muskulus. Topology Optimization of a Jacket Structure for an Offshore Wind Turbine with a Genetic Algorithm. In *11th World Congress on Structural and Multidisciplinary Optimization*, Sydney, 2015.

[28] MathWorks, Inc. *MATLAB Primer*, R2016a edition, 2016. `www.mathworks.com`.

[29] K. Mela. Resolving issues with member buckling in truss topology optimization using a mixed variable approach. *Structural and Multidisciplinary Optimization*, 50(6):1037 – 1049, 2014.

[30] E.J. Munoz Queupumil and M. Stolpe. Generalized Benders decomposition for topology optimization problems. *Journal of Global Optimization*, 51(1):149–183, 2011.

[31] M. Muskulus and S. Schafhirt. Design Optimization of Wind Turbine Support Structures A Review. *Journal of Ocean and Wind Energy*, 1(1):12–22, 2014.

[32] J. Oest, R. Sørensen, L.C.T. Overgaard, and E. Lund. Structural optimization with fatigue and ultimate limit constraints of jacket structures for large offshore wind turbines. *Structural and Multidisciplinary Optimization*, 55(3):779–793, 2017.

[33] L. Pasamontes, F.G. Torres, D. Zwick, S. Schafhirt, and M. Muskulus. Support structure optimization for offshore wind. In *Proceedings of the ASME 2014 33rd International Conference on Ocean, Offshore and Arctic Engineering*, pages 1–7, San Francisco, 2014. The American Society of Mechanical Engineers (ASME).

[34] C.B.W. Pedersen. Crashworthiness design of transient frame structures using topology optimization. *Computer Methods in Applied Mechanics and Engineering*, 193(6-8):653–678, 2004.

[35] N.L. Pedersen and A.K. Nielsen. Optimization of practical trusses with constraints on eigenfrequencies, displacements, stresses, and buckling. *Structural and Multidisciplinary Optimization*, 25(5-6):436–445, dec 2003.

[36] P. Pedersen and L. Jørgensen. Minimum mass design of elastic frames subjected to multiple load cases. *Computers and Structures*, 18(1):147–157, 1984.

[37] G.I.N. Rozvany. Difficulties in truss topology optimization with stress, local buckling and system stability constraints. *Structural Optimization*, 11:213–217, 1996.

[38] G.I.N. Rozvany. On design-dependent constraints and singular topologies. *Structural and Multidisciplinary Optimization*, 21:164–172, 2001.

[39] S. Schafhirt, D. Zwick, and M. Muskulus. Reanalysis of jacket support structure for computer-aided optimization of offshore wind turbines with a genetic algorithm. *Journal of Ocean and Wind Energy*, 1(4):209–216, 2014.

[40] J. Stegmann and E. Lund. Discrete material optimization of general composite shell structures. *International Journal for Numerical Methods in Engineering*, 62(14):2009–2027, 2005.

[41] M. Stolpe. On the reformulation of topology optimization problems as linear or convex quadratic mixed 0-1 programs. *Optimization and Engineering*, 8:163–192, 2007.

[42] M. Stolpe. Truss topology optimization with discrete design variables by outer approximation. *Journal of Global Optimization*, 61(1):139–163, 2014.

[43] M. Stolpe and K. Svanberg. Modeling topology optimization problems as linear mixed 0–1 programs. *International Journal for Numerical Methods in Engineering*, 57(5):723–739, 2003.

[44] A.B. Templeman. Discrete optimum structural design. *Computers and Structures*, 30(3):511–518, 1988.

[45] A.B. Templeman and D.F. Yates. A Segmental Method for the Discrete Optimum Design of Structures. *Engineering Optimization*, 6(3):145–155, 1983.

[46] A. Wächter and L.T. Biegler. On the Implementation of a Primal-Dual Interior Point Filter Line Search Algorithm for Large-Scale Nonlinear Programming. *Mathematical Programming*, 106(1):25–57, 2006.

[47] D.F. Yates, A.B. Templeman, and T.B. Boffey. The complexity of procedures for determining minimum weight trusses with discrete member sizes. *International Journal of Solids and Structures*, 18(6):487–495, 1982.

[48] D. Zwick, M. Muskulus, and G. Moe. Iterative optimization approach for the design of full-height lattice towers for offshore wind turbines. *Energy Procedia*, 24:297–304, 2012.

Paper V

K. Sandal, JADOP - JAcket Design OPtimization. To be submitted as a *Technical report at DTU Wind Energy.*

JADOP – JAcket Design OPtimization

Documentation

Kasper Sandal

Department of Wind Energy
Technical University of Denmark
Date: July 22, 2017

Nomenclature

ε	Axial strain	6
ξ, η, ζ	Normalized element coordinate system	5
A	Cross sectional area	6
d	Element diameter	5
E	Youngs modulus	6
$f(\mathbf{v})$	General objective function	14
G	Shear modulus	6
I	Second moment of area	6
k	Shear coefficient	6
l	Element length	5
n_d	Number of unconstrained degrees of freedom in the structure	11
n_{dof}	Number of degrees of freedom in the structure	11
s^{ax}	SCF for stress induced by axial loading	12
s^{mi}	SCF for stress induced by moment in-plane	12
s^{mo}	SCF for stress induced by moment out-of-plane	12
SCF	Stress concentration factor	12
t	Element wall thickness	5
u, v, w	Element displacement field	5
x, y, z	Global coordinate system	5
x_e, y_e, z_e	Element coordinate system	5

Notation

This chapter describes the notations of arrays and derivatives, and the general rules for subscripts and superscripts.

Arrays

This document uses a notation where bold capital letters are matrices, bold non-capitalized letters are vectors, and italic letters are scalars.

$$\mathbf{M} - \text{matrix} \tag{1}$$
$$\mathbf{v} - \text{vector} \tag{2}$$
$$S - \text{scalar} \tag{3}$$
$$s - \text{scalar} \tag{4}$$

Vectors are, unless otherwise specified, column vectors.

Derivatives

Consider the vector $\mathbf{x} \in \mathbb{R}^{n_x}$, and the function $\mathbf{v}(\mathbf{x}) : \mathbb{R}^{n_x} \to \mathbb{R}^{n_v}$. The Jacobian of $\mathbf{v}(\mathbf{x})$ with respect to $\mathbf{x}$ is denoted

$$\nabla \mathbf{v}(\mathbf{x}) = \frac{\mathrm{d}\mathbf{v}(\mathbf{x})}{\mathrm{d}\mathbf{x}} \in \mathbb{R}^{n_v \times n_x} \tag{5}$$

If we consider the function $f(\mathbf{x}, \mathbf{v}(\mathbf{x})) : \mathbb{R}^{n_x} \to \mathbb{R}$, the sensitivity of $f(\mathbf{x}, \mathbf{v}(\mathbf{x}))$ with respect to $\mathbf{x}$ is computed as

$$\frac{\mathrm{d}f(\mathbf{x}, \mathbf{v}(\mathbf{x}))}{\mathrm{d}\mathbf{x}} = \frac{\partial f(\mathbf{x}, \mathbf{v}(\mathbf{x}))}{\partial \mathbf{x}} + \frac{\partial f(\mathbf{x}, \mathbf{v}(\mathbf{x}))}{\partial \mathbf{v}(\mathbf{x})} \frac{\mathrm{d}\mathbf{v}(\mathbf{x})}{\mathrm{d}\mathbf{x}} \tag{6}$$

where partial derivatives and the chain rule are used to find the full derivative.

Subscripts and superscripts

Subscripts and superscripts are used to indicate additional information about a symbol, function, or variable. Subscripts generally represent indices, while superscripts are used to indicate more general information. Consider the displacement vector $\mathbf{u}$, with the following sub- and superscripts.

$$\mathbf{u}_e^l \tag{7}$$

Subscript e indicate that only the degrees of freedom of element e are included, and superscript l indicate that the degrees of freedom are given in local coordinates.

Contents

Chapter 1

Introduction

This report describes the theory and implementation of **JA**cket **D**esign **OP**timization - **JADOP**.

JADOP is an analysis and optimization software for frame structures implemented in Matlab [10]. Frames are often used to model wind turbine structures such as blades and tower, and are also effective for modelling support structures such as jackets as well. While wind turbine blades are complex structures with anisotropic properties, support structures are less so. In the current version of JADOP it is assumed that all structural members are thin-walled cylindrical members made of isotropic material. For jackets and towers, this assumptions does not give any significant limitations.

The jacket design problem can be approached on two levels. Level one regards the topology and overall design of the jacket. How many legs, how many sections, leg distance, height, and so forth. Level two regards the cross sectional dimensions, diameter and thickness, of each member in the structure. The jacket design problem on level two can be formulated as a sizing optimization problem, where the objective is to minimize mass or cost, and the design variables are the diameters and thicknesses of all the members. To ensure manufacturability, some variable bounds and geometric and symmetry constraints can be introduced.

The purpose of this documentation is to describe the finite element analysis and sensitivity analysis implemented in JADOP in detail. It is intended as a theory manual as well as a developers guide. A user manual is not included, as the (graphical) user interface is not fully determined in the current version.

Questions regarding this documentation can be directed to Kasper Sandal (kasp@dtu.dk).

Chapter 2

Finite element analysis

This chapter describes the finite element analysis used in JADOP. The assumptions for using beam elements are justified, and the structural problem is composed from the kinematic relation, the constitutive law and the physical equilibrium. The structural matrices are derived from the principle of virtual work, and both static and dynamic analysis is presented. Finally, stress evaluation in tubular joints according to relevant design guidelines is presented.

2.1 Assumptions

In this section the main assumptions of the finite element analysis in JADOP are presented and justified.

JADOP is developed for analysis and optimization of offshore wind turbine support structures, with emphasis on the jacket structure. The jacket structure is a space frame structure, and consists of tubular members which are welded together in K-joints, Y-joints, and X-joints. We assume that:

- the structure is built from thin-walled cylindrical members, such that the structural response, including local stresses, can be described by Timoshenko beam finite elements.
- axial stresses will dominate, such that the other stress components can be neglected.
- the stress concentrations along the welded joints can be approximated by analytic formulas.

The first assumption is common for these types of structures, and is in particular driven by the desire for easy modelling and computationally cheap analysis. The second and third assumptions are not forced by the beam element, but rather a consequence of the design guideline for fatigue analysis [6].

2.2 Timoshenko beam element

In this section, the two-noded Timoshenko beam element implemented in JADOP is presented, and applied to thin-walled cylinders.

Let a beam element be defined by two nodes with six degrees of freedom each, as shown in Figure 2.1. The element displacement vector $\mathbf{u}_e^l \in \mathbb{R}^{12}$ with respect to the local coordinate system is denoted

$$\mathbf{u}_e^l = \begin{pmatrix} u_1 & v_1 & w_1 & \theta_{x1} & \theta_{y1} & \theta_{z1} & u_2 & v_2 & w_2 & \theta_{x2} & \theta_{y2} & \theta_{z2} \end{pmatrix}^T \tag{2.1}$$

The element rotation matrix $\mathbf{T}_e \in \mathbb{R}^{12\times12}$ is defined as the rotation from global coordinate system (x, y, z) to local coordinate system (x_e, y_e, z_e), such that $\mathbf{u}_e^l = \mathbf{T}_e\mathbf{u}_e^g$. When the local coordinate system is normalized with respect to the diameter and length of the element, we refer to it as the *normalized element coordinate system*,

$$\begin{pmatrix} \xi & \eta & \zeta \end{pmatrix} = \begin{pmatrix} \frac{x_e}{l_e} & \frac{y_e}{d_e} & \frac{z_e}{d_e} \end{pmatrix} \tag{2.2}$$

where d and l are the element diameter and length, respectively.

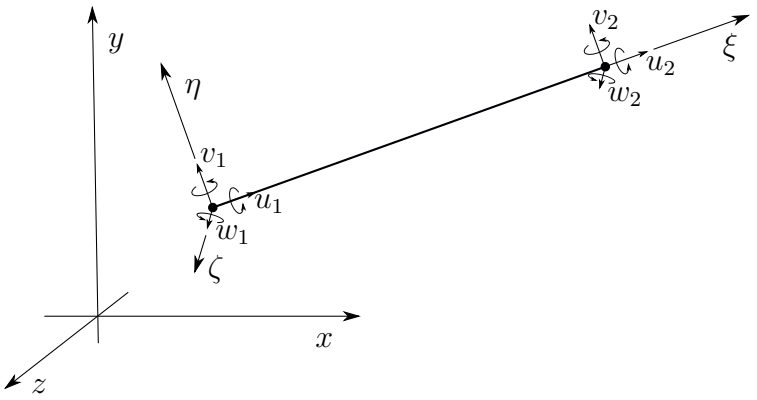

Figure 2.1: A beam element with global and local coordinate system, and local translation degrees of freedom $(u_1, v_1, w_1, u_2, v_2, w_2)$. Local rotational degrees of freedom $(\theta_{\xi1}, \theta_{\eta1}, \theta_{\zeta1}, \theta_{\xi2}, \theta_{\eta2}, \theta_{\zeta2})$ are drawn but not labelled.

Important cross section properties for a thin-walled cylinder are the area A, the second moment of inertia around the transverse axes $I_{yy} = I_{zz} = I$, and the shear coefficient $k_y = k_z = k$.

$$A(d,t) = \frac{\pi(d^2 - (d-2t)^2)}{4} \tag{2.3}$$

$$I(d,t) = \frac{\pi(d^4 - (d-2t)^4)}{64} \tag{2.4}$$

$$k(d,t) = \frac{6(\nu+1)^2}{4\nu^2 + 12\nu + 7 + \frac{20d^2(d-2t)^2}{(d^2+(d-2t)^2)^2}} \tag{2.5}$$

where the expression for the shear coefficient k_{shear} is adopted from [8], and ν is the Poisson's ratio. The second moment of inertia around the longitudinal axis is $I_{xx} = 2I$. While all three properties are functions of the diameter and thickness, it is common to assume the shear coefficient to be constant. Figure 2.2 shows that the shear coefficient is actuallly approximately constant for the d/t ratios we consider in this application. The SCF-validity bounds will be explained further in section 2.7. The default value of the shear stiffness in JADOP is 0.53, which is also the default value for thin walled cylindrical beam elements in the commercial finite element software Abaqus [4].

2.3 Constitutive law

In this section we apply plane stress assumptions, and link the remaining stress components to strain components through the constitutive law.

The beam is assumed to be a thin-walled cylinder, which means it can be analysed under the plane stress condition. This means the stress tensor can be reduced to only three independent

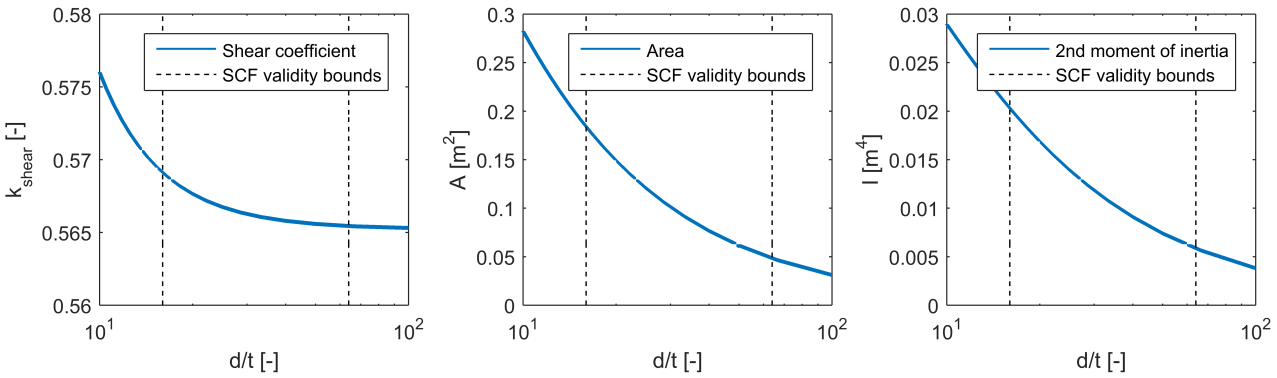

Figure 2.2: Shear coefficient, area, and inertia as functions of d/t ratio when $d = 1$.

components: axial stress, hoop stress, and shear stress. The hoop stress can be induced by a pressure difference between the inside and outside of the thin-walled cylinder. This can happen for offshore structures if the thin-walled cylinders are sealed, and the external water pressure is higher than the pressure on the inside. However, simple calculations shows that even at 50 meter water depth, the hoop stress will not exceed 1 percent of the yield stress for the d/t ratios we consider here. It is thus safe to neglect this contribution, and we are left with only two stress components: axial stress σ and shear stress τ. These contributions are found from the axial strain ε and shear strain γ by the constitutive law

$$\begin{pmatrix} \sigma \\ \tau \end{pmatrix} = \begin{pmatrix} E & 0 \\ 0 & G \end{pmatrix} \begin{pmatrix} \varepsilon \\ \gamma \end{pmatrix} \tag{2.6}$$

where E is the Youngs modulus, and

$$G = \frac{E}{2(1+\nu)} \tag{2.7}$$

is the shear modulus. The constitutive law (2.6) can also be written as

$$\boldsymbol{\sigma} = \mathbf{E}\boldsymbol{\varepsilon} \tag{2.8}$$

where $\mathbf{E}$ is referred to as the constitutive matrix. Note that this constitutive law is a simplified version of the general case.

2.4 Kinematics

In this section we relate the strains to displacements by kinematic relations, and introduce the shape functions to interpolate displacements between the nodes.

The strain components ε and γ are found from the displacement by kinematic relations:

$$\varepsilon = \frac{\partial u}{\partial x_e} = \frac{1}{l}\frac{\partial u}{\partial \xi}, \quad \text{, and,} \quad \gamma = \frac{1}{2}\frac{\partial u_\theta}{\partial x_e} = \frac{1}{2l}\frac{\partial u_\theta}{\partial \xi} \tag{2.9}$$

where u is the axial displacement field and

$$u_\theta = v\sin\theta + w\cos\theta \tag{2.10}$$

is the tangential displacement field, where $\theta = \tan^{-1}\frac{\eta}{\zeta}$.

The displacement vector $\mathbf{u}_e^l$ only contains values at the two end nodes. For the rest of the element volume we use interpolation functions, $\mathbf{N}(d,t,l) : \mathbb{R}^3 \to \mathbb{R}^{3\times 12}$, to evaluate the displacement field:

$$\begin{pmatrix} u \\ v \\ w \end{pmatrix} = \begin{pmatrix} \mathbf{n}_u^T \\ \mathbf{n}_v^T \\ \mathbf{n}_w^T \end{pmatrix} \mathbf{u}_e^l = \mathbf{N}\mathbf{u}_e^l \tag{2.11}$$

The shape functions are functions of the location in the element, (ξ, η, ζ), the cross sectional properties, $A = A(d,t)$, $I = I(d,t)$, and k, and the material properties E and G. The entries of the shape function matrix $\mathbf{N}$ are computed as [9]

$$\begin{pmatrix} (1-\xi) & 0 & 0 \\ 6\tilde{\Phi}(\xi-\xi^2)\eta & \tilde{\Phi}\left(1-3\xi^2+2\xi^3+\Phi(1-\xi)\right) & 0 \\ 6\tilde{\Phi}(\xi-\xi^2)\zeta & 0 & \tilde{\Phi}\left(1-3\xi^2+2\xi^3+\Phi(1-\xi)\right) \\ 0 & -(1-\xi)l\zeta & (1-\xi)l\eta \\ l\tilde{\Phi}\left(1-4\xi+3\xi^2+\Phi(1-\xi)\right)\zeta & 0 & \\ -l\tilde{\Phi}\left(1-4\xi+3\xi^2+\Phi(1-\xi)\right)\eta & 0 & \\ \xi & 0 & 0 \\ 6\tilde{\Phi}(-\xi+\xi^2)\eta & \tilde{\Phi}(3\xi^2-2\xi^3+\Phi\xi) & 0 \\ 6\tilde{\Phi}(-\xi+\xi^2)\zeta & 0 & \tilde{\Phi}(3\xi^2-2\xi^3+\Phi\xi) \\ 0 & -\xi l\zeta & \xi l\eta \\ l\tilde{\Phi}(-2\xi+3\xi^2+\Phi\xi)\zeta & 0 & -l\Phi\left(-\xi^2+\xi^3-\frac{\Phi}{2}(\xi-\xi^2)\right) \\ -l\tilde{\Phi}(-2\xi+3\xi^2+\Phi\xi)\eta & l\Phi\left(-\xi^2+\xi^3-\frac{\Phi}{2}(\xi-\xi^2)\right) & 0 \end{pmatrix}^T \tag{2.12}$$

where

$$\tilde{\Phi} = \frac{1}{1+\Phi} \quad \text{and,} \quad \Phi = \frac{12EI}{kGAl^2}. \tag{2.13}$$

If Φ is set equal to zero, the Timoshenko element becomes a Bernoulli-Euler element.

The strain-displacement matrix $\mathbf{B}(d,t,l) : \mathbb{R}^3 \to \mathbb{R}^{2\times 12}$ relates the strain to nodal displacements:

$$\begin{pmatrix} \varepsilon \\ \gamma \end{pmatrix} = \begin{pmatrix} \mathbf{b}_\varepsilon^T \\ \mathbf{b}_\gamma^T \end{pmatrix} \mathbf{u}_e^l = \mathbf{B}\mathbf{u}_e^l \tag{2.14}$$

where

$$\mathbf{b}_\varepsilon = \frac{1}{l}\frac{\partial \mathbf{n}_u}{\partial \xi}, \quad \text{and} \quad \mathbf{b}_\gamma = \frac{1}{2l}\left(\frac{\partial \mathbf{n}_v}{\partial \xi}\sin\theta + \frac{\partial \mathbf{n}_w}{\partial \xi}\cos\theta\right). \tag{2.15}$$

The entries of the strain displacement matrix $\mathbf{B}$ are computed as

$$\begin{pmatrix} -1/l & \\ 6\tilde{\Phi}(1-2\xi)\eta/l & \tilde{\Phi}(-6\xi^2+6\xi-\Phi)\sin\theta/l \\ 6\tilde{\Phi}(1-2\xi)\zeta/l & \tilde{\Phi}(-6\xi^2+6\xi-\Phi)\cos\theta/l \\ 0 & \zeta\sin\theta-\eta\cos\theta \\ \tilde{\Phi}\left(-4+6\xi-\Phi\right)\zeta & \tilde{\Phi}(1-4\xi+3\xi^2+\frac{\Phi}{2}(1-2\xi))\cos\theta \\ -\tilde{\Phi}\left(-4+6\xi-\Phi\right)\eta & \tilde{\Phi}(1-4\xi+3\xi^2+\frac{\Phi}{2}(1-2\xi))\sin\theta \\ 1/L & \\ 6\tilde{\Phi}(2\xi-1)\eta/l & \tilde{\Phi}(6\xi-6\xi^2+\Phi)\sin\theta/l \\ 6\tilde{\Phi}(2\xi-1)\zeta/l & \tilde{\Phi}(6\xi-6\xi^2+\Phi)\cos\theta/l \\ 0 & -\zeta\sin\theta+\eta\cos\theta \\ \tilde{\Phi}(-2+6\xi+\Phi)\zeta & \tilde{\Phi}(-2\xi+3\xi^2-\frac{\Phi}{2}(1-2\xi))\cos\theta \\ -\tilde{\Phi}(-2+6\xi+\Phi)\eta & \tilde{\Phi}(-2\xi+3\xi^2-\frac{\Phi}{2}(1-2\xi))\sin\theta \end{pmatrix}^T . \tag{2.16}$$

2.5 Physical equilibrium

In this section the structural matrices are derived from the principle of virtual work, and the static and dynamic equilibrium equations are presented.

We consider an ambiguous (or virtual) displacement field $\boldsymbol{\delta} = (\delta u, \delta v, \delta w)$ in an element volume, V_e. The energy balance between internal strain-energy $\boldsymbol{\varepsilon}(\boldsymbol{\delta})^T\boldsymbol{\sigma}$, acceleration forces $\rho\boldsymbol{a} = \rho(a_u, a_v, a_w)^T$, and external forces $\mathbf{f} = (f_u, f_v, f_w)^T$ can be written as

$$\int_{V_e} \boldsymbol{\varepsilon}(\boldsymbol{\delta})^T\boldsymbol{\sigma}\ \mathrm{d}V_e + \int_{V_e} \boldsymbol{\delta}^T\left(\rho\boldsymbol{a}\right)\ \mathrm{d}V_e = \int_{V_e} \boldsymbol{\delta}^T\mathbf{f}\ \mathrm{d}V_e \tag{2.17}$$

When the displacements, accelerations, and forces are discretized into nodal contributions

$$\boldsymbol{\delta} = \mathbf{N}\mathbf{T}_e\delta\mathbf{u}_e^g \tag{2.18}$$

$$\boldsymbol{a} = \mathbf{N}\mathbf{T}_e\ddot{\boldsymbol{u}}_e^g \tag{2.19}$$

$$\mathbf{f} = \mathbf{N}\mathbf{p}_e, \tag{2.20}$$

the energy balance can be reformulated to

$$\int_{V_e} \left(\mathbf{B}\mathbf{T}_e\delta\mathbf{u}_e^g\right)^T\left(\mathbf{E}\mathbf{B}\mathbf{T}_e\mathbf{u}_e^g\right)\ \mathrm{d}V_e + \int_{V_e} \left(\mathbf{N}\mathbf{T}\delta\mathbf{u}_e^g\right)^T\left(\rho\mathbf{N}\mathbf{T}_e\ddot{\boldsymbol{u}}_e^g\right)\ \mathrm{d}V_e = \int_{V_e} \left(\mathbf{N}\mathbf{T}_e\delta\mathbf{u}_e^g\right)^T\left(\mathbf{N}\mathbf{p}_e\right)\ \mathrm{d}V_e \tag{2.21}$$

Since this balance holds for any displacement field, it follows that

$$\mathbf{K}_e^g\mathbf{u}_e^g + \mathbf{M}_e^g\ddot{\mathbf{u}}_{\boldsymbol{e}}^{\boldsymbol{g}} = \mathbf{p}_e \tag{2.22}$$

where

$$\mathbf{K}_e^g = \mathbf{T}_e\mathbf{K}_e^l\mathbf{T}_e = \mathbf{T}_e^T\int_{V_e}\mathbf{B}^T\mathbf{E}\mathbf{B}\ \mathrm{d}V_e\mathbf{T}_e, \quad \text{and} \quad \mathbf{M}_e^g = \mathbf{T}_e^T\mathbf{M}_e^l\mathbf{T}_e = \int_{V_e}\mathbf{N}^T\left(\rho\mathbf{N}\right)\ \mathrm{d}V_e\mathbf{T}_e \tag{2.23}$$

The entries of the element stiffness matrix $\mathbf{K}_e^l(d,t,l) : \mathbb{R}^3 \to \mathbb{R}^{12\times 12}$ is computed as [3]

$$\mathbf{K}_e^l = \left(\begin{array}{cccccc:cccccc} X & 0 & 0 & 0 & 0 & 0 & -X & 0 & 0 & 0 & 0 & 0 \\ & Y_1 & 0 & 0 & 0 & Y_2 & 0 & -Y_1 & 0 & 0 & 0 & Y_2 \\ & & Y_1 & 0 & -Y_2 & 0 & 0 & 0 & -Y_1 & 0 & -Y_2 & 0 \\ & & & Z & 0 & 0 & 0 & 0 & 0 & -Z & 0 & 0 \\ & & & & Y_3 & 0 & 0 & 0 & Y_2 & 0 & Y_4 & 0 \\ & & & & & Y_3 & 0 & -Y_2 & 0 & 0 & 0 & Y_4 \\ \hdashline & & & & & & X & 0 & 0 & 0 & 0 & 0 \\ & & & & & & & Y_1 & 0 & 0 & 0 & -Y_2 \\ & & & \text{symmetric} & & & & & Y_1 & 0 & Y_2 & 0 \\ & & & & & & & & & Z & 0 & 0 \\ & & & & & & & & & & Y_3 & 0 \\ & & & & & & & & & & & Y_3 \end{array}\right) \tag{2.24}$$

where

$$X = \frac{EA}{l} \qquad Y_1 = \frac{12EI\bar{\Phi}}{l^3} \qquad Y_2 = \frac{6EI\bar{\Phi}}{l^2} \tag{2.25}$$

$$Y_3 = \frac{(4+\Phi)EI\bar{\Phi}}{l} \qquad Y_4 = \frac{(2-\Phi)EI\bar{\Phi}}{l} \qquad Z = \frac{2GI}{l} \tag{2.26}$$

The entries of the element mass matrix $\mathbf{M}_e^l(d,t,l) : \mathbb{R}^3 \to \mathbb{R}^{12\times 12}$ is computed as

$$\mathbf{M}_e^l = \rho L \left(\begin{array}{cccccc:cccccc} P_1 & 0 & 0 & 0 & 0 & 0 & P_2 & 0 & 0 & 0 & 0 & 0 \\ & Q_1 & 0 & 0 & 0 & Q_2 & 0 & Q_4 & 0 & 0 & 0 & -Q_5 \\ & & Q_1 & 0 & -Q_2 & 0 & 0 & 0 & Q_4 & 0 & Q_5 & 0 \\ & & & R_1 & 0 & 0 & 0 & 0 & 0 & R_2 & 0 & 0 \\ & & & & Q_3 & 0 & 0 & 0 & -Q_5 & 0 & Q_6 & 0 \\ & & & & & Q_3 & 0 & Q_5 & 0 & 0 & 0 & Q_6 \\ \hdashline & & & & & & P_1 & 0 & 0 & 0 & 0 & 0 \\ & & & & & & & Q_1 & 0 & 0 & 0 & -Q_2 \\ & & & \text{symmetric} & & & & & Q_1 & 0 & Q_2 & 0 \\ & & & & & & & & & R_1 & 0 & 0 \\ & & & & & & & & & & Q_3 & 0 \\ & & & & & & & & & & & Q_3 \end{array}\right) \tag{2.27}$$

where

$$P_1 = \frac{A}{3} \qquad P_2 = \frac{A}{6} \tag{2.28}$$

$$Q_1 = \frac{A\bar{\Phi}^2(70\Phi^2 + 147\Phi + 78)}{210} + \frac{6I\bar{\Phi}^2}{5l^2} \tag{2.29}$$

$$Q_2 = \frac{Al\bar{\Phi}^2(35\Phi^2 + 77\Phi + 44)}{840} - \frac{I\bar{\Phi}^2(5\Phi - 1)}{10l} \tag{2.30}$$

$$Q_3 = \frac{Al^2\bar{\Phi}^2(7\Phi^2 + 14\Phi + 8)}{840} + \frac{I\bar{\Phi}^2(10\Phi^2 + 5\Phi + 4)}{30} \tag{2.31}$$

$$Q_4 = \frac{A\bar{\Phi}^2(35\Phi^2 + 63\Phi + 27)}{210} - \frac{6I\bar{\Phi}^2}{5l^2} \tag{2.32}$$

$$Q_5 = \frac{Al\bar{\Phi}^2(35\Phi^2 + 63\Phi + 26)}{210} + \frac{I\bar{\Phi}^2(5\Phi - 1)}{10l} \tag{2.33}$$

$$Q_6 = \frac{-Al^2\bar{\Phi}^2(7\Phi^2 + 14\Phi + 6)}{840} + \frac{I\bar{\Phi}^2(5\Phi^2 - 5\Phi - 1)}{30} \tag{2.34}$$

$$R_1 = \frac{2I}{3} \qquad R_2 = \frac{I}{3} \tag{2.35}$$

For structures consisting of more than one element, the full stiffness and mass matrices are assembled from all the element matrices. We refer to $\mathbf{K} \in \mathbb{R}^{n_{dof} \times n_{dof}}$ and $\mathbf{M} \in \mathbb{R}^{n_{dof} \times n_{dof}}$ as the stiffness matrix and the mass matrix, respectively, where n_{dof} is the number of degrees of freedom in the structure. The assembly is performed by adding the element structural matrices to their respective degrees of freedom, and will be shown in section 3.1. The dynamic equilibrium equation can now be stated as

$$\mathbf{Ku} + \mathbf{M}\ddot{\boldsymbol{u}} = \mathbf{p} \tag{2.36}$$

where $\mathbf{u} \in \mathbb{R}^{n_{dof}}$, $\ddot{\boldsymbol{u}} \in \mathbb{R}^{n_{dof}}$, and $\mathbf{p} \in \mathbb{R}^{n_{dof}}$ are the displacement vector, the acceleration vector, and load vector.

In physical problems there is always a certain damping, which we model as Rayleigh damping $\mathbf{C} = \alpha\mathbf{M} + \beta\mathbf{K}$. The coefficients α and β are tuned to obtain the desired damping.

We can now solve the time dependent equilibrium equation

$$\mathbf{Ku}(t) + \mathbf{C}\dot{\mathbf{u}}(t) + \mathbf{M}\ddot{\boldsymbol{u}}(t) = \mathbf{p}(t) \tag{2.37}$$

with respect to displacements by discretizing it in the time domain and solving it with a Newmark integration [11]. For static problems, the equilibrium equation reduces to

$$\mathbf{Ku} = \mathbf{p} \tag{2.38}$$

which can be solved directly, as $\mathbf{u} = \mathbf{K}^{-1}\mathbf{p}$. In JADOP, the backslash operator in Matlab is used to solve the linear system of equations more efficiently.

2.6 Dynamic analysis

In this section we present the general eigenvalue problem, and how it is used to compute eigenfrequencies and mode shapes of the structure.

The generalized eigenvalue problem is stated as

$$\mathbf{K}\boldsymbol{\phi}_i = \lambda_i\mathbf{M}\boldsymbol{\phi}_i, \quad i = 1, \ldots, n_d \tag{2.39}$$

where $\boldsymbol{\phi}_i$ is the eigenvector corresponding to eigenvalue λ_i, and $n_d < n_{dof}$ is the number of unconstrained degrees of freedom in the structure. We assume the eigenvalues to be distinct and ordered, $\lambda_1 < \ldots < \lambda_{n_d}$. This is a realistic assumption, at least for the first couple of eigenfrequencies which are of interest for the application to offshore wind turbine jacket structures. Even though the structure is completely symmetric, there is an asymmetric rotor-nacelle-assembly mass matrix at the tower top which ensures that the bending modes as distinct.

The natural frequencies of the structure is computed as

$$\omega_i = \frac{\sqrt{\lambda_i}}{2\pi} \tag{2.40}$$

and the displacement field $\mathbf{u} = \boldsymbol{\phi}_i$ corresponds to the mode shape associated with eigenfrequency ω_i.

2.7 Stress in tubular welds

In this section the Stress Concentration Factors (SCFs) are introduced, and used to compute stresses in tubular welds and butt welds.

Fatigue failure is often the design driving design criterion for wind turbine support structures, and crack initiation generally occurs at or close to the welds. Fatigue damage is computed as a function of stress history, and it is therefore important to accurately estimate the stress in the welds.

The recommended practice for fatigue design of offshore structures [6] provides a methodology for computing fatigue in welds:

- The stress history shall be computed at eight hot spots equally spaced along the weld.
- The stress at the hot spots shall be computed as a sum of stress contributions from axial forces (ax), moments in-plane (mi), and moments out-of-plane (mo).
- Each stress contribution shall be premultiplied with a stress concentration factor (SCF) which is a function of joint geometry and dimensions.

The nominal stress at hot spot position $\mathbf{h} = (\xi_h, \eta_h, \zeta_h)$ in element e, is computed as $\sigma_{eh} = E\mathbf{b}_{eh}\mathbf{u}_e^l$, where the subscript ε is removed for brevity. The stress is decomposed by decomposing the strain displacement vector $\mathbf{b}_{eh} = \mathbf{b}_{eh}^{ax} + \mathbf{b}_{eh}^{mi} + \mathbf{b}_{eh}^{mo}$. The SCFs s_{eh}^{ax}, s_{eh}^{mi} and s_{eh}^{mo} are then premultiplied onto each strain-component, and the fatigue stress σ_{eh}^f is computed as

$$\sigma_{eh}^f = E\left(s_{eh}^{ax}\mathbf{b}_{eh}^{ax} + s_{eh}^{mi}\mathbf{b}_{eh}^{mi} + s_{eh}^{mo}\mathbf{b}_{eh}^{mo}\right)^T \mathbf{u}_e^l \tag{2.41}$$

where we now have assumed axial stress to be the dominating contribution to the nominal stress. If shear stress shall be included, it is important to note that it is the principal stress which should go into the fatigue stress, and not von Mises stress.

The SCF stress is referred to as the fatigue stress because it is only for fatigue limit state (FLS) computations the SCFs are used. In ultimate limit state (ULS) analysis, the SCFs are not included, but the stress is still evaluated in at least eight hot spots along the circumference of the element.

When there is a thickness transition along a member, such as when stubs and cans are used to reinforce the joints, we assume that there is a butt weld. Butt weld SCFs are simpler than the tubular joint SCFs, but the implementation is similar. For elements that are not part of a weld, the SCFs are all set to unity, i.e. $s_{eh}^{ax} = s_{eh}^{mi} = s_{eh}^{mo} = 1$.

Chapter 3

Optimization

This chapter introduces the design parametrization, and derives the sensitivities of the structural matrices, displacements, stresses, and eigenfrequencies. Both nested and simultaneous analysis and design [1] are considered.

3.1 Design parametrization

In this section the design parametrization of the jacket structure is defined, and variable linking is used to reduce the number of variables.

The jacket structure consists of thin-walled cylindrical elements, fully described by their diameter, wall thickness, and length. In JADOP, the mesh is kept constant in the optimization problem, and thus are diameter and thickness the two design variables associated with each element. The strain-displacement vector for a specific point h in element e can now be described as $\mathbf{b}_{eh} = \mathbf{b}_{eh}(d_e, t_e)$.

The design variable $\mathbf{x}\mathbb{R}^{2n_e}$ contains the diameters and thicknesses of all the finite elements in the jacket:

$$\mathbf{x} = \begin{pmatrix} \mathbf{d} \\ \mathbf{t} \end{pmatrix} \tag{3.1}$$

where n_e is the number of finite elements in the jacket. There are many more finite elements in the analysis model than there are independent cross sections in the structure. To eliminate dependent variables from the design variable, we define a Boolean matrix $\mathbf{B}_v \in \{0,1\}^{2n_e \times n_v}$ which maps the independent design variables $\mathbf{v} \in \mathbb{R}^{n_v}$ to the full design variable $\mathbf{x}$, such that $\mathbf{x} = \mathbf{B}_v\mathbf{v}$.

The stiffness and mass matrices can now be computed as functions of the design variable:

$$\mathbf{K}(\mathbf{v}) = \mathbf{K}_0 + \sum_{e=1}^{n_e} \mathbf{T}_e \mathbf{K}_e^l(\mathbf{v}) \mathbf{T}_e \tag{3.2}$$

$$\mathbf{M}(\mathbf{v}) = \mathbf{M}_0 + \sum_{e=1}^{n_e} \mathbf{T}_e \mathbf{M}_e^l(\mathbf{v}) \mathbf{T}_e \tag{3.3}$$

The ultimate and fatigue stress can be computed as a function of the design variable

$$\sigma_{eh}^u(\mathbf{v}, \mathbf{u}(\mathbf{v})) = E \mathbf{b}_{eh}^T(\mathbf{v}) \mathbf{T}_e \mathbf{u}_e^g(\mathbf{v}) \tag{3.4}$$

$$\sigma_{eh}^f(\mathbf{v}, \mathbf{u}(\mathbf{v})) = E \left(s_{eh}^{ax}(\mathbf{v}) \mathbf{b}_{eh}^{ax}(\mathbf{v}) + s_{eh}^{mi}(\mathbf{v}) \mathbf{b}_{eh}^{mi}(\mathbf{v}) + s_{eh}^{mo}(\mathbf{v}) \mathbf{b}_{eh}^{mo}(\mathbf{v}) \right)^T \mathbf{T}_e \mathbf{u}_e^g(\mathbf{v}) \tag{3.5}$$

Note that the SCFs are also design dependent.

3.2 Optimal design problem

The optimization problem considered in JADOP is

$$\begin{array}{ll} \underset{\mathbf{v}}{\text{minimize}} & f(\mathbf{v}) \\ \text{subject to} & \mathbf{b}_l \leq \mathbf{A}\mathbf{v} \leq \mathbf{b}_u \\ & \mathbf{g}_l \leq \mathbf{g}(\mathbf{v}) \leq \mathbf{g}_u \\ & \underline{\mathbf{v}} \leq \mathbf{v} \leq \overline{\mathbf{v}} \end{array} \tag{P}$$

where the linear constraints $\mathbf{A}\mathbf{v}$ generally enforce the SCF-validity range [6], the nonlinear constraints $\mathbf{g}(\mathbf{v})$ enforce stress, buckling, and frequency constraints, and the variable bounds $\underline{\mathbf{v}}$ and $\overline{\mathbf{v}}$ enforce positive design variables which can be manufactured.

3.3 Simultaneous analysis and design

In this section the difference between the nested analysis and design formulation and the simulataneous analysis and design formulations are described.

There are two main ways to formulate the continuous structural sizing optimization problem:

- Nested analysis and design: The design variable $\mathbf{v}$ is the only variable, and the displacements $\mathbf{u}$ are found by solving the equilibrium equation. Problem (P) is a nested formulation.
- Simultaneous analysis and design (SAND): In addition to the design variable $\mathbf{v}$, we introduce the displacement vector $\mathbf{u}$ as a state variable, and the equilibrium equation is posed as a non-linear equality constraint.

The advantage of using the latter is that the equilibrium equation does not have to be solved in each function call, and the sensitivities are simplified, which might give cheaper computations. The disadvantage is what we introduce many more variables, many more constraints, and that the optimization has to converge before giving useful results.

A reformulation of (P) to a SAND formulation is for the single load case situation

$$\begin{array}{ll} \underset{\mathbf{v},\mathbf{u}}{\text{minimize}} & f(\mathbf{v}) \\ \text{subject to} & \mathbf{b}_l \leq \mathbf{A}\mathbf{v} \leq \mathbf{b}_u \\ & \mathbf{g}_l \leq \mathbf{g}(\mathbf{v},\mathbf{u}) \leq \mathbf{g}_u \\ & \mathbf{0} \leq \mathbf{K}(\mathbf{v})\mathbf{u} - \mathbf{p}(\mathbf{v}) \leq \mathbf{0} \\ & \underline{\mathbf{v}} \leq \mathbf{v} \leq \overline{\mathbf{v}} \end{array} \tag{SAND}$$

where the non-linear constraints $\mathbf{g}(\mathbf{v},\mathbf{u})$ now is a function of $\mathbf{u}$ as well, and the equilibrium equation $\mathbf{K}(\mathbf{v})\mathbf{u} = \mathbf{p}$ is imposed as an extra non-linear equality constraint.

3.4 Sensitivity analysis

In this section the sensitivity of the stress, state equation, and eigenvalues are described.

The sensitivity of the ultimate stress with respect to the design variables is

$$\frac{\mathrm{d}\sigma_{eh}^{u}(\mathbf{v},\mathbf{u}(\mathbf{v}))}{\mathrm{d}\mathbf{v}} = E\left(\mathbf{u}_e^{l\,T}(\mathbf{v})\frac{\mathrm{d}\mathbf{b}_{eh}(\mathbf{v})}{\mathrm{d}\mathbf{v}} + \mathbf{b}_{eh}^{T}(\mathbf{v})\frac{\mathrm{d}\mathbf{u}_e^{l}}{\mathrm{d}\mathbf{v}}\right) \tag{3.6}$$

in the nested formulation, and

$$\frac{\mathrm{d}\sigma_{eh}^{u}(\mathbf{v})}{\mathrm{d}\mathbf{v}} = E\mathbf{u}_e^{l\,T}\frac{\mathrm{d}\mathbf{b}_{eh}(\mathbf{v})}{\mathrm{d}\mathbf{v}} \tag{3.7}$$

in the SAND formulation. The sensitivity of the fatigue stress is similar, but also includes all the dependencies on the SCFs.

The sensitivity of the displacement vector in the nested formulation is found from

$$\mathbf{u}(\mathbf{v})^T\frac{\mathrm{d}\mathbf{K}(\mathbf{v})}{\mathrm{d}\mathbf{v}} + \frac{\mathrm{d}\mathbf{u}(\mathbf{v})}{\mathrm{d}\mathbf{v}}\mathbf{K}(\mathbf{v}) - \frac{\mathrm{d}\mathbf{p}(\mathbf{v})}{\mathrm{d}\mathbf{v}} = 0 \tag{3.8}$$

The sensitivity of the state equation in the SAND formulation is

$$\frac{\mathrm{d}\big(\mathbf{K}(\mathbf{v})\mathbf{u} - \mathbf{p}(\mathbf{v})\big)}{\mathrm{d}\mathbf{v}} = \mathbf{u}^T\frac{\mathrm{d}\mathbf{K}(\mathbf{v})}{\mathrm{d}\mathbf{v}} - \frac{\mathrm{d}\mathbf{p}(\mathbf{v})}{\mathrm{d}\mathbf{v}} \tag{3.9}$$

$$\frac{\mathrm{d}\big(\mathbf{K}(\mathbf{v})\mathbf{u} - \mathbf{p}(\mathbf{v})\big)}{\mathrm{d}\mathbf{u}} = \mathbf{K}(\mathbf{v}) \tag{3.10}$$

The sensitivity of the eigenvalues are, under the assumption that the eigenvalues are distinct, given by [7]

$$\frac{\mathrm{d}\lambda_i}{\mathrm{d}\mathbf{v}_k} = \boldsymbol{\phi}_i^T\left(\frac{\mathrm{d}\mathbf{K}(\mathbf{v})}{\mathrm{d}\mathbf{v}_k} - \lambda_i\frac{\mathrm{d}\mathbf{M}(\mathbf{v})}{\mathrm{d}\mathbf{v}_k}\right)\boldsymbol{\phi}_i.$$

The model of the offshore wind turbine rotor-nacelle-assembly in JADOP ensures that the lowest eigenfrequencies are indeed distinct.

To derive the sensitivity of $\mathbf{K}(\mathbf{v})$, $\mathbf{M}(\mathbf{v})$, and $\mathbf{b}(\mathbf{v})$ we first define the element variable $\mathbf{x}_e = (d_e\ t_e)^T$, and compute

$$\frac{\mathrm{d}\tilde{\Phi}(\mathbf{x}_e)}{\mathrm{d}\mathbf{x}_e} = \frac{\mathrm{d}\tilde{\Phi}(\Phi)}{\mathrm{d}\Phi}\frac{\mathrm{d}\Phi(\mathbf{x}_e)}{\mathrm{d}\mathbf{x}_e} \tag{3.11}$$

where

$$\frac{\mathrm{d}\tilde{\Phi}(\Phi}{\mathrm{d}\Phi} = \frac{-1}{(\Phi+1)^2} \tag{3.12}$$

$$\frac{\mathrm{d}\Phi(\mathbf{x}_e)}{\mathrm{d}\mathbf{x}_e} = \frac{12E\frac{\mathrm{d}I(\mathbf{x}_e)}{\mathrm{d}\mathbf{x}_e}kGAL^2 - 12EIkGL^2\frac{\mathrm{d}A(\mathbf{x}_e)}{\mathrm{d}\mathbf{x}_e}}{(kGAL^2)^2} \tag{3.13}$$

$$\frac{\mathrm{d}A_e(\mathbf{x}_e)}{\mathrm{d}\mathbf{x}_e} = \begin{pmatrix}\pi t_e \\ \pi(d_e - 2t_e)\end{pmatrix} \tag{3.14}$$

$$\frac{\mathrm{d}I_e(\mathbf{x}_e)}{\mathrm{d}\mathbf{x}_e} = \begin{pmatrix}\frac{\pi}{16}\left(d_e^3 - (d-2t_e)^3\right) \\ \frac{\pi}{8}\left((d-2t_e)^3\right)\end{pmatrix} \tag{3.15}$$

The sensitivity of the stiffness matrix, mass matrix, and strain-displacement vector with respect to $\mathbf{x}$ can now be computed relatively straight forward, as they are only functions of $\tilde{\Phi}$, Φ, A and I. The Boolean matrix is then used to map the sensitivity to $\mathbf{x}$ to the sensitivity to $\mathbf{v}$

$$\frac{\mathrm{d}\mathbf{K}(\mathbf{v})}{\mathrm{d}\mathbf{v}} = \frac{\mathrm{d}\mathbf{K}(\mathbf{x}(\mathbf{v}))}{\mathrm{d}\mathbf{x}}\mathbf{B}_v \tag{3.16}$$

$$\frac{\mathrm{d}\mathbf{M}(\mathbf{v})}{\mathrm{d}\mathbf{v}} = \frac{\mathrm{d}\mathbf{M}(\mathbf{x}(\mathbf{v}))}{\mathrm{d}\mathbf{x}}\mathbf{B}_v \tag{3.17}$$

$$\frac{\mathrm{d}\mathbf{b}_{eh}(\mathbf{v})}{\mathrm{d}\mathbf{v}} = \frac{\mathrm{d}\mathbf{b}_{eh}(\mathbf{x}(\mathbf{v}))}{\mathrm{d}\mathbf{x}}\mathbf{B}_v \tag{3.18}$$

From the above relation it is apparent that

$$\mathbf{B}_v = \frac{\mathrm{d}\mathbf{x}(\mathbf{v})}{\mathrm{d}\mathbf{v}} \tag{3.19}$$

Chapter 4

Validation with Abaqus

To validate the implementation of finite element analysis in JADOP, the structural model is exported to Abaqus. Static response and eigenfrequencies are compared. The interpretation of the OC4 jacket with the NREL 5 MW turbine is chosen as the reference structure.

4.1 Static analysis

An extreme thrust force of 10 MN is applied to the structure, and the structural response **u** computed in JADOP and Abaqus are compared. Some properties of the displacement vectors are given in Table 4.1, and a visual representation is shown in Figure 4.1.

Table 4.1: Static structural response in Jadop and Abaqus.

	JADOP	Abaqus
Norm of **u**	18.2009	18.1983
Max of **u**	6.2624	6.2640

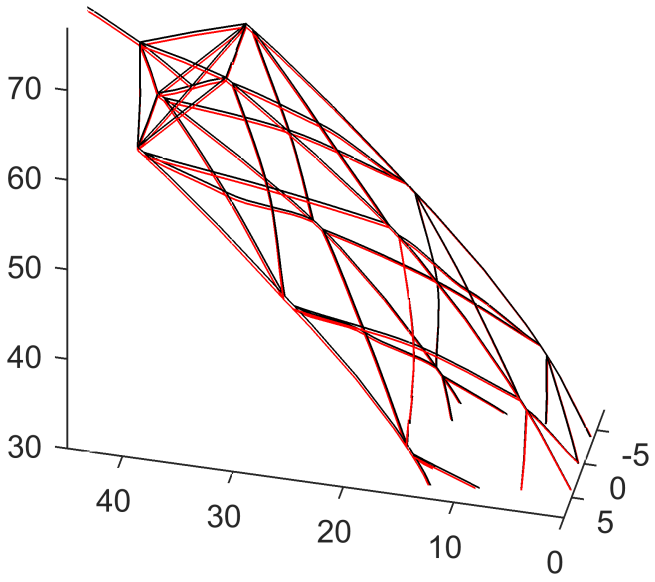

Figure 4.1: Structural response times 50 under a 10 MN load. Jadop in black, Abaqus in red.

The structural responses are in very good agreement, though a small difference can be observed. A closer investigation indicate that the difference has to do with the boundary condition. This is because the error in the displacement vector is not accumulated throughout

the structure, but exists even very close the the boundary condition. An explanation to this has not been reached, but it is concluded instead that the agreement is sufficiently good.

4.2 Dynamic analysis

The ten first eigenfrequencies are computed in both JADOP and Abaqus, and they are compared in Table 4.2.

Table 4.2: Eigenfrequencies computed in JADOP and Abaqus.

	Jadop	Abaqus
1	0.3127	0.3126
2	0.3135	0.3134
3	1.1121	1.1122
4	1.1233	1.1234
5	1.5772	1.5730
6	2.6140	2.6158
7	2.8991	2.9015
8	3.9679	3.8518
9	5.1838	5.1839
10	5.5431	5.5499

The agreement of the ten first eigenfrequencies computed in Jadop and Abaqus is very good. The largest relative difference is in frequency number eight, where Jadop computes three percent higher frequency than Abaqus. With the exception of frequency number five, eight, and ten, the disagreement is lower than 0.1 percent. However, this difference is actually because the Abaqus model uses a lumped mass matrix, and the JADOP model uses a consistent mass matrix.

4.3 Mesh dependency

The above mentioned validation data are based on the coarsest mesh allowed in JADOP, which is two finite elements per part. Considering that each member in the jacket consists of three parts, and that the tower consists of approximately ten parts, this gives a reasonably fine mesh. As shown in the previous validation, it compares well with Abaqus for both static and dynamic analysis.

The validation was also performed for a finer discretization, with maximum finite element length of 1 meter. This has almost no implication for the static response, but does explain some of the deviation between JADOP and Abaqus in the dynamic response. Table 4.3 shows the relative error of the ten first eigenfrequencies, as reported in Table 4.2, when compared with the eigenfrequencies of the finer discretization in Abaqus. Information about the two meshes are given in Table 4.4.

Table 4.3: Relative error in eigenfrequency calculations.

	Jadop [%]	Abaqus [%]
1	-0.0485	-0.0799
2	-0.0501	-0.0829
3	-0.0437	-0.0360
4	-0.0419	-0.0356
5	-0.0179	-0.2853
6	-0.0702	0
7	-0.1031	-0.0207
8	-0.2029	-3.1237
9	0.0029	0.0039
10	-0.2105	-0.0882

Table 4.4: Information about the two different meshes.

	Coarse mesh	Fine mesh
Number of elements	572	2157
Number of DOFs	3078	12588

Table 4.3 shows that the eigenfrequencies computed with the coarse mesh in JADOP is actually more accurate than those computed with the coarse mesh in Abaqus. This is most likely because the Abaqus model by default uses lumped mass matrices, while JADOP uses consistent mass matrices.

Based on these investigations, it is concluded that the finite element implementation in JADOP shows good agreement with Abaqus. It is also recommended that the coarse model can be used for all purposes.

Chapter 5

Model library

JADOP is developed specifically for design of jacket structures, although the analysis and optimization methods are applicable to any type of frame structure. This chapter describes the current model library. First the structural model is described. Then follows a description of how two specific structures. Finally, a discussion about current limitations and future possibilities is presented.

5.1 Structural model

This section describes the structural model in JADOP, with focus on the parametric mesh of the jacket. The structural model in JADOP, see Figure 5.1, consists of

- Foundations, one in each of the four corners of the square jacket base.
- A four-legged symmetric jacket with straight battered legs.
- A transition piece.
- A tower.
- A turbine model.

The foundation is modelled as a six-degree-of-freedom node, where specialized stiffness, damping and mass matrices can be implemented. The parameters controlling the jacket design are

- Bottom leg distance.
- Top leg distance (must be smaller than bottom leg distance).
- Number of sections (also called bays).
- Stub length and can length (only relevant of joints are reinforced with stubs and cans).
- K-joint eccentricity (the distance between the intersecting braces on the in a joint).

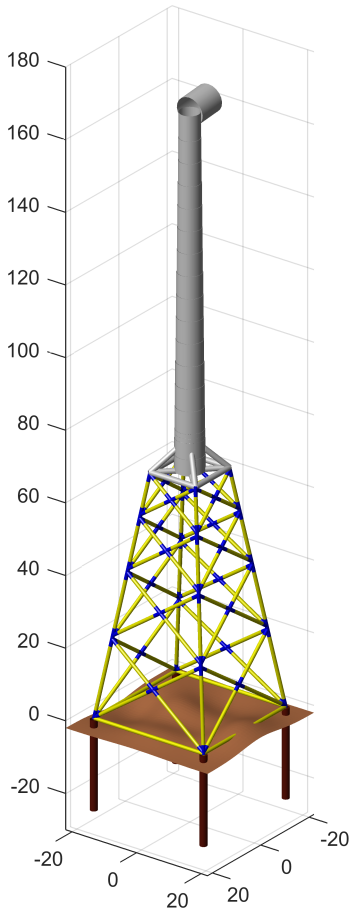

Figure 5.1: Visualization of the offshore wind turbine model in JADOP.

The transition piece design is currently limited to a pyramid-type frame structure with diagonal stiffeners in the base. The parameters controlling the transition piece design are

- Batter angle. This can be set to for example 45 degrees, such that the transition piece height changes with the top leg distance of the jacket
- Maximum and minimum transition piece height. This is to make sure the transition-piece is not allowed to become too large or too small. Specifically, it is important that the height of the transition piece is smaller than the tower sections.

The tower is assumed to begin at the bottom of the transition piece and end at the hub height, and both diameter and thickness is assumed to vary linearly from bottom to top. JADOP only supports cylindrical members at the current time, and therefore the tower is modelled in sections, with discrete jumps in thickness and diameter. However, since there are many sections describing the tower, this is assumed to be sufficient for modelling first few eigenfrequencies correctly. The parameters controlling the tower are

- Tower top diameter.
- Diameter increase per meter from the top (tower coning).
- Tower top thickness.
- Thickness increase per meter from the top.
- Hub height (Tower height = Hub height - (Jacket height - Water depth)).
- Tower section height (Must be larger than transition piece height).

At the top of the tower is the turbine. However, no aeroelastic simulations are available in JADOP, and therefore the rotor is not modelled at all. Instead, an equivalent mass matrix with the total rotor-nacelle-assembly (RNA) mass, and equivalent inertias with respect to the tower top node, are provided. This is a major simplification, but it gives a good estimate of the first few eigenfrequencies.

All parts of the structure are modelled with at least two finite elements. However, there is also a parameter for maximum mesh length, which can be adjusted to obtain a finer discretization.

5.2 NREL 5 MW RWT on OC4 jacket

The Upwind reference jacket [5], which was also used in the OC4 project [12], is a well-known reference structure in the literature. It is designed for 50 meter water depth.

Figure 5.2 shows the Upwind jacket in detail, and the interpretation in JADOP to the right. Leg distance at the bottom and top, number of sections, and cross section dimensions in the jacket are the same. The cross section dimensions in JADOP are tuned such that the transition piece mass is the same as the original one. The transition piece height is also the same.

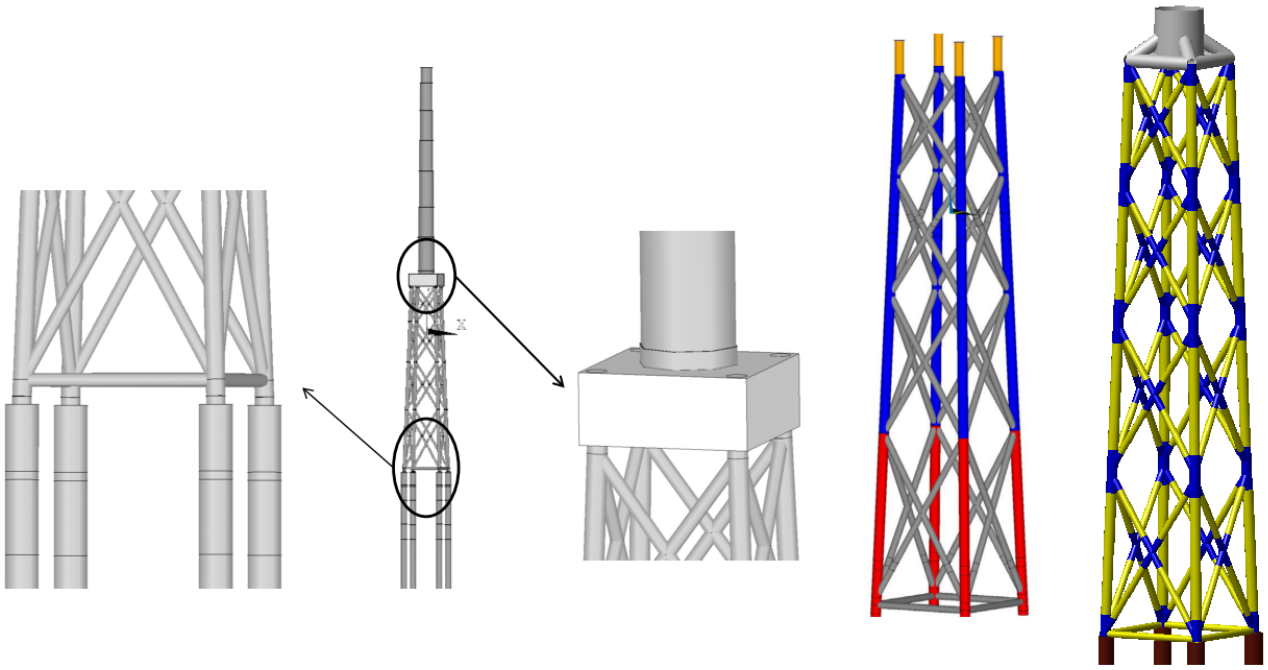

Figure 5.2: The OC4 jacket and the JADOP interpretation of it. The main difference is in the transition piece, since OC4 has a solid concrete transition piece.

Since the models are not identical, there are some minor differences in the eigenfrequencies of the two models. In addition to the different transition pieces, there are some small differences in the lowest part of the jacket as well. The Upwind jacket assumes the connection to the piles to be 6 meters above the seabed, while JADOP assumes this connection to at the seabed. Furthermore, there is zero eccentricity in OC4, while in JADOP the eccentricity has to be a positive value, although it can be as low as desired.

5.3 DTU 10 MW RWT on INNWIND.EU jacket

The INNWIND.EU reference jacket [2] was developed by Ramboll for the DTU 10 MW reference wind turbine in 50 m water depth. It is increasingly being used as a reference structure, as the industry is clearly moving towards larger turbines that 5 MW.

Figure 5.3 shows the INNWIND.EU jacket in detail, and the interpretation in JADOP to the right. Leg distance at the bottom and top, and the number of sections in the jacket are the same. The cross sectional dimensions of the INNWIND.EU reference jacket has not been implemented in JADOP, partly because the X-joints are non-symmetric for manufacturing reasons, and this is not supported in the current version of JADOP. The transition piece is not identical either, but it has the same height, and the cross sectional dimensions are also tuned such that the mass is the same.

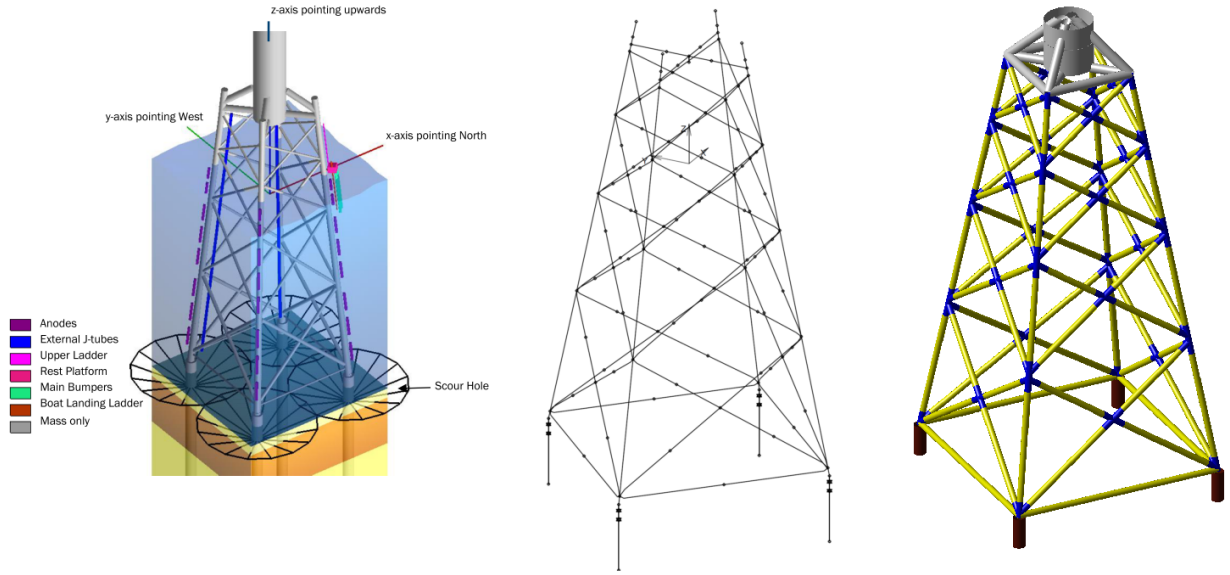

Figure 5.3: The INNWIND.EU jacket and the JADOP interpretation of it.

5.4 Turbines

The Upwind reference jacket was designed to support the NREL 5 MW reference wind turbine, and the Innwind.EU jacket was designed to support the DTU 10 MW reference turbine. Significant details are provided in Table 5.1. The frequency range is necessary to create correct frequency constraints in the optimal design problem. The allowable frequency for the first bending mode is generally given as the soft-stiff range (between 1P and 3P), with a ten percent safety margin, as shown in Table 5.1.

Table 5.1: Turbine properties required in JADOP.

	NREL 5 MW	DTU 10 MW
Hub height [m]	90	113
RNA-mass [tons]	350	676
Equivalent I_{xx}[m^4]	2.34e7	1.66e8
Equivalent I_{yy}[m^4]	1.69e7	1.27e8
Equivalent I_{zz}[m^4]	1.54e7	1.27e8
1P Frequency range [Hz]	0.115-0.2017	0.10-0.158
3P Frequency range [Hz]	0.345-0.6051	0.30-0.474
Allowable range [Hz]	0.2219-0.3105	0.174-0.27

5.5 Limitations

The parametric jacket model in JADOP can be easily adopted to approximate other jacket designs by only changing a few parameters. However, the interpretations are not exact. Below is a short list of limitations:

Number of legs: In the current model, only four-legged jacket is supported. The number of legs should ideally be a parameter (≥ 3).

Multiple transition pieces: In the current model, a pyramid-shaped transition piece is assumed, but this should be extended to more realistic alternatives.

Conical elements: Some jackets are designed with conical elements, and the tower is almost always built using conical elements.

Load library: To compare results from JADOP with results from the literature, the same structure is not enough, one also needs the same load cases and constraints.

By addressing these limitations, the design freedom could be significantly increased, making the parametric model able to better suit many types of structures. By creating a load case library, it would also be easier to compare the optimization results from JADOP with results from the literature.

Chapter 6

Conclusions

A documentation and theory manual of the analysis and optimization software JADOP is presented.

A finite element analysis based on Timoshenko beam elements is used to model the full offshore wind turbine structure, except the rotor-nacelle-assembly, which is simplified. An optimal design problem for sizing of diameters and thicknesses of the jacket members is formulated using both nested and simultaneous analysis and design (SAND) formulations. Analytical gradients of both displacements and stresses are given. Following the design guidelines, the method of stress concentration factors is followed, and also this is solved with analytical gradients.

The software is organized in a way that allows it to be used for several purposes, and it is currently used by several researchers pursuing various goals. The aim is to update this documentation continuously, such that new features are included when they are finished.

6.1 Contributions

The evolution of JADOP has been a team effort by Kasper Sandal and Alexander Verbart, without very clear distinction of responsibilities. The first version of the code was made by Kasper Sandal, and here are his main contributions:

- **Jacket model:** Parameterized mesh, local coordinate system, element and node numbering, variable linking, implementation of Boolean matrix.
- **Static analysis:** Timoshenko beam element stiffness and mass matrices, global matrix assembly, boundary conditions, modal analysis.
- **Loads:** Make Jadop communicate with the load model, implement rotor load time series, implement Morison equation wave load, damage equivalent load.
- **Static optimization:** Static optimization in the SAND formulation, frequency constraint, SCF-validity constraints.
- **Piles:** Implement pile model and pile capacity constraints for optimization.
- **Post-processing:** Wireframe plot, node number plot, element number plot, 3D element plot, and wave surface plots.

Alexander Verbart came into the project when an early version of the code was developed, and he have had the following main contributions:

- **Structure:** Organize and design the code in an hierarchy that allows it to grow without systematically.
- **Boolean matrix:** The idea and first implementations of the Boolean matrix.
- **Domains:** Design, constraint, and visualization domains.
- **Transient analysis:** Implement time integration.
- **Stresses:** Shape functions, strain-displacement matrix, and stress calculation.
- **Transient optimization:** Optimization in the Nested formulation, stress constraints.
- **Multiple loading:** Implementation of a systematic way of dealing with multiple loading conditions.
- **Post-processing:** Stress plot.

Mathias Stolpe has supervised the development, and has contributed specifically with code for exporting frame structures to Abaqus and interfaces to various optimization solvers.

Load models have been provided by Signe Schløer and Henrik Bredmose from DTU Wind Energy. Pile models has been provided by Chiara Lahti and Varvara Zania from DTU Civil Engineering.

6.2 Acknowledgement

JADOP is developed in the strategic research project ABYSS: Advancing BeYond Shallow waterS - Optimal design of offshore wind turbine support structures (`www.abyss.dk`). The project is funded by the Danish Council for Strategic Research, Grant no. 1305-00020B. The funding is gratefully acknowledged.

Bibliography

[1] J. S. Arora and Q. Wang. Review of formulations for structural and mechanical system optimization. *Structural and Multidisciplinary Optimization*, 30(4):251–272, 2005.

[2] T. Borstel. Design report - reference jacket. Technical Report D4.3.1, INNWIND.EU, 2013.

[3] R. D. Cook, D. S. Malkus, M. E. Plesha, and R. J. Witt. *Concepts and Applications of Finite Element Analysis*. John Wiley & Sons, fourth edition, 2007.

[4] Dassault Systèmes. *ABAQUS Documentation*, 6.14 edition, 2014. `www.3ds.com`.

[5] W. de Vries. Final report WP 4 . 2 Support Structure Concepts for Deep Water Sites. Technical report, Delft University of Technology, 2011.

[6] DNVGL. RP-C203 Fatigue design of offshore steel structures. Technical report, DNVGL, 2014.

[7] R. L. Fox and M. P. Kapoor. Rate of change of eigenvalues and eigenvectors. *AIAA Journal*, 6(12):2426–2429, 1968.

[8] J. R. Hutchinson. Shear Coefficients for Timoshenko Beam Theory. *Journal of Applied Mechanics*, 68(1):87–92, 2001.

[9] Y. A. Khulief. Shape Functions of Three-Dimensional Timoshenko Beam Element. *Journal of Sound and Vibration*, 259(2):473–480, 2003.

[10] MathWorks, Inc. *MATLAB Primer*, R2015a edition, 2015. `www.mathworks.com`.

[11] N. M. Newmark. A Method of Computation for Structural Dynamics. *Journal of the Engineering Mechanics Division*, 85(3):6794, 1959.

[12] F. Vorpahl, W. Popko, and D. Kaufer. Description of a basic model of the "UpWind reference jacket" for code comparison in the OC4 project under IEA Wind Annex 30. Technical report, Fraunhofer Institute for Wind Energy and Energy System Technology IWES, 2011.

$\sqrt{17}$
$\Omega \int \delta e^{i\pi} = -1$
{2.7182818284}ϑωερτυθιοπσδφγηξκλ
$\chi^2 \sum \gg \approx \lambda$
!